Equilibrium oxygen, hydrogen and carbon isotope fractionation factors applicable to geologic systems

Chapter · February 2019

CITATIONS
18

READS
404

3 authors, including:

Thomas Chacko
University of Alberta
124 PUBLICATIONS **5,269** CITATIONS
SEE PROFILE

David Robert Cole
The Ohio State University
363 PUBLICATIONS **10,092** CITATIONS
SEE PROFILE

1 Equilibrium Oxygen, Hydrogen and Carbon Isotope Fractionation Factors Applicable to Geologic Systems

Thomas Chacko

Department of Earth and Atmospheric Sciences
University of Alberta
Edmonton, Alberta T6G 2E3, Canada

David R. Cole and Juske Horita

Chemical and Analytical Sciences Division
Oak Ridge National Laboratory
Oak Ridge, Tennessee 37831

INTRODUCTION

As demonstrated by the chapters in this short course, stable isotope techniques are an important tool in almost every branch of the earth sciences. Central to many of these applications is a quantitative understanding of equilibrium isotope partitioning between substances. Indeed, it was Harold Urey's (1947) thermodynamically based estimate of the temperature-dependence of $^{18}O/^{16}O$ fractionation between calcium carbonate and water, and a recognition of how this information might be used to determine the temperatures of ancient oceans, that launched the science of stable isotope geochemistry. The approach pioneered by Urey has since been used to estimate temperatures for a wide range of geological processes (e.g. Emiliani 1955; Anderson et al. 1971; Clayton 1986; Valley, this volume). In addition to their geothermometric applications, equilibrium fractionation data are also important in the study of fluid-rock interactions, including those associated with diagenetic, hydrothermal, and metamorphic processes (Baumgartner and Valley, this volume; Shanks, this volume). Finally, a knowledge of equilibrium fractionation is a necessary first step in evaluating isotopic disequilibrium, a widespread phenomenon that is increasingly being used to study temporal relationships in geological systems (Cole and Chakraborty, this volume).

In the fifty-four years since the publication of Urey's paper, equilibrium fractionation data have been reported for many minerals and fluids of geological interest. These data were derived from: (1) theoretical calculations following the methods developed by Urey (1947) and Bigeleisen and Mayer (1947); (2) direct laboratory experiments; (3) semi-empirical bond-strength models; and (4) measurement of fractionations in natural samples. Each of these methods has its advantages and disadvantages. However, the availability of a variety of methods for calibrating fractionation factors has led to a plethora of calibrations, not all of which are in agreement. In this chapter, we evaluate the major methods for determining fractionation factors. We also compile data on oxygen, hydrogen, and carbon isotope fractionation factors for geologically relevant mineral and fluid systems. Our compilation focuses primarily on experimental and natural sample calibrations of fractionations factors as large compilations of theoretical (Richet et al. 1977; Kieffer 1982) and bond-strength (e.g. Hoffbauer et al. 1994; Zheng 1999a) calibrations already exist in the literature. The chapter begins with a general overview of the theoretical basis of stable isotope fractionation, and theoretical methods for calculating fractionation factors. The reader is referred to the earlier review papers of Richet et al. (1977), Clayton (1981), O'Neil (1986) and Kyser (1987), and the recent textbook by Criss (1999) for more detailed

1529-6466/00/0043-0001$10.00

discussion of theoretical topics. Our emphasis will be on advances in the determination of fractionation factors and on our understanding of the variables that control isotopic fractionation behavior made since the publication of *Reviews in Mineralogy*, Volume 16 (Valley et al. 1986).

THEORETICAL BACKGROUND

Comparison of cation and isotope exchange reactions

The equilibrium fractionation of isotopes between substances is analogous in many ways to the partitioning of cations (such as Fe and Mg) between minerals. Both processes can be described in terms of chemical reactions in which isotopes or cations are exchanged between two coexisting phases. For example, the partitioning of Fe and Mg between orthopyroxene and olivine can be described by the reaction:

$$FeSiO_3 + 1/2\ Mg_2SiO_4 = MgSiO_3 + 1/2\ Fe_2SiO_4$$

where the equilibrium constant, K_1, for this reaction is:

$$K_1 = \frac{(a^{opx}_{MgSiO_3})(a^{ol}_{Fe2SiO_4})^{1/2}}{(a^{opx}_{FeSiO_3})(a^{ol}_{Mg2SiO_4})^{1/2}}$$

where a_i^p is the thermodynamic activity of component i in phase p. Assuming ideal mixing of Fe and Mg on the octahedral sites of orthopyroxene and olivine, K_1 can be recast as:

$$K_1 = \frac{(Mg/Fe)_{opx}}{[(Mg/Fe)^2_{ol}]^{1/2}} = \frac{(Mg/Fe)_{opx}}{(Mg/Fe)_{ol}}$$

Similarly, the partitioning of ^{18}O and ^{16}O between olivine and orthopyroxene is described by the reaction:

$$1/3\ MgSi^{16}O_3 + 1/4\ Mg_2Si^{18}O_4 = 1/3\ MgSi^{18}O_3 + 1/4\ Mg_2Si^{16}O_4$$

Assuming ideal mixing of oxygen isotopes among the different oxygen sites in olivine and orthopyoxene, this gives an equilibrium constant, K_2, of:

$$K_2 = \frac{[(^{18}O/^{16}O)^3_{opx}]^{1/3}}{[(^{18}O/^{16}O)^4_{ol}]^{1/4}} = \frac{(^{18}O/^{16}O)_{opx}}{(^{18}O/^{16}O)_{ol}} = \alpha_{opx-ol}$$

If the reaction is written such that one mole of ^{18}O and ^{16}O atoms are exchanged between the two minerals, K_2 is equal to $\alpha_{opx\text{-}ol}$, the oxygen isotope fractionation factor between orthopyroxene and olivine.

As with all chemical reactions, the standard state Gibbs free energy change for an isotope exchange reaction at a given pressure and temperature is related to the equilibrium constant by:

$$\Delta G^o_R(T, P) = \Delta H^o_R - T\Delta S^o_R + P\Delta V^o_R = -RT \ln K \quad (1)$$

In principle, the free energy change and in turn the equilibrium constant for such reactions can be calculated from conventional thermodynamic data (molar enthalpy, entropy, volume data) on the end-member isotopic species denoted in the reaction. This approach, however, is generally not practicable because of the paucity of thermodynamic data on isotopically 'pure' end-members. Moreover, even if such data were widely available, the Gibbs free energy changes associated with most isotope exchange reactions

are too small (typically a few tens of joules or less, compared to thousands of joules for cation exchange reactions) to permit precise calculations using classical thermodynamic methods.

Despite its limitations, the discussion above is useful for illustrating the formal similarities between cation and isotope exchange reactions. Equation (1) also shows that equilibrium constants for all exchange reactions are dependent on temperature. More specifically, ln K varies linearly with T^{-1} if ΔG^o_R is independent of temperature. This T^{-1} temperature-dependency generally applies to cation exchange reactions because values of ΔG^o_R for such reactions are approximately constant over a wide range of temperatures. In the case of isotope exchange reactions, however, ΔG^o_R varies significantly with temperature, which results in higher order temperature-dependencies (T^{-2}). The effect of pressure on ln K is determined by the volume change for the reaction. For most isotope exchange reactions, ΔV^o_R is small, resulting in correspondingly small pressure effects on ln K. However, as discussed further below, pressure effects can be significant for hydrogen isotope fractionations, particular those involving water.

QUANTUM MECHANICAL REASONS FOR ISOTOPIC FRACTIONATION

The existence of small but significant free energy changes in isotope exchange reactions implies energetic differences between chemical species differing only in their isotopic composition. These energy differences are entirely a quantum mechanical phenomenon arising from the effect of atomic mass on the vibrational energy of molecules. Consider a diatomic molecule, which can be represented by two masses, m_1 and m_2, attached by a spring (Fig. 1a). The force (F) exerted on the masses is equal to the displacement (x) of the spring from the rest position times the force constant (k) of the spring (i.e. the spring's stiffness):

$$F = -kx,$$

The potential energy, PE, of the spring is given by the equation:

$$PE = kx^2/2$$

which defines a parabola with a minimum potential energy when the spring is at the rest position (x = 0), and increasing potential energy when the spring is compressed (-x) or stretched (+x) from that position (Fig. 1b). The vibrational frequency, ν, of the spring is given by:

$$\nu = \frac{1}{2\pi}\sqrt{\frac{k}{\mu}} \tag{2}$$

where μ is the reduced mass and given by:

$$\mu = \frac{m_1 m_2}{m_1 + m_2}$$

Derivation of the equations given above can be found in most introductory physics or physical chemistry textbooks. McMillan (1985) also provides a helpful summary.

In its simplest form, the spring-chemical bond analogy is referred to as the harmonic oscillator approximation. Several facets of this analogy are useful to keep in mind. Firstly, the rest position of the spring corresponds to the optimal distance between the nuclei of the two atoms, and the minimum in the potential energy curve. If the atoms are pushed closer or pulled further away than this optimal distance, electrical forces act to

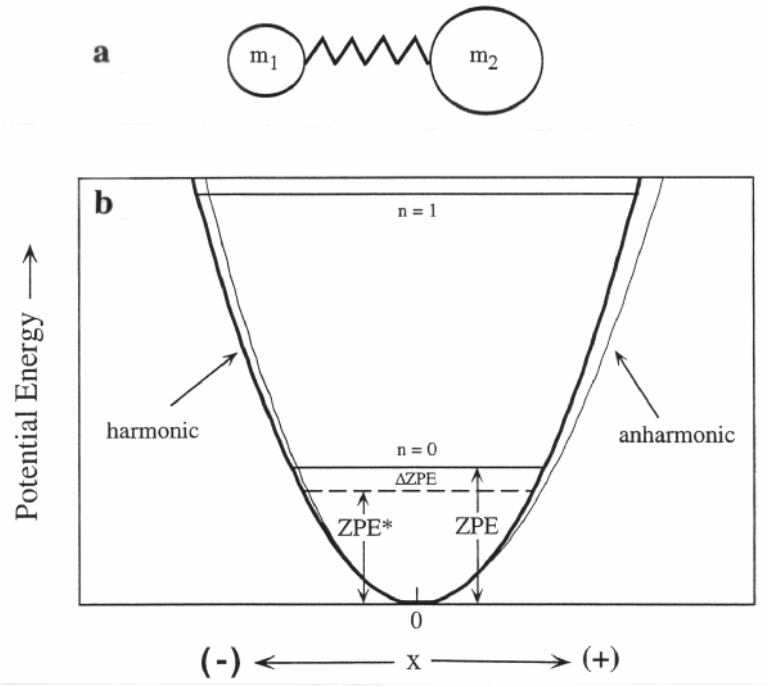

Figure 1. (A) Drawing of a spring with two masses attached (simple harmonic oscillator), which is an analogue for a diatomic molecule. (B) Schematic plot showing variation in the potential energy of harmonic (and anharmonic) oscillators as they are displaced from the rest position (x = 0). Energy levels are given by values of n. The zero point energy (ZPE) is the difference in energy between the bottom of the potential energy well and the energy of the ground vibrational state (n = 0). Note that the zero point energy of a molecule made with the heavy isotope (ZPE*) is lower than that of the molecule made with the light isotope. The magnitude of ΔZPE (ZPE-ZPE*) for a substance exerts a major control on its isotopic fractionation behavior.

restore the atoms towards the equilibrium position. Secondly, a strong chemical bond can be thought of as a stiff spring (i.e. a spring with a large force constant). It follows from Equation (2) that, all else being equal, strong bonds generally have higher vibrational frequencies than weak bonds. Thirdly, according to the Born-Oppenheimer approximation, isotopic substitution has no effect on the force constant of a bond. The magnitude of the force constant is determined by the electronic interaction between atoms, and is independent of the masses of the two nuclei. Thus, the potential energy curves of molecules comprising heavy and light isotopes of an element are identical.

Given the last statement, classical mechanics predicts no energy differences between two molecules that differ only in their isotopic composition. At a temperature of absolute zero, both molecules should have energies corresponding to the bottom of their identical potential energy wells. Quantum theory, however, indicates that the vibrational energy, E, is quantized and given by:

$$E = (n + 1/2)h\nu \quad (3)$$

where n corresponds to the energy levels 0, 1, 2, 3, etc., and h is Planck's constant. Thus, even at absolute zero, where all molecules are in the ground state (n = 0), the vibrational energy of these molecules lies some distance above the bottom of the potential energy well. The energy difference between the bottom of the potential energy well and the

energy of ground vibrational state is referred to as the zero point energy or ZPE (Fig. 1b). Importantly, although the potential energy curves of molecules made up of light and heavy isotopes of an element are identical, their ZPE's are different because of the effect of mass on vibrational frequency. More specifically, it can readily be shown from Equation (2) that the ratio of the vibrational frequencies of isotopically heavy and light molecules of a particular compound is given by:

$$\frac{\nu^*}{\nu} = \sqrt{\frac{\mu}{\mu^*}} \tag{4}$$

where the asterisks denote the molecule containing the heavy isotope. Because of the inverse relationship between frequency and mass, the heavy molecule has a lower vibrational frequency, and hence a lower ZPE than the light molecule (Fig. 1b). This implies that a isotopically heavy molecule is always energetically more stable than its isotopically light counterpart.

It should be clear from the discussion above that *all* substances will be stabilized by heavy isotope substitution, and thus prefer to form bonds with the heavy isotope. The key issue for partitioning of isotopes *between* substances is the preference of one substance over another for the heavy isotope. This is determined by the degree to which a molecule's vibrational energy is lowered by heavy isotope substitution. At low temperatures, where all molecules are in their ground state, the magnitude of energy lowering is, to a good approximation, given by:

$$\Delta ZPE = ZPE - ZPE^* = 1/2\ h(\nu - \nu^*) = 1/2\ h\Delta\nu \tag{5}$$

In a competition for the heavy isotope, the substance with the larger ΔZPE (Fig. 1b) is more stabilized by the isotopic substitution, and therefore takes the lion's share of the heavy isotope. It should be noted that with increasing temperature, a progressively larger fraction of molecules are excited to higher energy levels ($n > 0$). In those cases, ΔZPE remains an important factor, but not the only factor in determining isotope fractionation behavior.

Earlier in this section, we stated that strong bonds tend to have higher vibrational frequencies than weak bonds. By rearranging terms in equation (4), it can be shown that, other things being equal, bonds with high vibrational frequency undergo larger frequency shifts (Δν) on isotope substitution than bonds with low vibrational frequency.

$$\Delta\nu = \nu - \nu^* = \nu\left(1 - \sqrt{\frac{\mu}{\mu^*}}\right) \tag{6}$$

From Equation (5), it follows that large frequency shifts lead to large ΔZPE, and consequently an affinity for the heavy isotope. The important generalization that stems from Equations (5) and (6) is that the heavy isotope favors substances with strong bonds. An example of this correlation between bond strength and heavy isotope partitioning is the sequence of ^{18}O enrichment observed in coexisting silicate minerals. Taylor and Epstein (1962) noted that minerals with abundant Si-O bonds are enriched in the heavy isotope of oxygen (^{18}O) relative to minerals with fewer Si-O bonds. This correlation reflects the high strength and therefore high vibrational frequency of Si-O bonds relative to other cation-oxygen bonds in silicates, and the effect of these parameters on ΔZPE.

The discussion above is based on the harmonic oscillator approximation, which is the simplest model for representing the energetics of a molecule. In this model, the potential energy curve is symmetrical and the energy levels are equally spaced. More

realistic models, such as that of Morse (1929), have asymmetric potential energy curves, non-uniformly spaced energy levels, and numerically different values of ZPE than given in the harmonic model. Despite these differences, the general principles outlined in this section also apply to the more complex models.

CALCULATING FRACTIONATION FACTORS

Theory

The detailed calculation of isotopic fractionation factors follows the approach of Urey (1947) and Bigeleisen and Mayer (1947), and the reader is referred to those papers for further explanation of the equations given below. A summary of the nomenclature used in these equations is given in Appendix 1. The equations were originally derived for ideal gases, and require additional approximations if applied to liquids or solids. The calculation of fractionation factors involves the partition function, Q, a statistical mechanical parameter that describes all possible energy states of a substance. The equilibrium constant for an isotope exchange reaction can be expressed as a ratio of the partition functions of the two sides of the reaction. For example, consider a generalized isotope exchange reaction between substances A and B:

$$aA + bB^* = aA^* + bB$$

where a and b represent stoichiometric coefficients, and the asterisk, here and in all subsequent references, denotes the substance made with the heavy isotope. The equilibrium constant, $K_{A\text{-}B}$, for this reaction can be expressed as:

$$K_{A\text{-}B} = \frac{(Q^*)^a_A (Q)^b_B}{(Q)^a_A (Q^*)^b_B} = \frac{(Q^*/Q)^a_A}{(Q^*/Q)^b_B} \tag{7}$$

To a good approximation, the total partition function (Q) for each species in the reaction is the product of the translational (tr), rotational (rot), and vibrational (vib) partition functions:

$$Q = Q_{tr} \times Q_{rot} \times Q_{vib} \tag{8}$$

Taking these partition functions individually, the translational partition function is given by:

$$Q_{tr} = \frac{(2\pi M k_b T)^{3/2}}{h^3} V$$

where M is the molecular weight, k_b is Boltzmann's constant and V is the volume of the system. Fortunately, the partition function of each species in the reaction need not be evaluated in the calculation of the equilibrium constant, only the ratio of partition functions of a species and its isotopically substituted derivative (e.g. $[Q^*]_A/[Q]_A$). Because all ideal gases occupy the same volume at a given pressure and temperature, all terms except molecular weight cancel in the ratio of translational partition functions:

$$(Q^*/Q)_{tr} = \left(\frac{M^*}{M}\right)^{3/2}$$

Similarly, most terms cancel in the calculation of the ratio of rotational partition functions. For diatomic molecules and linear polyatomic molecules, this ratio is given by:

$$(Q^*/Q)_{rot} = \frac{\sigma I^*}{\sigma^* I}$$

where I is the moment of inertia and σ is the symmetry number, which is the number of equivalent ways of orienting a molecule in space. For example, σ = 1 for heteronuclear diatomic molecules (e.g. NO or HD), and σ = 2 for homonuclear diatomic molecules (e.g. O_2). The rotational partition function ratio for non-linear polyatomic molecules is:

$$(Q^*/Q)_{rot} = \frac{\sigma}{\sigma^*}\left(\frac{I_A^* I_B^* I_C^*}{I_A I_B I_C}\right)^{1/2}$$

where I_A, I_B, and I_C are the three principal moments of inertia.

In the harmonic oscillator approximation, the vibrational partition function ratio is given by:

$$(Q^*/Q)_{vib} = \prod_i \frac{e^{-U_i^*/2}}{e^{-U_i/2}} \frac{1-e^{-U_i}}{1-e^{-U_i^*}}$$

where $U_i = h\nu_i/k_bT$ and i is a running index of vibrational modes. There is only one vibrational mode for diatomic molecules (i = 1). For linear and non-linear polyatomic molecules consisting of s atoms, there are 3s-5 and 3s-6 vibrational modes, respectively, all of which must be considered in the calculation of Q*/Q.

Combining the contributions of translational, rotational and vibrational partition functions yields:

$$(Q^*/Q) = \left(\frac{M^*}{M}\right)^{3/2} \frac{\sigma I^*}{\sigma^* I} \frac{e^{-U_i^*/2}}{e^{-U_i/2}} \frac{1-e^{-U_i}}{1-e^{-U_i^*}}$$

for diatomic molecules and:

$$(Q^*/Q) = \left(\frac{M^*}{M}\right)^{3/2} \frac{\sigma}{\sigma^*}\left(\frac{I_A^* I_B^* I_C^*}{I_A I_B I_C}\right)^{1/2} \prod_i \frac{e^{-U_i^*/2}}{e^{-U_i/2}} \frac{1-e^{-U_i}}{1-e^{-U_i^*}}$$

for polyatomic molecules. The moments of inertia can be removed from the expressions through use of the Teller-Redlich spectroscopic theorem (Urey 1947). This yields:

$$(Q^*/Q) = \left(\frac{m^*}{m}\right)^{3r/2} \frac{\sigma}{\sigma^*} \prod_i \frac{\nu_i^*}{\nu_i} \frac{e^{-U_i^*/2}}{e^{-U_i/2}} \frac{1-e^{-U_i}}{1-e^{-U_i^*}} \quad (9)$$

where m* and m are the atomic weights of the isotopes being exchanged, and r is the number of atoms of the element being exchanged present in the molecule (e.g. r = 1 for oxygen exchange in CO; r = 2 for oxygen exchange in CO_2). Equation (9) forms the basis for the calculation of fractionation factors for gaseous substances.

Several features of Equation (9) are noteworthy (cf. Richet et al. 1977; Criss 1999). The first three terms on the right hand side of the equation ($[m^*/m]^{3r/2}$, $[\sigma/\sigma^*]$, $[\nu^*/\nu]$) which take into account the effect of translation and rotation on (Q*/Q), are independent of temperature. The fourth term ($e^{-Ui^*/2}/e^{-Ui/2}$) varies with temperature, but is mainly controlled by the ZPE difference of the isotopically heavy and light molecules. The last term ($[1-e^{-Ui}]/[1-e^{-Ui^*}]$) relates to the spacing of energy levels. At low temperatures, where nearly all molecules are in the ground vibrational state, this term is close to unity, and therefore does not contribute appreciably to Q*/Q. The term has a progressively larger effect on Q*/Q as temperature increases. Finally, the mass term ($[m^*/m]^{3r/2}$) in Equation (9) cancels in the calculation of an equilibrium constant ($[Q^*/Q]_A/[Q^*/Q]_B$). That is, the mass term for one molecule (A) taken to the stoichiometrically appropriate

exponent equals that for the other molecule (B) involved in the exchange reaction. Thus, the mass term need not be considered for our purposes. By convention, partition function ratios with the mass term omitted are called reduced partition function ratios, and sometimes referred to by the symbol *f*. *f* is formally defined as:

$$f = \frac{Q^*}{Q}\left(\frac{m}{m^*}\right)^{3r/2} \tag{10}$$

In tabulations of partition function calculations (e.g. Richet et al. 1977), reduced partition ratios are commonly reported as $f^{1/r} = \beta$ values, or 1000 ln β values. In such cases, the fractionation factor between two substances is simply:

$$\alpha_{(A\text{-}B)} = \beta_A/\beta_B \text{ and } 1000 \ln \alpha_{(A\text{-}B)} = 1000 \ln \beta_A - 1000 \ln \beta_B$$

The input data required in calculating fractionation factors are the vibrational frequencies of all chemical species participating in an isotope exchange reaction. In many cases, however, frequencies have only been measured for molecules made with the abundant isotope (e.g. ^{16}O); the frequencies of molecules containing the rare isotope (e.g. ^{18}O) must be calculated. The simplest way to calculate the unknown frequencies is through the harmonic oscillator approximation (Eqn. 4). More rigorous and accurate calculations of frequencies require force-field models, which are available for many common gaseous molecules (e.g. Richet et al. 1977).

An example calculation

As an example, we show the calculation of the $^{18}O/^{16}O$ fractionation factor between CO_2 and CO. Such calculations were computationally laborious in Urey's time but today can readily be done on a spreadsheet. The exchange reaction controlling oxygen isotope fractionation in the CO_2-CO system is:

$$C^{18}O + 1/2\ C^{16}O_2 = C^{16}O + 1/2\ C^{18}O_2$$

with an equilibrium constant given by:

$$K_{CO_2-CO} = \frac{Q^{1/2}_{C^{18}O_2}}{Q^{1/2}_{C^{16}O_2}}\frac{Q_{C^{16}O}}{Q_{C^{18}O}} = \frac{(Q^*/Q)^{1/2}_{CO_2}}{(Q^*/Q)_{CO}} = \alpha_{(CO_2-CO)}$$

For isotope exchange reactions written as above involving only isotopically pure molecules (e.g. pure $C^{16}O$ or $C^{18}O$), the symmetry number of a molecule and its isotopic derivative are identical. Therefore, $\sigma/\sigma^* = 1$, and the term need not be included in the calculations. The vibrational frequencies used in our calculations are the same as those on which Urey's (1947) calculations are based. However, Urey corrected these frequencies for anharmonicity (zero-order frequencies), whereas we used observed (measured) fundamental frequencies with no anharmonicity correction (see discussions in Bottinga 1969a, p. 52; McMillan 1985, p. 15; and Polyakov and Kharlashina 1995, p. 2568). Vibrational frequencies are generally reported in wave numbers (ω), which have units of cm^{-1}. For partition function calculations, wave numbers must be converted to units of sec^{-1} by multiplying by c, the velocity of light ($\nu = c\omega$).

There is one vibrational mode for diatomic molecules such as CO, and four (3s-5) vibrational modes for linear tri-atomic molecules such as CO_2. The four modes of CO_2 correspond to different vibrational motions of the CO_2 molecule, the symmetric stretching vibration (ω_1), the asymmetric stretching vibration (ω_3), and two lower-frequency bending vibrations (ω_2) (Fig. 2). The two bending modes are referred to as degenerate because they have the same vibrational frequency. Therefore, although it is

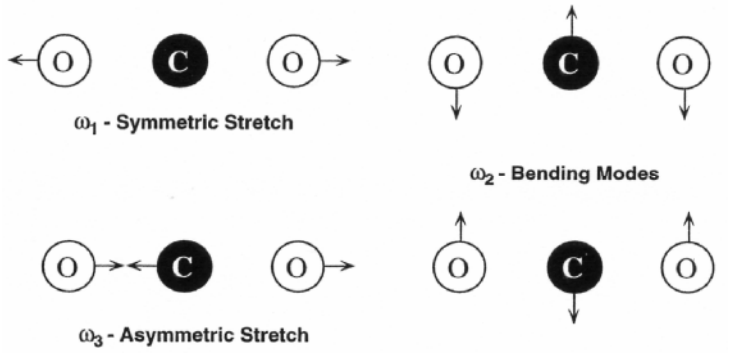

Figure 2. Vibrational modes of the CO_2 molecule, the symmetric stretching vibration (ω_1), the asymmetric stretching vibration (ω_3), and the two bending vibrations (ω_2). Note that ω_1 only involves movement of oxygen atoms, whereas ω_2 and ω_3 involve movement of both oxygen and carbon atoms. This results in a larger ^{18}O frequency shift ($\Delta\nu$) for the ω_1 vibration.

listed only once in Table 1, ω_2 must be counted twice in calculating the partition function ratio of CO_2 using Equation (9). Note also that the magnitude of frequency shifts ($\Delta\nu$) for the isotopically substituted CO_2 molecule varies with vibrational mode (Table 1). The largest shift is associated with the ω_1 vibration, which relates to the fact that this vibrational mode involves only movement of oxygen atoms, whereas the other three modes involve the movement of both oxygen and carbon atoms (Fig. 2). The reduced mass of the $^{12}C^{16}O_2$ molecule undergoing the ω_1, ω_2 and ω_3 vibrations is then given by:

$$\mu_{\omega 1} = \frac{m_o m_o}{m_o + m_o} \qquad \mu_{\omega 2,\omega 3} = \frac{2 m_o m_c}{2 m_o + m_c}$$

(see Polyakov and Kharlashina 1995) where m_o and m_c are the masses of the ^{16}O and ^{12}C atoms, respectively. As a result of these relationships, the change in reduced mass on ^{18}O substitution ($[\mu/\mu^*]^{1/2}$), and therefore the frequency shift, is significantly greater for the ω_1 vibration than for the other vibrational modes.

Table 1 shows the contribution of individual terms to the total and reduced partition function ratios of CO and CO_2. The dominant contributor to the reduced partition function ratios of both molecules is the ZPE term, particularly at low temperatures. Thus, as noted above, isotope partitioning between substances is strongly influenced by the magnitude of ΔZPE (cf. Bigeleisen 1965). The large frequency shift associated with the ω_1 vibration of the CO_2 molecule results in a large ΔZPE, and therefore a tendency for CO_2 to concentrate the heavy isotope at low temperature. At higher temperature, the magnitudes of vibrational frequencies (high ν) play an increasingly important role in isotope partitioning. In the case of the CO_2-CO system, the high vibrational frequency of the CO molecule results in a so-called crossover in fractionations between 0 and 500°C (crossover occurs at 289°C). That is, at T > 289°C, ^{18}O partitions into CO rather than into CO_2. Such crossovers are entirely consistent with equilibrium fractionation of isotopes, and, as noted by Urey (1947), Stern et al. (1968) and Spindel et al. (1970), are not uncommon in gaseous substances.

The calculations above are made on the basis of the harmonic oscillator approximation, and include no explicit corrections for anharmonicity. The effects of anharmonicity can be incorporated by using calculated zero-order frequencies rather than observed fundamental frequencies (see above), and by adding anharmonic corrections to the ZPE and energy level spacing terms of Equation (9) (Urey 1947; Bottinga 1968; Richet et al. 1977). Urey (1947) included anharmonic effects in his calculations of partition function

Table 1. Calculation of $^{18}O/^{16}O$ fractionation factors between CO_2 and CO.

Vibrat. mode	T(°C)	[1]ω (cm^{-1})	[1]ω* (cm^{-1})	[2]$(m^*/m)^{3r/2}$	ν*/ν	$e^{-U^*/2}/e^{-U/2}$	$(1-e^{-U})/(1-e^{-U^*})$	Q*/Q	[4]$f^{1/r}$ = β
CO		**$^{12}C^{16}O$**	**$^{12}C^{18}O$**						
ω_0	0	2140.8	2089.1	1.193728	0.975843	1.145914	1.000004	1.334870	1.118236
ω_0	500	2140.8	2089.1	1.193728	0.975843	1.049296	1.001920	1.224662	1.025914
CO_2		**$^{12}C^{16}O_2$**	**$^{12}C^{18}O_2$**						
ω_1	0	1345.4	1268.3	1.424987	0.942681	1.225194	1.000420		
[3]ω_2 (2)	0	661.7	651.6	1.424987	0.984695	1.027031	1.001735		
ω_3	0	2349.5	2313.5	1.424987	0.984695	1.099334	1.000001		
	0							1.829239	1.133000
ω_1	500	1345.4	1268.3	1.424987	0.942681	1.074391	1.013936		
[3]ω_2 (2)	500	661.7	651.6	1.424987	0.984695	1.009468	1.007904		
ω_3	500	2349.5	2313.5	1.424987	0.984695	1.034025	1.000886		
	500							1.496899	1.024922
					K (0°C) = 1.013203		**1000lnα (0°C) = 13.12 ‰**		
					K (500°C) = 0.999033		**1000lnα (500°C) = -0.97 ‰**		

(1) Observed fundamental vibrational frequencies for CO and CO_2 corresponding to zero-order frequencies (corrected for anharmonicity) given in Urey (1947). The vibrational frequencies of the $C^{18}O$ and $C^{18}O_2$ molecules (ω*) were calculated using Equation (4) (see text).

(2) The term r in the exponent represents the number of atoms of the isotope being exchanged present in the molecule (e.g., r = 1 for CO and 2 for CO_2).

(3) ω_2 for the CO_2 molecule is degenerate. That is, two vibrational modes of the molecule have this frequency.

(4) *f* is the reduced partition function ratio where $f = (Q^*/Q)\,(m/m^*)^{3r/2}$. The equilibrium constants listed above are for the isotope exchange reaction given in the text; $K\,(CO_2\text{-}CO) = \alpha\,(CO_2\text{-}CO) = \{(Q^*/Q)^{0.5}_{CO2}/(Q^*/Q)_{CO}\} = \beta_{CO2}/\beta_{CO}$.

ratios for CO_2 and CO. Because we used the same vibrational frequencies as Urey, his results in the CO_2-CO system can be compared directly with those given in Table 1. For the five temperatures (273-600 K) for which Urey reported fractionation factors, our calculations neglecting anharmonicity are within 0.04 to 0.35‰ of his. Thus, the net effect of anharmonicity on fractionation factors in this system is relatively small, albeit in some cases outside measurement error. In their detailed partition function ratio calculations for gaseous molecules, Richet et al. (1977) showed that the largest anharmonic correction is to the ZPE term but that the magnitude of this correction decreases with increasing with temperature. The anharmonic correction to the energy level spacing term is much smaller but increases with increasing temperature. For most gaseous substances, the net effect of including the anharmonicity terms is to decrease the calculated β value (Urey 1947; Richet et al. 1977). Thus, in the calculation of fractionation factors from β values, the anharmonicity correction for one substance is often partly cancelled by the anharmonicity correction for the other substance in the exchange couple. More detailed discussions of anharmonicity are given in Bottinga (1968), Richet et al. (1977), Gillet et al. (1996) and Polyakov (1998).

Calculation of fractionation factors for gases, liquids and fluids

Following the original compilation by Urey (1947), several studies have calculated fractionation factors involving geologically relevant gaseous molecules. The most sophisticated and widely cited of these studies is that of Richet et al. (1977), who reported oxygen, hydrogen, carbon, sulfur, nitrogen and chlorine isotope fractionation factors for a large number of gaseous species. Their calculations used the latest (at the time) spectroscopic data and theoretical models, and included anharmonicity terms for all the gaseous species considered. In general, their calculated fractionation factors are in good agreement with experimental data.

Although the basic principles still hold, isotopic fractionation theory developed for ideal gases is not directly applicable to liquids. Indeed, it has long been known from experiments that gases fractionate isotopes relative to liquids of the same composition. For example, the equilibrium hydrogen and oxygen isotope fractionation between liquid and gaseous H_2O is 73 and 9.2‰, respectively, at 25°C (Majoube 1971b; Horita and Wesolowski 1994). These large fractionations are the result of two effects in the condensed phase (Bigeleisen 1961; Van Hook 1975). First, translational and rotational energy levels, which for free moving gaseous molecules are well represented by an energy continuum, become quantized in liquids because of interactions among molecules. Thus, whereas there is no isotope fractionation associated solely with translation or rotation in gases, there is such a fractionation in the liquid phase. This effect favors partitioning of the heavy isotope into a liquid relative to a gas of the same composition. The second effect relates to the influence of intermolecular interactions on the vibrational characteristics of individual molecules in the liquid. Thus, vibrational frequencies of substance measured in the gas phase are not identical to those of the same substance in the liquid phase. This second effect may cause isotopic fractionation in the opposite direction to the first (Bigeleisen 1961), and lead to a crossover in liquid-vapor fractionations, as has been documented for D/H fractionations in the $H_2O_{(l)}$-$H_2O_{(v)}$ system.

We are not aware of any direct calculations of partition function ratios for supercritical fluids. However, experimentally determined oxygen and carbon isotope fractionations in the CO_2-calcite system at supercritical conditions are in good agreement with fractionations derived from theoretical calculations (Chacko et al. 1991; Scheele and Hoefs 1992; Rosenbaum 1994). This suggests that supercritical CO_2 is well represented by the ideal gas approximation as the calculations were made on this basis (Rosenbaum

1997). The same conclusion does not appear to hold for H_2O (Bottinga 1968; Clayton et al. 1989; Rosenbaum 1997; Driesner 1997). For example, oxygen partition function ratios for supercritical H_2O derived empirically from mineral-H_2O exchange experiments are distinctly lower than those calculated using the ideal gas approximation (Rosenbaum 1997). As first suggested by Bottinga (1968), this discrepancy may be due to the non-ideality of H_2O under supercritical conditions, and the effect of this non-ideality on the vibrational frequencies of the H_2O molecule. Another possible reason for the discrepancy is the solubility of minerals in water at elevated pressures and temperatures. Thus, partition function ratios of H_2O derived empirically from mineral-H_2O experiments may be different from those of a pure H_2O fluid at comparable P-T conditions (Hu and Clayton, in press).

Calculation of fractionation factors for minerals

Principles. Partition function ratios can also be calculated for minerals, but these calculations are complex and require a number of approximations. The general approach is to treat a mineral as a large molecule consisting of 3s independent oscillators, where s is the number of atoms in the unit cell. For example, quartz, which contains 9 atoms in its unit cell (Si_3O_6), has a total of 27 vibrational modes. Of these, 24 (3s-3) are so-called optical modes because their vibrational frequencies are derived from optical spectroscopic techniques (e.g. IR or Raman spectroscopy). The optical modes are subdivided into internal modes, which concern the vibrational motions of individual functional groups within the mineral (e.g. Si-O in silicates and CO_3 in carbonates), and external modes, which correspond to vibrations of the mineral lattice. The remaining 3 modes are referred to as acoustic modes because they relate to sound velocity. The frequencies of the acoustic modes are typically derived from heat capacity and spectroscopic data using Debye-Einstein models (e.g. Bottinga 1968; Kawabe 1978). Using these data, the partition function ratio for the unit cell in the harmonic approximation is given by (Kieffer 1982):

$$(Q^*/Q) = \prod_{i=1}^{3s} \frac{e^{-U_i^*/2}}{e^{-U_i/2}} \frac{1-e^{-U_i}}{1-e^{-U_i^*}} \tag{11}$$

Equation (11) for minerals is similar to Equation (9) for gases but ignores translational and rotational contributions to the partition function, as such motions are restricted or absent in solids (Bottinga 1968). In detailed calculations, the three acoustic modes are treated separately from the optical modes because each acoustic mode represents a continuous spectrum of vibrations rather than a single vibrational frequency. As such, the acoustic modes are best evaluated by means of Debye functions rather than the Einstein functions typically used to treat the optical modes (see Eqn. 6 in Bottinga (1968) for the mathematical details of dealing with the acoustic modes). The total partition function ratio given by Equation (11) can be converted to a reduced partition function ratio using Equation (10) (Kieffer 1982), but r in the case of minerals is the number of atoms being exchanged in the unit cell (e.g. r = 6 for oxygen exchange in quartz).

The largest uncertainty in the calculation of partition function ratios for minerals is the magnitude of frequency shifts on isotope substitution. Because direct spectroscopic measurements of minerals made with the less abundant isotope are not widely available, these shifts must usually be calculated or estimated in some other way. The detailed approach to calculating frequency shifts employs the methods of lattice dynamics to determine force constants for each vibrational mode, from which the vibrational frequencies for a mineral and its isotopic derivative can be predicted (e.g. Bottinga 1968;

Elcombe and Hulston 1975; Kawabe 1978). Kieffer (1982) took a less detailed approach in calculating oxygen isotope partition function ratios for 11 silicate minerals, calcite and rutile. As input for her calculations, Kieffer used the measured spectra for the ^{16}O forms of minerals, divided the vibrational modes for these minerals into four groups, and then developed a set of rules for estimating the frequency shift associated with each group on ^{18}O substitution. Importantly, she applied the same rules to each mineral considered in her study, which resulted in an internally consistent set of partition function ratios. Most of Kieffer's calculated fractionation factors are in excellent agreement with experimental data (Clayton and Kieffer 1991).

Table 2. Calculation of oxygen isotope partition function ratio for quartz at 25°C.

ω (cm^{-1})	(1)shift factor	(2)g_i	(3)$f(x)^{gi}$	Q*/Q	*f*	1000 lnβ
[a]102	0.96522	1	1.03675	5.3344	1.8435	101.95
[a]122	0.96522	1	1.03705			
[a]164	0.96522	1	1.03786			
128	0.93828	2	1.14019			
205.6	0.93677	1	1.07279	$\ln (Q^*/Q)_{optical} = 1.56455$		
263.1	0.95173	2	1.11772	$\ln (Q^*/Q)_{acoustic} = 0.10963$		
354.3	0.97883	1	1.02662	$\ln (Q^*/Q)_{total} = 1.67418$		
363.5	0.97387	1	1.03332			
393.8	0.9647	1	1.04688			
401.8	0.95744	1	1.05741			
450	0.9426	2	1.17246			
463.6	0.95513	1	1.06491			
509	0.9426	1	1.08850			
697.4	0.98179	2	1.06803			
796.7	0.98795	1	1.02450			
808.6	0.98417	2	1.06652			
1066.1	0.96398	2	1.20647			
1083	0.96602	1	1.09400			
1160.6	0.95614	2	1.28109			
1231.9	0.965	1	1.11031			

(1) Frequency shift factor (ω^*/ω)

(2) g^i is the degeneracy of the i^{th} vibrational mode

(3) $f(x)^{gi} = [(e^{-Ui*/2})/(e^{-Ui/2})][(1-e^{-Ui})/(1-e^{-Ui*})]^{gi}$. Frequencies and frequency shift factors taken from compilation of Polyakov and Kharlashina (1994) except for the shift factors of the three acoustic modes (denoted by the (a) superscript), which were calculated using the high-temperature product rule (see text).

Example calculation for quartz. We show, as an example, the calculation of a partition function ratio for quartz at 25°C (Table 2). The input data are taken from the compilation of frequencies and frequency shifts factors (ω^*/ω) given in Polyakov and Kharlashina (1994), with minor modifications (see below). The shift factors in this compilation are mostly from Sato and McMillan (1987), who directly measured the spectrum of ^{18}O quartz. The degeneracy column in the table gives the number of vibrational modes with a particular frequency, and therefore the number of times that mode must be counted in the calculations. Including degeneracies, there are 27 vibrational modes.

(Q*/Q) was calculated by substituting ω and ω* for each vibrational mode into Equation (11). For the sake of simplicity, all the vibrational modes, including the acoustic modes, were represented by Einstein functions. More rigorous calculations would treat the acoustic modes using Debye functions. Given a value for (Q*/Q), *f* and β values are given by:

$$f = (\mathrm{Q}^*/\mathrm{Q})\left(\frac{\mathrm{m}_{16}}{\mathrm{m}_{18}}\right)^9 \qquad 1000\ \ln\beta = \frac{1}{6}1000\ \ln f$$

When divided into contributions of optical and acoustic modes, the three low frequency acoustic modes contribute only about 6% to the partition function ratio for quartz (Table 2). The percentage is similarly low or lower in most minerals (O'Neil 1986). Thus, imperfect information on the acoustic frequencies typically does not lead to large errors in calculated partition function ratios.

The 1000 ln β value for quartz at 25°C given in Table 2 (101.95) can be compared to values of 102.04 and 104.54 calculated by Kieffer (1982; corrected for a rounding error by Clayton et al. 1989) and Clayton and Kieffer (1991), respectively. The 2.6‰ difference in the results of these calculations is primarily due to differences in the input vibrational frequency data, and illustrates the sensitivity of theoretical calculations to these input data. It should be noted, however, that same input data yield 1000 ln β values of 11.43 (this study), 11.55 (Kieffer 1982), and 11.71 (Clayton and Kieffer 1991) at 1000 K, a range of only 0.3‰. Thus, the absolute magnitude of the discrepancy decreases markedly with increasing temperature, a consequence of the way that uncertainties in the input data propagate with temperature in Equations (9) or (11) (Richet et al. 1977; Clayton and Kieffer 1991; Farquhar 1995).

High-temperature product rule. An important consideration in partition function calculations for minerals is ensuring the proper high-temperature limiting behavior. That is, ln *f* should go to zero as temperature goes to infinity (see below). However, this requirement is not always met in the calculations because of rounding errors and uncertainties in frequency shift factors. The problem can be avoided through use of the high-temperature product rule (Becker 1971; Kieffer 1982; Chacko et al. 1991):

$$\prod_{i=1}^{3s}\left(\frac{\omega}{\omega^*}\right)^{g_i} = \left(\frac{\mathrm{m}^*}{\mathrm{m}}\right)^{3r/2}$$

where g_i is the degeneracy of a vibrational mode. If the product of the frequency shift factors for all vibrational modes does not equal the quantity on the right hand side of the equation, ln *f* will not go to zero at infinite temperature. To correct the problem, one or more of the frequency shift factors must be adjusted so as to satisfy the equation. Typically, it is the shift factors for the lower frequency modes that are modified (O'Neil et al. 1969; Kieffer 1982; Chacko et al. 1991). In Table 2, the shift factors for the acoustic modes of quartz were changed to fulfill the product rule. It should be emphasized that this procedure can be quantitatively important, and affects partition function ratios at both high and low temperature. In the case of the CO_2-calcite system, calculations that utilized the product rule gave results in much better agreement with experimental data than those that did not (Chacko et al. 1991).

Other theoretical methods. In addition to the procedure described above, three other theoretical methods have been developed for calculating fractionation factors involving minerals. The first is based on computer simulation of crystal structures and first principles prediction of their thermodynamic properties (Patel et al. 1991; Dove et al.

1994). Reduced partition function ratios for calcite and a number of silicate minerals calculated using this approach are within 13% of those calculated by traditional methods. Fractionation factors (at 1000 K) derived from these calculations are within 1‰ and, in many cases, within 0.5‰ of those given by experiments. These early results suggest that the *ab initio* approach to calculating fractionation factors is promising, and should be pursued. At present, however, the approach may not be sufficiently accurate to provide quantitatively reliable fractionation factors. The second of the alternative methods, which is based on thermodynamic perturbation theory, can be applied to single element substances such as graphite or diamond (Polyakov and Kharlashina 1995). The method uses only heat capacity data for the minerals of interest as input. Application of this method to the diamond-graphite and calcite-graphite systems yielded results in good agreement with more standard theoretical calculations (Bottinga 1969b), and natural sample data (Valley and O'Neil 1981; Kitchen and Valley 1995), respectively. The third method is also based on thermodynamic perturbation theory but uses Mössbauer data as input (Polyakov 1997; Polyakov and Mineev 2000). The method can be applied to two-element compounds if one of the elements (e.g. Fe) has a Mössbauer-sensitive isotope. Polyakov and Mineev (2000) used this approach to calculate iron, sulfur, and oxygen isotope reduced partition function ratios for a number of minerals. Iron isotope fractionations derived with this approach are in agreement with fractionations calculated using more traditional theoretical methods and vibrational spectroscopic data (Schauble et al. 2001).

VARIABLES INFLUENCING THE MAGNITUDE OF FRACTIONATION FACTORS

Temperature

Temperature is in many cases the single most important variable in controlling isotope fractionation behavior. Bigeleisen and Mayer (1947), Urey (1947), Stern et al. (1968), Bottinga and Javoy (1973), and Criss (1991) evaluated the temperature-dependence of fractionation factors from a theoretical perspective. The following is based largely on the lucid explanation provided in Criss' (1991) paper. Written in logarithmic form, the reduced partition function ratio of a diatomic gas (see Eqn. 9) is given by:

$$\ln f = \ln\left[\frac{\sigma}{\sigma^*}\frac{\nu^*}{\nu}\right] + \left[\frac{U - U^*}{2}\right] + \ln\left[\frac{1 - e^{-U}}{1 - e^{-U^*}}\right] \tag{12}$$

As noted previously, the quantity $[(1–e^{-U})/(1–e^{-U^*})]$ is approximately unity at low temperature. Thus, at low temperature, Equation (12) reduces to:

$$\ln f \cong \ln\left[\frac{\sigma}{\sigma^*}\frac{\nu^*}{\nu}\right] + \left[\frac{U - U^*}{2}\right] \tag{13}$$

Because $U = h\nu/k_bT$, this equation is of the form y = constant + slope (T^{-1}), with a slope given by $\Delta ZPE/k_b$. The equation indicates that reduced partition function ratios, and in turn fractionation factors ($\ln \alpha$), vary linearly with respect to T^{-1} at low temperature. The same relationship applies to polyatomic molecules but in that case both terms in Equation (13) are summations over all vibrational modes of the molecule.

At high temperature, the last term on the right-hand side of Equation (12) is significantly greater than zero and must be considered in the calculation. Criss (1991) expanded this term in a Taylor series, which, after canceling like terms, gives the following equation for diatomic molecules:

$$\ln f = \ln\left[\frac{\sigma}{\sigma^*}\right] + \left[\frac{U^2 - U^{*2}}{24}\right] - \left[\frac{U^4 - U^{*4}}{2880}\right] + \left[\frac{U^6 - U^{*6}}{181{,}440}\right] - \left[\frac{U^8 - U^{*8}}{9{,}676{,}800}\right] + \ldots$$

The higher order terms (terms 3 and above on the right hand side) become vanishingly small at high temperature, which results in:

$$\ln f \cong \ln\left[\frac{\sigma}{\sigma^*}\right] + \left[\frac{U^2 - U^{*2}}{24}\right] \quad (14)$$

This equation is of the form y = constant + slope (T^{-2}), and implies that fractionation factors vary linearly with respect to T^{-2} at high temperature. Note also that $\ln f \rightarrow 0$ as $T \rightarrow \infty$ provided that the symmetry numbers of a molecule and its isotopic derivative (σ/σ^*) are the same.

The theoretical considerations discussed above provide insight into the expected temperature-dependence of fractionation factors at low- and high-temperature limits. The exact temperatures at which these limits occur depend on the substance being considered. Bigeleisen and Mayer (1947) showed that the reduced partition function ratios approach the T^{-1} and T^{-2} temperature-dependencies when values of $hc\omega/k_bT$ are >20 and <2, respectively. Therefore, gaseous molecules, which commonly have vibrational frequencies in the range 2000-3000 cm^{-1}, only enter the T^{-1} region at temperatures below -53°C. Minerals, which typically have vibrational frequencies of ~1000 cm^{-1}, enter the T^{-1} region at even lower temperature. The T^{-2} temperature-dependency requires temperatures in excess of 1100 and 600°C for most gases and minerals, respectively.

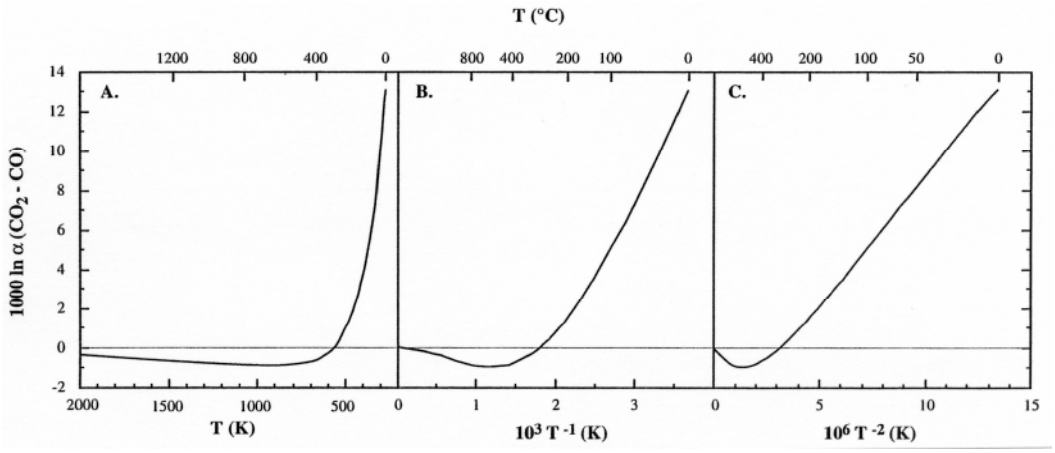

Figure 3. Calculated oxygen isotope fractionation factors between CO_2 and CO plotted as a function of (A) T, (B) 10^3T^{-1}, and (C) 10^6T^{-2}. Note that the variation in the fractionation factor with temperature cannot be represented by any one simple function of temperature. Calculations follow the procedure outlined in the text.

It should be apparent from the discussion above that geologically relevant temperatures are transitional between the high- and low-temperature limits for many substances. Thus, fractionation factors between substances cannot be represented as a simple function of temperature over a broad temperature range (Clayton 1981). This is illustrated in Figure 3, which shows calculated oxygen isotope fractionations in the CO_2-CO system as a function of T, T^{-1} and T^{-2}. With increasing temperature, the magnitude of the fractionation factor in this system first decreases, changes sign and increases, and then finally decreases and approaches zero. None of the plots are linear over the entire

temperature range, although individual segments of each plot are approximately linear. Because of these complexities, equations describing the variation of ln α with temperature take a number of forms. For lower temperature fractionations (T < 100°C), one commonly finds equations of the form ln $\alpha = A(T^{-1}) + B$ or ln $\alpha = A(T) + B$, where A and B are constants. Higher temperature fractionations are generally represented by ln $\alpha = A(T^{-2})$, ln $\alpha = A(T^{-2}) + B$, or ln $\alpha = A(T^{-2}) + B(T^{-1}) + C$. Simple equations such as these are useful in interpolating fractionation data but should not be used to extrapolate fractionations outside the prescribed temperature range. Numerical representation of fractionation curves over a broader temperature range requires more complex equations. For example, Clayton and Kieffer (1991) used third-order polynomial expressions in T^{-2} to represent reduced partition function ratios for minerals between 400 K and infinite temperature (see also Polyakov and Kharlashina 1995; Horita 2001).

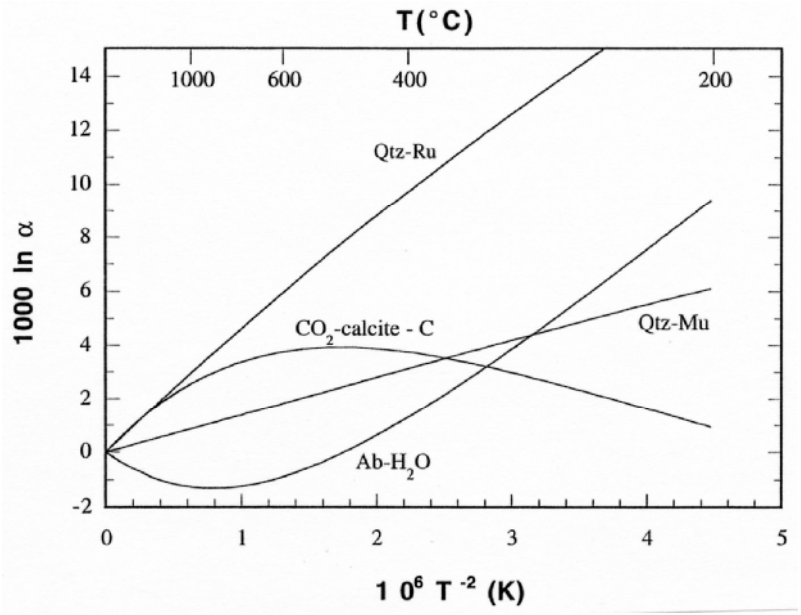

Figure 4. Temperature-dependence of oxygen or carbon isotope fractionation factors in some representative mineral-fluid and mineral-mineral systems as indicated by theoretical calculations. All curves are for oxygen isotope fractionations except for CO_2-calcite, which is for carbon isotope fractionations. Note the relative linearity of mineral-mineral fractionation curves compared to mineral-fluid fractionation curves. Reduced partition function ratios of quartz, rutile, and muscovite taken from Clayton and Kieffer (1991) and Chacko et al. (1996). Calculations for CO_2, calcite and H_2O taken from Chacko et al. (1991) and Richet et al. (1977).

It is instructive to compare the temperature-dependence of fractionation factors in some representative mineral-fluid and mineral-mineral systems (Fig. 4). The exact magnitude of fractionation factors shown on the plot may not be accurate because of uncertainties inherent to the theoretical calculations on which they are based. However, theory does place strict constraints on the temperature-dependence of fractionation factors, and hence the basic shape of fractionation curves (Clayton and Kieffer 1991). The shapes of oxygen isotope fractionation curves in most mineral-H_2O systems are broadly similar to the albite-H_2O system shown on the figure (Bottinga and Javoy 1973; Matthews et al. 1983a). At low temperatures, ^{18}O is concentrated in the mineral whereas, at higher temperatures, it partitions into the H_2O fluid. Analogous to the CO_2-CO example given above, this complex temperature-dependency results from the very high vibrational frequencies (1600-3900 cm^{-1}) but small ^{18}O frequency shifts of the water

molecule relative to those of most minerals (~1000 cm^{-1}). Similarly, large differences in the vibrational characteristics of CO_2 and calcite result in a parabolically shaped fractionation curve for carbon and oxygen (not shown) fractionations in the CO_2-calcite system. Although no calculations are available, experimental data suggest that hydrogen isotope fractionation factors between hydrous minerals and water also have complex temperature-dependencies (e.g. Vennemann and O'Neil 1996). Mineral-mineral systems typically show a simpler temperature-dependency (Fig. 4). At temperatures above 600°C, oxygen isotope fractionations between anhydrous minerals (e.g. quartz-rutile) are approximately linear through the origin when plotted against T^{-2} (e.g. Bottinga and Javoy 1973). The same conclusion appears to hold for fractionations between anhydrous and hydrous minerals (quartz-muscovite), although detailed calculations have only been reported for one hydrous mineral, muscovite (Kieffer 1982; Chacko et al. 1996). At temperatures below 600°C, some mineral-mineral fractionation curves become significantly non-linear. Thus, straight-line extrapolations of these curves to lower temperature can result in the calculation of erroneous fractionation factors, especially at temperatures below 400°C.

Pressure

Oxygen isotope fractionations. Isotopic fractionation is generally thought to be independent of pressure. However, in specific cases, pressure can lead to significant changes in the magnitude of fractionation factors. From classical thermodynamics, the effect of pressure on an equilibrium constant is given by:

$$\left(\frac{\partial \ln K}{\partial P}\right)_T = -\frac{\Delta V_R}{RT}$$

The volume change associated with an isotope exchange reaction is predictably small, but is not zero because of minor differences in the molar volumes of a molecule and its isotopic derivative. These differences arise because of the anharmonicity of vibrations, which results in slightly greater mean bond lengths for the isotopically light molecule (Clayton et al. 1975). Clayton (1981) estimated a volume decrease in calcite on ^{18}O substitution of approximately 0.0025 cm^3 per mole of oxygen. Most of this volume change is cancelled by a similar magnitude change for the other phase participating in the isotope exchange reaction. Therefore, the net pressure effect on oxygen isotope fractionation factors is expected to be small, on the order of 0.003‰ per kbar (at 1000 K) in most cases (Clayton 1981). Clayton et al. (1975) directly investigated this problem through experiments in the calcite-water system at 500°C. Mineral-water systems are particularly conducive to showing pressure effects because the volume change of the water molecule on ^{18}O substitution is expected to be much smaller than that of most minerals. Therefore, ΔV_R for mineral-water reactions should be significantly larger than for many other isotope exchange reactions. Nevertheless, Clayton et al. found no measurable change of fractionation factors in the calcite-water system between 1 and 20 kbar. This result was subsequently corroborated in the quartz-water and albite-water systems (Matsuhisa et al. 1979; Matthews et al. 1983b)

Polyakov and Kharlashina (1994) took a different approach to investigating pressure effects on isotope fractionation. Using the methods of mineral physics, they examined the influence of pressure (or volume) on vibrational frequencies. This is given by:

$$\gamma_i = -\left(\frac{\partial \ln \nu_i}{\partial \ln V}\right)_T$$

where γ_i is the mode Grüneisen parameter of the i^{th} vibrational mode. The magnitude of

this parameter for a given substance can be obtained from molar volume, heat capacity, thermal expansion and compressibility data for that substance. The effect of pressure on β values is then given by:

$$\left(\frac{\partial \beta}{\partial P}\right)_T = -\frac{\gamma T}{B_T}\left(\frac{\partial \beta}{\partial T}\right)_V$$

where B_T is the isothermal bulk modulus of the substance. Using this approach, Polyakov and Kharlashina (1994) calculated changes in the ln β values of a number of minerals associated with a 10 kbar increase in pressure (Fig. 5). They also suggested that their calculated 10-kbar pressure effect could be extrapolated in approximately linear fashion; that is, the effect at 20 kbar should be about twice that at 10 kbar. For oxygen isotopes, the changes in ln β values are very small, except at low temperature. At temperatures of 500°C and above, ln β values of all the minerals investigated shift by less than 0.2‰, and fractionation factors between minerals by less than 0.1‰. Similar to the findings of Clayton et al. (1975), this suggests that pressure effects on oxygen isotope fractionation between minerals will be close to or within analytical uncertainty, except for changes in pressure of greater than 20-30 kbar.

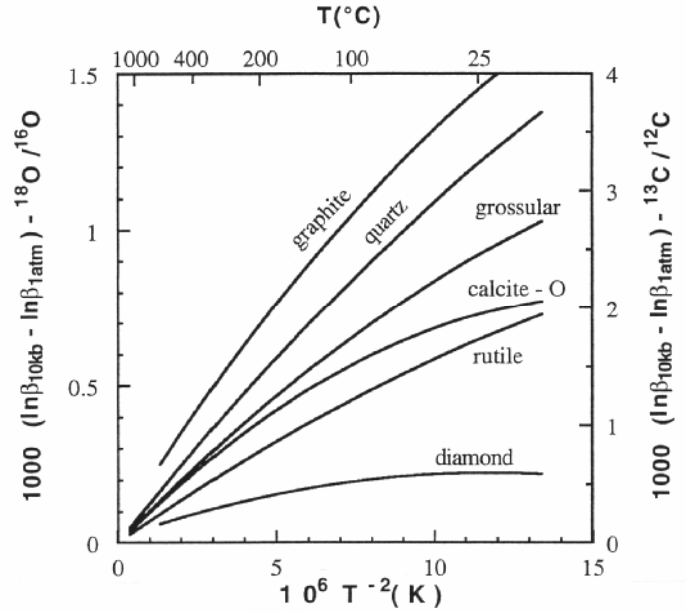

Figure 5. The effect of a 10 kbar pressure increase on the 1000 ln β values of minerals (after Polyakov and Kharlashina 1994). The curves for quartz, grossular, calcite and rutile (oxygen isotope fractionation) are calculated from the equations given in that paper. The curves for graphite and diamond (carbon isotope fractionation) are interpolated from their figure 7. Note that the effect of pressure on oxygen isotope fractionations between minerals is small except at low temperature (T < 300°C) or very high pressure (ΔP > 20 kbar). In contrast, the pressure effect on carbon isotope fractionations involving graphite is significant even at high temperature.

Carbon isotope fractionations. The same conclusion does not hold for carbon isotope fractionation factors involving graphite. Polyakov and Kharlashina (1994) noted that the β values of graphite are much more strongly affected by pressure than those of calcite or diamond (Fig. 5). As a consequence, the pressure effect on carbon isotope fractionations in the diamond-graphite and calcite-graphite systems is significant, even at high temperature. The pressure effect on graphite is, in fact, large enough to induce a

fractionation crossover in the diamond-graphite system, with graphite becoming the ^{13}C-enriched phase at high pressure.

Hydrogen isotope fractionations. Several recent studies indicate that pressure is an important variable in the hydrogen isotope fractionation behavior of hydrous mineral-H_2O systems. Using spectroscopic data on high temperature and pressure H_2O as input, Driesner (1997) calculated large pressure effects on the D/H reduced partition function ratio of water. The effects were largest at the critical temperature of water (374° C), where the calculations predict a 20‰ decrease in the reduced partition function ratio from 0.2 to 2 kbar. Driesner assumed that the effect of pressure on the reduced partition function ratios of hydrous minerals would be much smaller than on those of the water molecule. Therefore, most of the calculated shifts for water should translate to similar magnitude shifts in mineral-H_2O fractionation factors. Horita et al. (1999) tested this hypothesis with experiments in the brucite-water system. At 380° C, they found a 12.4‰ increase in brucite-H_2O fractionations associated with a pressure increase from 0.15 to 8 kbar (Fig. 6). This change in fractionation factor is well outside experimental error and represents the first unequivocal demonstration of a pressure effect on D/H fractionations. Significantly, more than one half of the total change in the fractionation factor occurs from 0.15 to 0.54 kbar, which is the region of P-T space characterized by the proportionately largest increase in the density of water. The direction of the pressure effect documented by Horita et al. (1999) is the same as that indicated by Driesner's (1997) calculations, but its magnitude is markedly smaller. It must be emphasized, however, that pressure effects on brucite-water D/H fractionation are substantial, and in fact larger than temperature effects in this system over the temperature range from 200 to 600° C (Horita et al., in press) (Fig. 7).

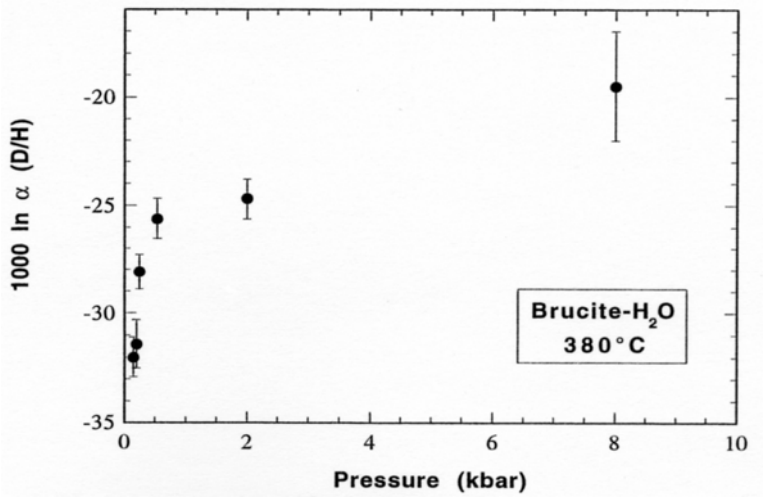

Figure 6. Pressure effect on D/H fractionations in the brucite-H_2O system at 380° C (after Horita et al. 1999). Note that increasing pressure decreases water's affinity for deuterium. The largest change in the fractionation factors occurs below 0.5 kbar, which is the region of P-T space with the proportionately largest increase in the density of water.

Although experimental details are not given, Mineev and Grinenko (1996) also report significant pressure effects on D/H fractionations in the serpentine-H_2O system at 100 and 200° C. They suggest that the large discrepancy between the experimental serpentine-water calibration of Sakai and Tatsumi (1978), and the natural sample calibration of Wenner and Taylor (1973) can be attributed to differences in pressure. Similarly, the differences in tourmaline-H_2O D/H fractionations obtained by Blamart

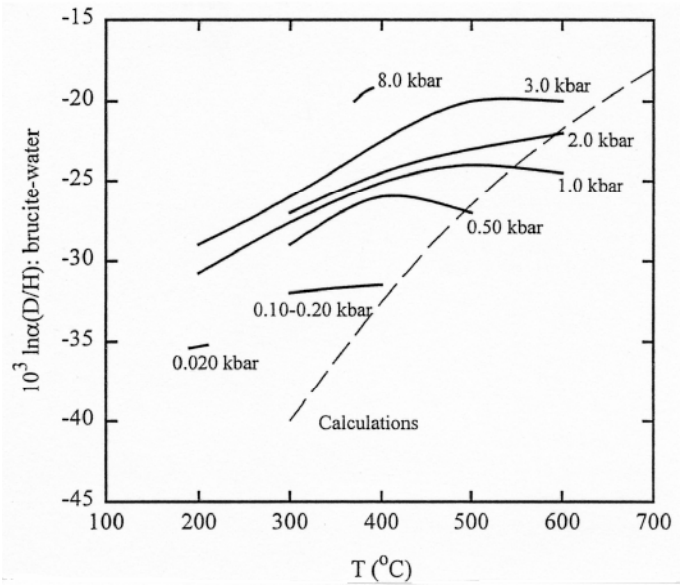

Figure 7. Experimental results of brucite-water D/H fractionation as a function of temperature and pressure. The calculated curve (dashed) is based on theoretical calculations for brucite at 0 kbar (Horita et al., in press), and water (Richet et al. 1977). The calculated curve has large errors (±20‰ at 300°C to ±15‰ at 700°C). The experiments indicate that the effect of pressure on D/H fractionations in this system is larger than the effect of temperature from 200-500°C. Modified after Horita et al. (in press).

et al. (1989) and Jibao and Yaqian (1997) can in part be attributed to differences in experimental pressures. In all the cases investigated thus far, the effect of increasing pressure is to decrease the water molecule's affinity of deuterium. Although the direction of the pressure effect seems well established from both theory and experiment, the magnitude of the effect and the relative contributions of mineral and water to that effect need to be evaluated with additional experiments and calculations.

Mineral composition

Even if isotope fractionation factors are well determined for the compositional end-member of a particular mineral, application of these data to the full range of geological samples commonly requires additional information on how compositional variation in that mineral or mineral group affects fractionation behavior. Compositional effects on fractionation factors have been investigated in a number of different ways including theoretical calculations, experiments, natural sample data, and bond-strength methods. We defer our discussion of bond-strength methods to a later section but see Zheng (1999b) for an application of this methodology to the assessment of fractionations in carbonate and sulfate minerals.

Compositional effects in carbonates. The classic experimental study of O'Neil et al. (1969), which was later refined by Kim and O'Neil (1997), systematically investigated the effect of cation substitution on the oxygen isotope fractionation behavior of carbonate minerals. Figure 8 shows experimentally determined carbonate-H_2O fractionation factors at 240°C plotted against the radius and mass of the divalent cation. Although there is an overall negative correlation between the fractionation factor and both of these variables, the correlation with mass is considerably better. This suggests that cation mass rather than radius is the major variable controlling fractionations between carbonates (O'Neil et

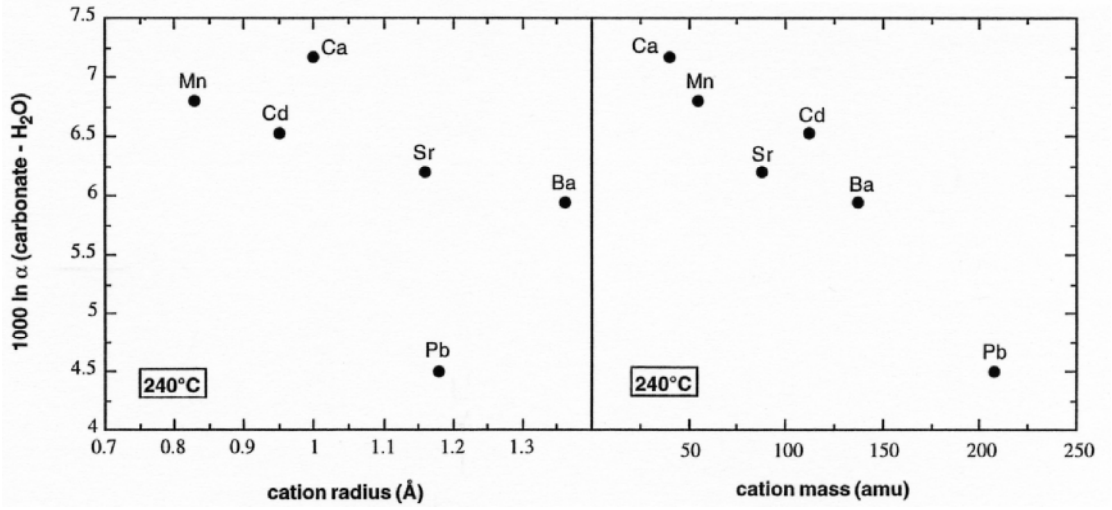

Figure 8. The effect of cation substitution on carbonate-H_2O fractionation factors at 240°C (O'Neil et al. 1969; Kim and O'Neil 1997). Note that the change in fractionation factor with cation substitution correlates with both cation radius and cation mass; however, the correlation with mass is considerably better suggesting that cation mass is dominant variable.

al. 1969; Kim and O'Neil 1997). Golyshev et al. (1981) reached the opposite conclusion on the basis of lattice dynamical calculations for a large number of carbonate minerals. It should be noted, however, that Golyshev et al.'s calculated ln β values are at least as well correlated with cation mass as with cation radius. Both O'Neil et al. and Golyshev et al. pointed out that cation radius mainly affects the internal frequencies of the CO_3 ion, whereas cation mass affects the lattice vibrations (acoustic and external optical frequencies). Notably, the frequencies of the lattice vibrations are much more strongly modified by cation substitution than are the internal frequencies.

Compositional effects in silicates. Compositional effects are also important in the oxygen isotope fractionation behavior of silicate minerals. The effects are complex, however, because of the large number of substitution mechanisms that operate in these minerals. Table 3 summarizes some of the major substitutions and their estimated effects on isotope fractionation (cf. Kohn and Valley 1998a). Of the common substitution schemes, the plagioclase substitution has the largest isotopic effect. Experimental data (O'Neil and Taylor 1967; Matsuhisa et al. 1979; Clayton et al. 1989) and theoretical calculations (Kieffer 1982) indicate a 1.05 to 1.2‰ fractionation between albite and anorthite at 1000 K. This fractionation reflects the higher Si to Al ratio of albite, and the affinity of the Si-O bond relative to the Al-O bond for ^{18}O (Taylor and Epstein 1962). In contrast to plagioclase, K ↔ Na substitution in the alkali feldspars, which does not affect the Si to Al ratio, has no measurable isotopic effect (Schwarcz 1966; O'Neil and Taylor 1967).

Like the plagioclase substitution, the jadeite ($NaAlSi_2O_6$)-diopside ($CaMgSi_2O_6$) substitution also involves Al, but Al in this case substitutes into an octahedral rather than a tetrahedral site. As demonstrated by a comparison of experimental data in the diopside-H_2O and jadeite-H_2O systems (Matthews et al. 1983a), the isotopic effect of this substitution is an enrichment in ^{18}O (Δ(jd-di) = 0.99‰ at 1000 K). Another substitution involving Al, the Tschermak substitution ($[Al^{oct}Al^{tet}] \leftrightarrow [M^{2+}Si]$), can be significant in pyroxenes, amphiboles and micas. Unfortunately, there are no data with which to evaluate its isotopic effect directly. A crude estimate can be obtained by combining the measured isotopic effects of the plagioclase and jadeite substitutions. The large ^{18}O depletion associated with replacement of Si by Al in the tetrahedral site (plagioclase) should be mostly cancelled by ^{18}O enrichment associated with replacement of a divalent

Table 3. Effect of compositional substitutions on oxygen isotope fractionation in silicates.

Substitution	Example	Experimental	Theoretical	Natural
NaSi↔CaAl	plagioclase	[1]1.05, [2]1.07, [3]1.09	[4]1.2	----
NaAl↔Ca(Mg,Fe)	jadeite-diopside	[5]0.99	----	----
K↔Na	alkali feldspar	[2]0	----	[6]0
Fe↔Mg	pyroxene, garnet	[5]0.08	[7]0	----
Mn↔Ca	garnet	[8]0	----	----
(Fe,Mg)↔Ca	pyroxene	[9,10]0.49	[4]0.4	[11]0.55-0.75
(Fe,Mg)↔Ca	garnet	----	[4]0.18, [7]0.12	[11]0.5
Al^{3+}↔Fe^{3+}	garnet	[12]1.3	[4]0.5, [7]0.45	[11]0.7
F↔OH	phlogopite	[13]0.52	----	----

Notes: Substitution schemes are written such that the left-hand side has the greater affinity for ^{18}O. Experimental, theoretical and natural (sample) refer to the methodology used to evaluate the magnitude of the fractionation factor. All fractionations are reported at 1000 K and refer to the isotopic fractionation between end-members. For example, the numbers listed for the plagioclase substitution represent the fractionation between end-member albite and anorthite at 1000 K.

Sources of data: 1 = Clayton et al. (1989); 2 = O'Neil and Taylor, (1967); 3 = Matsuhisa et al. (1979); 4 = Kieffer (1982); 5 = Matthews et al. (1983a); 6 = Schwarcz (1966); 7 = Rosenbaum and Mattey (1995); 8 = Lichtenstein and Hoernes (1992); 9 = Chiba et al. (1989); 10 = Rosenbaum et al. (1994); 11 = Kohn and Valley (1998b); 12 = Taylor (1976); 13 = Chacko et al. (1996).

cation by Al in the octahedral site (jadeite). Therefore, the net effect of Tschermak substitution is a relatively small depletion in ^{18}O. Following the approach of Kohn and Valley (1998a), we estimate the magnitude of that depletion at 1000 K to be ~0.1‰ for amphiboles, ~0.2‰ for micas, and ~0.4‰ for pyroxenes per mole of Al substitution in the tetrahedral site.

Fe^{2+}-Mg^{2+} substitutions are common in many silicate minerals. Experimental data on calcic clinopyroxenes ($Ca[Fe,Mg]Si_2O_6$) at 700° C indicate no significant difference in mineral-H_2O fractionation factors between Fe and Mg end-members (Matthews et al. 1983a). Similarly, calculated reduced partition function ratios of pyrope ($Mg_3Al_2Si_3O_{12}$) and almandine ($Fe_3Al_2Si_3O_{12}$) garnet are identical (Rosenbaum and Mattey 1995). Collectively, these observations suggest that the isotopic effect of Fe-Mg substitution in silicates is negligible, at least at high temperature. The same may be true for Ca-Mn substitutions as mineral-H_2O experiments with grossular ($Ca_3Al_2Si_3O_{12}$) and spessartine ($Mn_3Al_2Si_3O_{12}$) garnets gave identical fractionations at 750° C (Lichtenstein and Hoernes 1992). In contrast to Ca-Mn, there does appear to be a small but significant isotopic effect associated with Ca-Mg and Ca-Fe^{2+} substitutions. Theoretical calculations (Kieffer 1982), and data from experiments (Chiba et al. 1989; Rosenbaum et al. 1994) and natural samples (Kohn and Valley 1998b) indicate fractionations of 0.4, 0.5 and 0.55-0.75‰ respectively, between orthopyroxene ($[Fe,Mg]_2Si_2O_6$) and calcic clinopyroxene at 1000 K. Similarly, calculations and natural sample data suggest a 0.1 to 0.5‰ fractionation between pyrope-almandine and grossular garnet at 1000 K (Kieffer 1982; Rosenbaum and Mattey 1995; Kohn and Valley 1998b).

There is also a significant isotopic effect associated with the Fe^{3+}-Al^{3+} substitution mechanism. Taylor (1976) reported a 1.7‰ fractionation between grossular and andradite ($Ca_3Fe^{3+}{}_2Si_3O_{12}$) garnet in hydrothermal experiments at 600° C, which translates to a 1.3‰ fractionation at 1000 K. Theoretical calculations (Kieffer 1982; Rosenbaum and Mattey 1995), and natural sample data (Kohn and Valley 1998b) indicate smaller

fractionation of 0.5 to 0.8‰ at that temperature.

The generalizations that stem from the above observations are similar to the ones made long ago by Taylor and Epstein (1962). Namely, the dominant compositional variable affecting oxygen isotope fractionations between silicates is the identity of the tetrahedral cation. With the exception of Al, the octahedral and cubic (8-fold) cations are of secondary importance, although, as shown in Table 3, not insignificant in all cases. Monovalent cations have little effect on oxygen isotope fractionations.

There is good overall agreement between theory, experiment and natural sample data as regards the direction, and, in some cases, the magnitude of isotopic effects associated with compositional substitutions in silicates. This agreement is encouraging because it suggests that fractionation factors for silicate solid solutions can be predicted by combining fractionation data for end-members with the estimated isotopic effects of the various substitution mechanisms. The reader is referred to the paper of Kohn and Valley (1998a) for an elegant methodology for making such calculations.

Compositional effects on hydrogen isotope fractionation. As was the case with oxygen, hydrogen isotope fractionation factors are also influenced by mineral composition. The exact nature of the compositional dependence, however, remains unclear. From the results of their pioneering exchange experiments between micas, amphiboles and water, Suzuoki and Epstein (1976) concluded that the identity of the octahedral cation is the key compositional variable in the hydrogen isotope fractionation behavior of hydrous minerals. This observation can be rationalized by noting that the hydroxyl unit is more closely associated with the octahedral cations than with other cations in these mineral structures. Of the common octahedral cations, Al has the greatest affinity for deuterium, followed closely by Mg. Fe, on the other hand, has a strong affinity for hydrogen over deuterium. Suzuoki and Epstein (1976) suggested that these compositional effects are systematic and might be used to predict fractionation factors regardless of mineral species. Their proposed equation, which is applicable from 400 to 850° C, is:

$$1000 \ln \alpha (\text{mineral-}H_2O) = -22.4 (10^6 T^{-2}) + 28.2 + (2 X_{Al} - 4 X_{Mg} - 68 X_{Fe})$$

where X_{Al}, X_{Mg} and X_{Fe} are the mole fractions of each cation in the octahedral site. This equation correctly predicts the magnitude (but not the temperature-dependence) of brucite-H_2O fractionation factor (Satake and Matsuo 1984; Horita et al. 1999) to within 10‰ at 400 and 500° C. It is also supported in a general way by natural sample data, which suggest a negative correlation between the δD values of minerals and their Fe/Mg ratio (e.g. Marumo et al. 1980). There are, however, a number of complicating factors. Minerals such as boehmite, epidote and chlorite, which show a significant degree of hydrogen bonding (i.e. hydrogen exists as O-H--O units rather than O-H units), partition deuterium less strongly than predicted by the equation (Suzuoki and Epstein 1976; Graham et al. 1980, 1987). Additionally, a detailed study of hydrogen isotope fractionations between amphiboles and water does not show the compositional dependence indicated by Suzuoki and Epstein's equation, and suggests that the A-site cation in amphiboles may also play a role in hydrogen isotope partitioning (Graham et al. 1984). The issue of compositional effects on D/H fractionations remains largely unresolved and awaits further experimental studies.

Solution composition

The presence of dissolved species in the fluid phase can impact fractionation factors to a comparable or larger degree than the largest mineral composition effects. This effect applies specifically to fractionations between an aqueous fluid, and some other mineral,

gas or fluid phase. The seminal work on the isotopic solution effect, or ‘salt effect’ as it is commonly known, was done by H. Taube in the 1950s. This and subsequent work clearly demonstrated that the effects of many dissolved salts of geochemical interest on isotopic fractionation are non-trivial at or near room temperature (Taube 1954; Sofer and Gat 1972 1975; Stewart and Friedman 1975; Bopp et al. 1977; O'Neil and Truesdell 1991; Kakiuchi 1994). However, there was little information on the salt effect at elevated temperatures, and the available data were controversial with respect to the temperature and concentration-dependency of the effect (e.g. Truesdell 1974). In an attempt to resolve the controversy, several investigators carried out studies of oxygen and hydrogen isotope salt effects at elevated temperature, using a variety of experimental techniques (Matsuhisa et al. 1979, quartz- and albite-water at 600 and 700°C; Graham and Sheppard 1980, epidote-water 250-550°C; Kendall et al. 1983, calcite-water at 275°C; Kazahaya 1986, liquid-vapor to 345°C; Zhang et al. 1989, quartz-water at 180-550°C; Zhang et al. 1994, cassiterite- and wolframite-water at 200-420°C; Poulson and Schoonen 1994, dissolved HCO_3-water at 100-300°C; Driesner 1996, Driesner and Seward 2000, liquid-vapor at 50-413°C and calcite-water at 350-500°C; Kakiuchi 2000, liquid-H_2O vapor). Some of these studies described a complex dependence of the isotope effects on temperature and solution composition with large uncertainties (Graham and Sheppard 1980; Kazahaya 1986; and Poulson and Schoonen 1994). Other studies observed little or no effect of dissolved salts on oxygen isotope fractionation in mineral-water systems (Matsuhisa et al. 1979; Kendall et al. 1983; Zhang et al. 1989, 1994). In perhaps the most comprehensive set of studies, Horita et al. (1993a,b; 1994, 1995a,b; 1996, 1997) investigated the effect of a number of dissolved salts, particularly NaCl, on isotopic partitioning from room temperature to 500° C.

Terminology. The magnitude of the salt effect is conventionally represented by:

$$\Gamma = \frac{\alpha_{\text{A-aqueous soln}}}{\alpha_{\text{A-pure water}}} \tag{15}$$

where A is a reference phase with which both pure water and the salt-bearing solution are exchanged in separate experiments. Water vapor is commonly used as the reference phase at lower temperatures, whereas minerals are used at higher temperature. Although Γ is formally defined as an activity-composition ratio (see Horita et al. 1993a for details), in practice, it is a measure of how much the fractionation factor between phase A and an aqueous fluid changes as material is dissolved into the fluid.

Single salt solutions. Horita et al. (1993a,b; 1995a) determined values of Γ in single salt solutions (NaCl, KCl, $MgCl_2$, $CaCl_2$, Na_2SO_4, $MgSO_4$) by means of the $H_2O_{(v)}$-$H_2O_{(l)}$ equilibration method at temperatures from 50 to 350° C. Figure 9 shows representative results from the 100° C experiments.For hydrogen isotopes, Γ_H is greater than one for all of the salt solutions studied, and increases with salt concentration. Magnitudes of the effects are in the order $CaCl_2 \geq MgCl_2 > MgSO_4 > KCl \approx NaCl > Na_2SO_4$ at the same molality. Γ_O, on the other hand, is slightly less than or very close to 1, except for KCl solutions at 50°C. The measured salt effect trends for both hydrogen and oxygen are linear with the molalities of the salt solutions, and either decrease with temperature, or are nearly constant over the temperature range 50-100°C. Salt solutions of divalent cations (Ca and Mg) exhibit much larger oxygen isotope effects than those of monovalent cations (Na and K). Magnitudes of the oxygen isotope effects in NaCl solutions, and of hydrogen isotope effects in Na_2SO_4 and $MgSO_4$, increase slightly from 50 to 100° C. The systematic changes ofΓ with temperature and molality permit fitting of data for each salt to simple equations. A summary of these equations is given in Table 4. These data indicate that the identity of the cation largely controls oxygen isotope salt

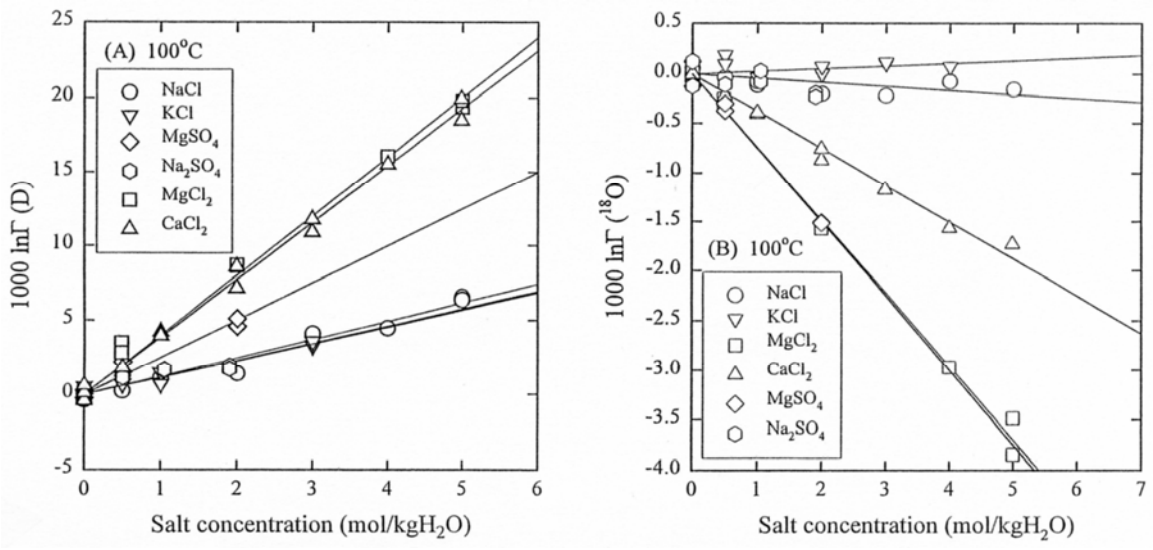

Figure 9. Experimental determined isotope salt effects (103 lnΓ) reported by Horita et al. (1993a) for (A) D/H and (B) $^{18}O/^{16}O$ fractionation at 100° C plotted against molality of the salt solution. The data were obtained by measuring the isotopic composition of water vapor over pure water and over salt solutions of the same isotopic composition. The solid lines are linear regressions with zero intercept through the data of each salt composition. Note that $MgCl_2$ and $CaCl_2$ have the largest (positive) D/H salt effects whereas $MgCl_2$ and $MgSO_4$ have the largest (negative) $^{18}O/^{16}O$ salt effect.

Table 4. Isotope salt effects determined by vapor-liquid equilibration.

Salt	Isotopes	Function (*m*; molality & T: K)	T Range (°C)
NaCl:	D/H	$10^3\ln\Gamma = m(0.01680T - 13.79 + 3255/T)$	10-350
	$^{18}O/^{16}O$	$10^3\ln\Gamma = m(-0.033 + 8.93\times10^{-7}T^2 - 2.12\times10^{-9}T^3)$	10-350
KCl:	D/H	$10^3\ln\Gamma = m(-5.1 + 2278.4/T)$	20-100
	$^{18}O/^{16}O$	$10^3\ln\Gamma = m(-0.612 + 230.83/T)$	25-100
$MgCl_2$:	D/H	$10^3\ln\Gamma = 4.14m$	50-100
	$^{18}O/^{16}O$	$10^3\ln\Gamma = m(0.841 - 582.73/T)$	25-100
$CaCl_2$:	D/H	$10^3\ln\Gamma = m(0.0412T - 31.38 + 7416.8/T)$	50-200
	$^{18}O/^{16}O$	$10^3\ln\Gamma = m(0.2447 - 211.09/T)$	50-200
Na_2SO_4:	D/H	$10^3\ln\Gamma = 0.86m$	50-100
	$^{18}O/^{16}O$	$10^3\ln\Gamma = -0.143m$	50-100
$MgSO_4$:	D/H	$10^3\ln\Gamma = m(8.45 - 2221.8/T)$	50-100
	$^{18}O/^{16}O$	$10^3\ln\Gamma = m(0.414 - 432.33/T)$	0-100

Regressions are based on data reported by Horita et al. (1993a,b, 1995a).
For the definition of Γ, see Equation (15).

effects in water. This can be rationalized by noting that cations interact strongly with the negatively-charged dipole of water molecules. Sofer and Gat (1972) pointed out that the ionic charge to radius ratio (ionic potential) of cations correlates positively with the measured oxygen isotope salt effects. For the same reason, it is expected that anions control hydrogen isotope salt effects, but their relationship is more complex. For example, there is a positive correlation between the radius of alkali and halogen ions and the magnitude of hydrogen isotope salt effects (Horita et al. 1993a).

Complex salt solutions. Isotope salt effects have also been investigated in complex salt solutions consisting of mixtures of two or more salts in the system Na-K-Mg-Ca-Cl-SO_4-H_2O (Horita et al. 1993b). Some of the mixed salt solutions examined in that study were similar to natural brine compositions, such as from the Salton Sea geothermal system. The measured oxygen and hydrogen isotope salt effects in mixed salt solutions to very high ionic strengths (2-9) agree closely with calculations based on the assumption of a simple additive property of the isotope salt effects of individual salts in the solutions:

$$10^3 \ln \Gamma_{\text{mixed salt soln}} = \Sigma\,(10^3 \ln \Gamma_{\text{single salt soln}}) = \Sigma\,\{m_i(a_i + b_i/T)\}$$

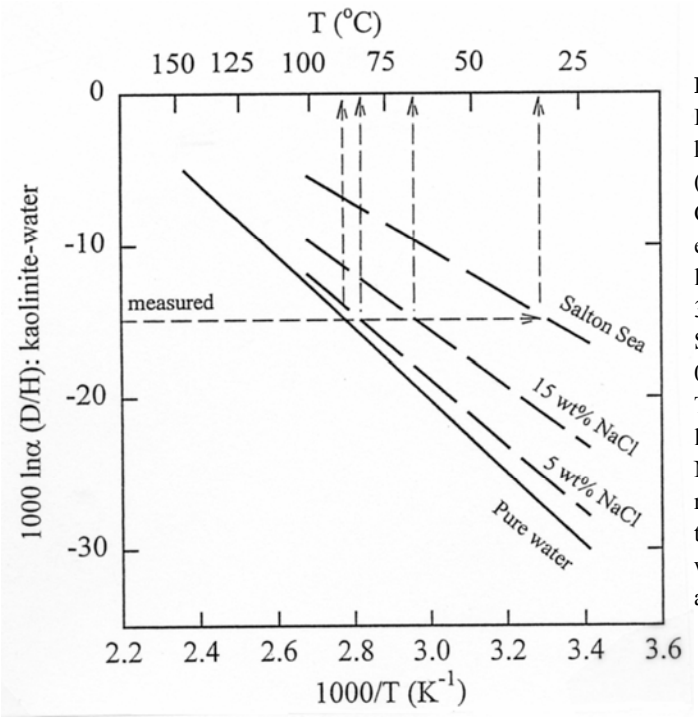

Figure 10. Calculated salt effects on D/H fractionation in the system kaolinite-water from 0 to 150° C (modified after Horita et al. 1993b). Calculations are based on the empirical equations given in Table 4. The dashed lines are the calculated curves for 1 and 3 molal NaCl solutions, and a synthetic Salton Sea brine (3.003 molal NaCl + 0.502 molal KCl + 0.990 molal $CaCl_2$). The kaolinite-pure water curve (solid line) is from Liu and Epstein (1984). Note that neglect of the salt effect could result in large errors in calculated temperatures and/or fluid compositions when mineral-water fractionation data are applied to natural samples

Figure 10 illustrates the effect of salinity and salt composition on the kaolinite-water D/H fractionation factor, calculated assuming that the salt effect on minerals is the same as the salt effect on water vapor coexisting with the brine (Horita et al. 1993b). The effects of 1 and 3 m NaCl solutions and a representative Salton Sea brine composition (Williams and McKibben 1989) are shown as examples. The fractionation factor between kaolinite and pure water is taken from Liu and Epstein (1984). Note that the temperature of formation of a diagenetic phase calculated from the isotopic compositions of coexisting brine and mineral could be incorrect by as much as 80° C, or the calculated hydrogen isotope composition of the brine at a known temperature could be in error by as much as 15‰if the salt effect on isotopic pa rtitioning is ignored. Discrepancies reported in the literature between temperatures obtained from mineral-water isotope geother-mometers, and temperatures derived from bore hole measurements, fluid inclusions, or other chemical geothermometers could result from neglect of isotope salt effects.

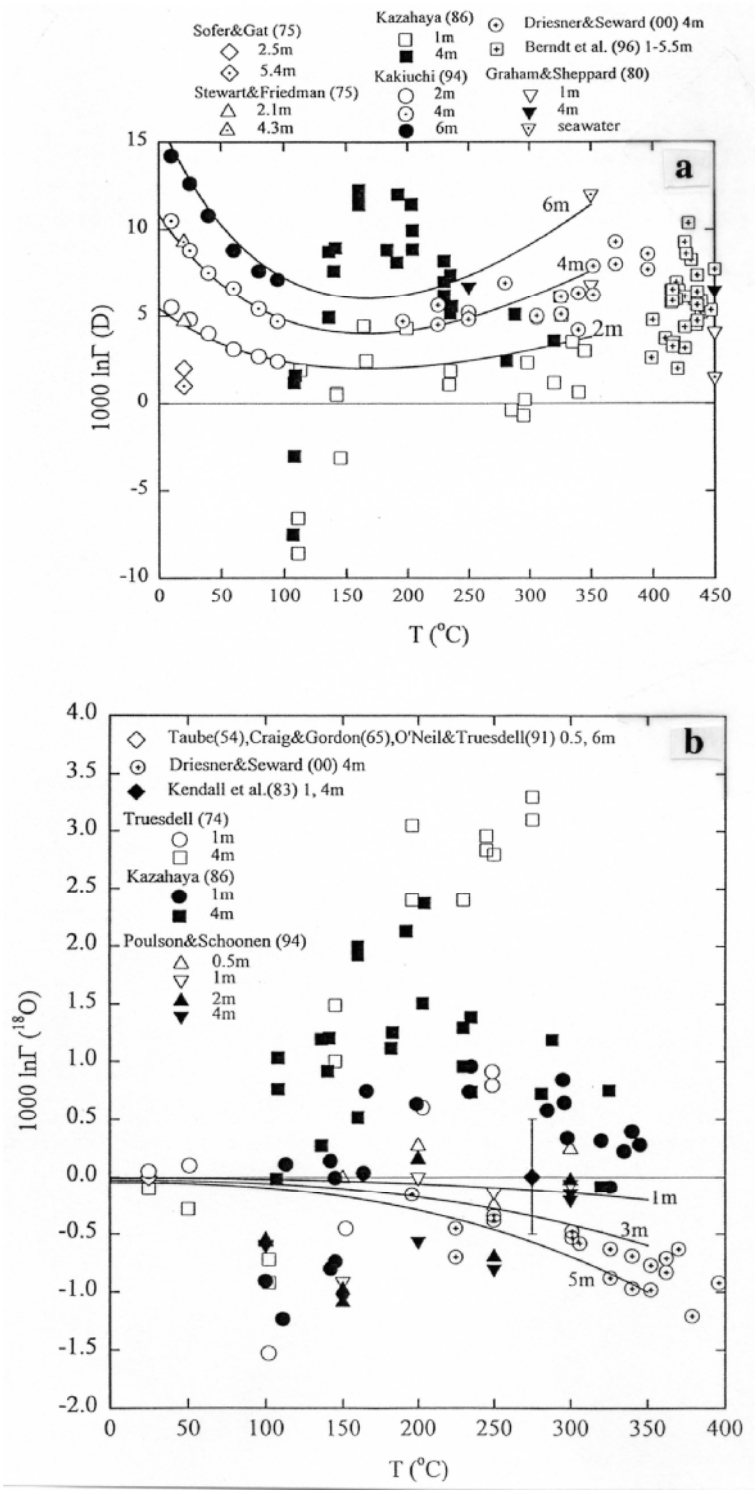

Figure 11. (A) Hydrogen isotope salt effects in NaCl solutions to 450°C. Plotted points represent data obtained from liquid-vapor equilibration, H_2-water equilibration, and mineral-water exchange experiments. (B) Oxygen isotope salt effects in NaCl solutions to 400°C. Plotted points represent data from liquid-vapor equilibration, CO_2-water equilibration, and mineral-water exchange experiments. Solid curves are based on the liquid-vapor equilibration experiments of Horita et al. (1995a).

Salt effect at high temperature. Horita et al. (1995a), Berndt et al. (1996), Shmulovich et al. (1999) and Driesner and Seward (2000) extended the results for liquid-vapor equilibration of NaCl solutions to 600° C.The results from Horita et al. (1995a) to 350° C are shown in Figure 11. The value of $10^3 \ln \Gamma(^{18}O/^{16}O)$ is always negative and its magnitude increases with increasing temperature. In contrast, the magnitude of $10^3 \ln \Gamma(D/H)$ decreases from 10°C to about 150°C, and then increases gradually to 350°C. The fractionation factors for both oxygen and hydrogen isotopes approach zero smoothly at the critical temperature of a given NaCl solution. The systematic nature of these results indicates that the complex temperature and concentration-dependencies of salt effects reported by Truesdell (1974) and Kazahaya (1986) are an experimental artifact.

Another aspect to be considered in liquid-vapor experiments is that the vapor pressure and density of water vapor in equilibrium with pure water compared to that in equilibrium with NaCl solutions are different at a given temperature. With increasing temperature, water vapor becomes more dense and non-ideal, and the formation of water clusters (dimer, trimer, etc.) becomes significant. On the basis of molecular dynamics and *ab initio* calculations, Driesner (1997) suggested that water clusters partition hydrogen isotopes much differently than the water monomer. Thus, the effect of NaCl on liquid-vapor isotope partitioning may reflect not only the isotope salt effect in liquid water, but also changes in the isotopic properties of water vapor. Furthermore, with increasing temperature, the concentration of NaCl in water vapor also increases, possibly causing an isotope salt effect in the vapor phase as well. Therefore, although the liquid-vapor equilibration method can provide the most precise results on the isotope salt effect, application of high-temperature data obtained with this technique may not be straightforward.

In an attempt to document the salt effect on D/H fractionation at elevated temperatures, Horita et al. (unpublished) conducted a study of the system brucite ($Mg[OH]_2$)-H_2O±NaCl±$MgCl_2$ from 200 to 500° C and salt concentrations up to 5 molal. Dissolved NaCl and $MgCl_2$ consistently increased D/H fractionation factors by a small amount at all temperatures studied (Fig. 12). These data can be compared to data obtained on the epidote-water+NaCl system by Graham and Sheppard (1980). The results of the two studies are generally consistent, although the latter show slightly larger D/H effects. In contrast to the results for hydrogen isotopes, recent studies in the system calcite-H_2O-NaCl (Horita et al. 1995a; Hu and Clayton, in press) indicate that the oxygen isotope salt effect is negligible from 300-700° C and 1 to 15 kbar.

Combined effects. Because temperature, pressure and solution composition all affect the physical properties of water, these three variables can act in concert to influence fractionation factors (Horita et al., in press; Hu and Clayton, in press). Increases in pressure and NaCl concentration both work to decrease the fluid's affinity for deuterium. The isotopic effect is most pronounced at low pressures and NaCl concentrations, which relates to the fact that the largest changes in the density of the fluid occurs over this region of pressure-composition space. It appears that the fractionation factor and the density of aqueous NaCl solutions are closely related to each other. With additional systematic experiments, empirical equations can be designed that relate the isotope salt effects and the density of aqueous solutions.

METHODS OF CALIBRATING FRACTIONATION FACTORS

As noted at the beginning of the chapter, the four main methods for calibrating fractionation factors are theoretical calculations, semi-empirical bond-strength models, natural sample data, and laboratory experiments. Theoretical methods have already been

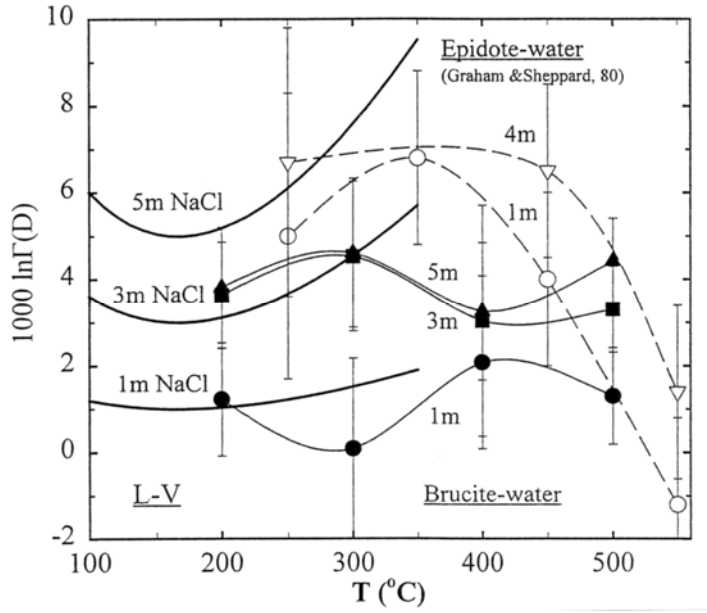

Figure 12. The effect of NaCl on the hydrogen isotope fractionation (10^3 lnΓ) obtained from experiments involving liquid-vapor equilibration (solid bold curves) compared to those obtained from brucite-water (solid curves, Horita et al., in press) and epidote-water (dashed curves, Graham and Sheppard 1980) partial exchange results. Data from Horita et al. (in press); Solid circles = 1 molal NaCl, Solid squares = 3 molal NaCl, Solid triangles = 5 molal NaCl. Data from Graham and Sheppard (1980): Open, inverted triangles = 4 molal NaCl, Open circles = 1 molal NaCl.

discussed at length. Below, we critically summarize key elements of the other three calibration methods.

Semi-empirical bond-strength calibration

This method of calibration has been applied specifically to determining oxygen isotope fractionation factors involving minerals. The method is based on the observation that the sequence of ^{18}O enrichment in minerals is correlated with average cation-oxygen bond strengths in those minerals (Taylor and Epstein 1962; Garlick 1966). As noted previously, statistical mechanical theory predicts such a correlation because bond strength relates to vibrational frequency, and in turn ZPE differences between isotopic species. Bond-strength methods, which include the original methodology of Taylor and Epstein (1962), the site potential method (Smyth and Clayton 1988; Smyth 1989), and the increment method (Schütze 1980; Richter and Hoernes 1988; Hoffbauer et al. 1994; Zheng 1999a and references cited therein), attempt to quantify the relationship between bond strength and isotopic fractionation. All of these methods involve two major steps: (1) formulate an internally consistent measure of bond strength, and (2) link bond strength to fractionation factors.

Taylor and Epstein method. Taylor and Epstein (1962) focussed on three major bond types in silicate minerals, the Si-O-Si bond (e.g. quartz), the Si-O-Al bond (e.g. anorthite) and the Si-O-M^{2+} bond (e.g. olivine). They assigned $\delta^{18}O$ values to each of these bond types on the basis of their isotopic analyses of quartz, anorthite and olivine in igneous rocks, and suggested that the $\delta^{18}O$ values of other silicates could be estimated through linear combination of these three bond types. Quartz-albite and quartz-diopside fractionation factors calculated with this method are in excellent agreement with those

determined experimentally (Clayton et al. 1989; Chiba et al. 1989). Savin and Lee (1988) and Saccocia et al. (1998) applied a modified version of this method to calculating fractionation factors for phyllosilicate minerals.

Site-potential method. Smyth (1989) developed the site potential model for calculating electrostatic site energies associated with various anion sites in minerals. In essence, an anion's site potential is the energy (in electron volts) required to remove that anion from its position in the crystal. Thus, an oxygen site potential provides a convenient monitor of how strongly bound that oxygen atom is within the mineral structure. Given data on individual oxygen sites in a mineral, a mean oxygen site potential for the mineral can be calculated from a weighted average of all of the oxygen sites. Smyth used this approach to calculate mean oxygen site potentials for 165 minerals. Following Smyth and Clayton (1988), Figure 13a plots experimentally determined quartz-mineral fractionation factors versus the difference in mean quartz-mineral site potentials. With the exception of forsterite, anhydrous and hydrous silicate minerals show a good linear correlation on this plot, which suggests that the trend may be useful in predicting fractionation factors for other silicates. Calcite, apatite and oxide minerals, however, fall well off the silicate trend. The poor fit of the oxide minerals can be attributed to neglect of cation mass in the site potential model (Smyth and Clayton 1988). It is well known that cation mass affects vibrational frequencies and frequency shifts on isotopic substitution. Thus, the significantly greater mass of cations in the oxide minerals relative to those in silicates would be expected to cause differences in their isotopic fractionation behavior. The deviation of calcite and apatite from the silicate trend is likely

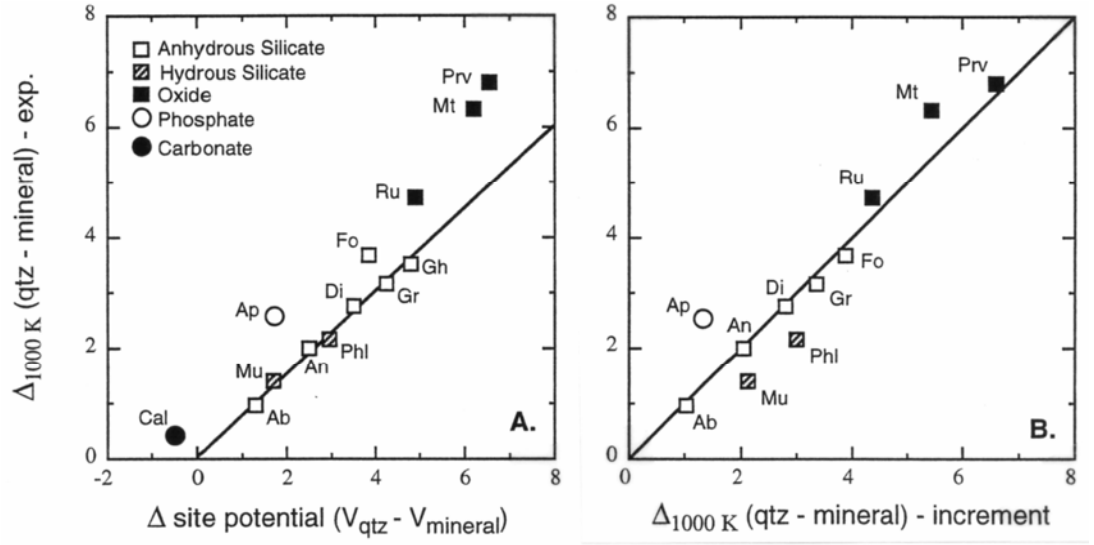

Figure 13. Comparison of quartz-mineral fractionation factors given by bond-strength methods and experiments at 1000 K (modified after Chacko et al. 1996). (A) Comparison with the oxygen site potential model of Smyth (1989) where V_{qtz} and $V_{mineral}$ are the mean oxygen site potentials of quartz and the mineral of interest, respectively. A least-squares regression through the origin fitted to all silicate data points except forsterite yields the equation: Δ_{1000K}(qtz-mineral) = 0.751 ($V_{qtz} - V_{mineral}$). (B) Comparison of experimental data with the increment method calculations of Zheng (1993 1996 1997 1999a). Note that Zheng applied a low-temperature 'correction' factor (D) in his earlier papers (e.g., Zheng 1991 1993). That correction factor was not applied in some later studies (Zheng 1997 1999a). For internal consistency, the correction factor must be applied to all minerals or not at all. Following Zheng (1999a), the correction factor was not included in calculating fractionation factors for the minerals shown on the plot. The line represents 1:1 correspondence. Designations: Ab = albite; An = anorthite; Ap = apatite; Cal = calcite; Di = diopside; Fo = forsterite; Gh = gehlenite; Gr = grossular; Mt = magnetite; Mu = muscovite; Prv = $CaTiO_3$-perovskite; Ru = rutile. Sources of experimental data: Clayton et al. (1989), Chiba et al. (1989), Gautason et al. (1993), Fortier and Lüttge (1995), Rosenbaum and Mattey (1995), and Chacko et al. (1989, 1996).

fractionation behavior. The deviation of calcite and apatite from the silicate trend is likely due to the strongly covalent nature of bonding in carbonate and phosphate functional groups (Smyth and Clayton 1988). The site potential model, on the other hand, assumes that bonding in crystals is fully ionic (Smyth 1989). The site potential method also provides no direct indication of the temperature-dependence of isotopic fractionation.

Increment method. The increment method is also based on bond strengths but attempts to incorporate the effect of cation mass in its parameterization. Although they differ in detail, the various formulations of this method assign ^{18}O increment values ($i_{ct\text{-}O}$) for individual cation-oxygen bonds, which are then referenced to the increment value for the silicon-oxygen bond. Increment values are calculated from data on cation valence and coordination number, and cation-oxygen bond lengths. Cation mass effects are incorporated by treating the cation-oxygen pair as a diatomic molecule, and calculating the change in the reduced mass of this molecule on ^{18}O substitution (Eqn. 4). Empirically derived parameters are also included for strongly-bonded and weakly-bonded cations, and the OH^- group in hydrous silicates is treated separately. The total ^{18}O increment value for a mineral (I-^{18}O), which is a weighted average of the increment values of its constituent cation-oxygen bonds, is an indication of the mineral's *relative* affinity for ^{18}O. To calculate fractionation factors, this relative scale of ^{18}O enrichment must be linked to an absolute scale derived from experiments or statistical mechanical theory. The reduced partition ratios of quartz obtained from experiments or theory have generally been used to make this link. Figure 13b shows a comparison of fractionation factors at 1000 K given by the increment method calculations of Zheng (1993 1996 1997 1999a) with those indicated by experiments. There is good agreement between the two approaches for anhydrous silicates. However, hydrous silicates, apatite, and to a lesser extent, oxide minerals, deviate from the 1:1 correspondence line. Comparisons with other formulations of the increment method (e.g. Hoffbauer et al. 1994) give broadly similar results. These comparisons suggest that, although useful for anhydrous silicates, the increment method in its current form does not adequately deal with the effects of cation mass, hydroxyl groups or covalent bonding on fractionation behavior.

Summary. Bond-strength methods are in wide use because of the relative ease of determining fractionation factors for a large number of minerals with this approach. It must be emphasized, however, that these methods do not comprise a separate theory of isotopic fractionation. They are a derivative approach in which bond strengths serve as a proxy for the vibrational energies that are the root cause of fractionation. Thus, at best, bond-strength methods are only as good as the various parameterizations that go into linking bond strengths to vibrational energies, and ultimately to fractionation factors. In general, the mathematical forms of these parameterizations are not rigorously grounded in theory. The statements above are not meant to imply that bond-strength methods have no value. In cases where experiments have not been done or where theoretical calculations have not been made, these methods may provide a reasonable interim estimate of fractionation factors. Such estimates must, however, be regarded with caution until confirmed by independent methods.

Natural sample calibration

In principle, isotopic analyses of natural samples can also be used to calibrate fractionation factors. Effective use of the natural sample method, however, requires that several stringent criteria be met. (1) The phases being calibrated first attained isotopic equilibrium at some temperature, and subsequently retained their equilibrium isotopic compositions, (2) equilibration temperatures in the samples of interest are well determined by independent methods, and (3) the geothermometers used to determine

temperature equilibrated (or re-equilibrated) at the same conditions as the isotopic system being calibrated. Rigorous application of these criteria significantly limits the number of samples suitable for use with this calibration method (cf. Kohn and Valley 1998b,c). Moreover, for many samples, it is difficult to demonstrate unambiguously that these criteria have been met. Despite the potential pitfalls, the natural sample method has been widely applied, and can in favorable cases provide important insights on isotope fractionation behavior. In this regard, Valley (this volume) describes how micro-analytical techniques can be used to select the optimal samples for use in natural sample calibrations.

Probably the most widely used set of natural sample calibrations is that of Bottinga and Javoy (1975). With oxygen isotope data on minerals from a large number of igneous and metamorphic rocks serving as input, these workers followed a bootstrap procedure for calibrating fractionation factors. More specifically, they estimated temperatures for individual samples with modified laboratory calibrations (Bottinga and Javoy 1973) of oxygen isotope geothermometers comprising feldspar, and one of quartz, muscovite or magnetite. They then empirically calibrated fractionation factors for other minerals (pyroxene, olivine, garnet, amphibole, biotite, and ilmenite) present in the same samples. The validity of this approach depends critically on whether all the minerals involved in the calibration preserved their equilibrium isotopic compositions (Clayton 1981). On the basis primarily of concordancy of the isotopic temperatures that they obtained, Bottinga and Javoy (1975) argued that most of the samples that they examined were in fact in isotopic equilibrium. Deines (1977) came to the opposite conclusion upon detailed statistical evaluation of the same body of isotopic data. It is also now well established from laboratory diffusion data, and from numerical modeling of natural sample data that the minerals involved in these calibrations have markedly different susceptibilities to re-equilibration, and thus are not likely to be in equilibrium in samples that have cooled slowly from high temperature (e.g. Giletti 1986; Eiler et al. 1992; Farquhar et al. 1993; Jenkin et al. 1994; Kohn and Valley 1998b,c). Therefore, purely on theoretical grounds, the approach to natural sample calibration taken by Bottinga and Javoy (1975) is suspect. Nevertheless, some of the mineral-pair fractionation factors reported in that study are in good agreement with the best available experimental calibrations. This agreement is probably fortuitous as two out of the three reference calibrations (feldspar-muscovite, feldspar-magnetite) used in the Bottinga and Javoy study are in substantial disagreement with the same set of experimental data.

The natural sample method is most likely to be successful with rocks formed at low temperatures, with rapidly cooled volcanic rocks, and with isotopically refractory minerals (e.g. garnet, graphite) in more slowly cooled rocks. Minerals formed in low-temperature environments are less susceptible to diffusional re-equilibration on cooling. They can, however, undergo changes in their isotopic compositions through recrystallization during processes such as diagenesis or deformation. Provided that this has not occurred, and that the mineral or minerals being calibrated have not become isotopically zoned during growth, the fractionations measured in such samples may yield reliable estimates of equilibrium fractionation factors. This approach to calibration also requires that the initial formation conditions of the mineral (temperature, the isotopic composition of the fluid, etc.) are well characterized. Examples of natural calibrations using low-temperature samples include the calcite-H_2O and gibbsite-H_2O oxygen isotope calibrations of Epstein et al. (1953) and Lawrence and Taylor (1971), respectively.

The very rapid cooling associated with the formation of volcanic rocks makes it likely that any phenocryst minerals present in these rocks retain their original isotopic composition. Thus, if these phenocrysts initially crystallized in isotopic equilibrium (cf.

well suited for use in natural sample calibrations. We are not aware of any calibrations based exclusively on the analysis of minerals in volcanic rocks.

In part because of improvements in analytical techniques over the past decade, there has been an increase in natural sample calibrations involving refractory minerals found in slowly cooled metamorphic and igneous rocks. Examples include calcite-graphite carbon isotope fractionations (Valley and O'Neil 1981; Wada and Suzuki 1983; Dunn and Valley 1992; Kitchen and Valley 1995), and garnet-zircon, garnet-pyroxene, garnet-staurolite, garnet-kyanite, and quartz-kyanite oxygen isotope fractionations (Valley et al. 1994; Sharp 1995; Kohn and Valley 1998b,c). The low diffusion rates of oxygen or carbon in these minerals greatly reduce the possibility of re-equilibration effects on cooling, and in that respect make them well suited for natural sample calibration. A concern with highly refractory mineral pairs, however, is the persistence of lower-temperature isotopic compositions during prograde metamorphic evolution. A possible example of this problem is found in the calcite-graphite system. The temperature coefficient of fractionations in this system given by two independent theoretical calibrations (Chacko et al. 1991; Polyakov and Kharlashina 1995) is in excellent agreement with that given by two high-temperature (T > 650° C) natural sample calibrations (Valley and O'Neil 1981; Kitchen and Valley 1995) (Fig. 14). In contrast, three other natural sample calibrations (Wada and Suzuki 1983; Morikiyo 1984; Dunn and Valley 1992), based primarily on data from lower-temperature samples (T = 270-650° C), indicate temperature coefficients that are higher by a factor of 1.5-2.0. Extrapolation of the lower temperature natural sample calibrations to the high-temperature limit ($\ln \alpha = 0$) requires the shape of the calcite-graphite fractionation curve

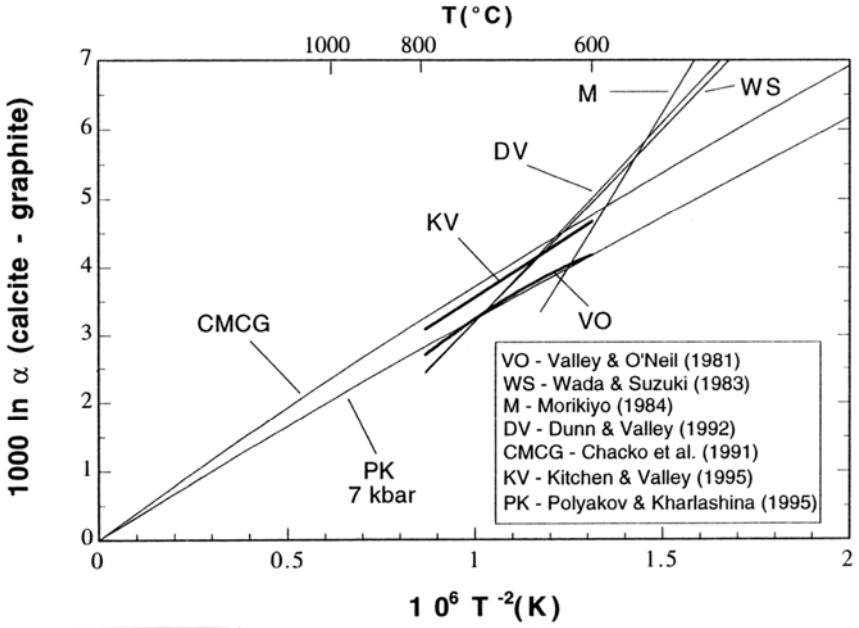

Figure 14. Comparison of theoretical (Chacko et al. 1991; Polyakov and Kharlashina 1995) and natural sample (Valley and O'Neil 1981; Wada and Suzuki 1983; Morikiyo 1984; Dunn and Valley 1992; Kitchen and Valley 1995) calibrations of the calcite-graphite fractionation factor. Note that the three lower-temperature natural sample calibrations (WS, M and DV) require a much different shape for the fractionation curve than indicated by the theoretical calculations. See text for discussion.

to be distinctly convex towards the temperature axis. This is in marked contrast to the weakly concave shape indicated by the theoretical calculations. Although the approximations required in making theoretical calculations result in significant uncertainty in the absolute magnitude of calculated fractionations, the calculations do place strict constraints on the basic shape of fractionation curves (Clayton and Kieffer 1991; Chacko et al. 1991). It is unlikely, therefore, that the shape of the fractionation curve implied by the Wada and Suzuki (1983), Morikiyo (1984), and Dunn and Valley (1992) calibrations is correct. Chacko et al. (1991) suggested that the deviation of the low-temperature natural sample data points from the calculated curve is due to the incomplete equilibration of calcite-graphite pairs at temperatures below about 650°C (see also discussion in Dunn and Valley 1992). If this interpretation is correct, calcite-graphite pairs formed at lower temperatures are unsuitable for use in natural sample calibrations, or for stable isotope thermometry.

Similar problems can occur in refractory silicate mineral pairs if the two minerals being calibrated formed at different temperatures, or if either one of the minerals formed over a range of temperatures in a prograde metamorphic sequence. In the first case, isotopic equilibrium may never have been established between the two minerals, whereas, in the second case, one or both minerals may be isotopically zoned. Sharp (1995), Kohn and Valley (1998c) and Tennie et al. (1998) noted these possibilities for natural sample calibrations involving the highly refractory minerals kyanite and garnet. Kohn and Valley (1998c) argued convincingly, however, that such problems can be overcome by carefully selecting samples with the appropriate textural and petrological characteristics. This screening process requires a detailed understanding of the metamorphic reaction history of samples.

Experimental calibration

Philosophy and methodology of experiments. Laboratory experiments are the most direct method of calibration in that they require the least number of *a priori* assumptions, and also generally permit control of the variables that may influence fractionation factors. The other calibration methods, although perhaps valid, must be regarded as tentative until confirmed by laboratory experiments. The reader is referred to the detailed reviews of experimental methods provided by O'Neil (1986) and Chacko (1993) as only the major points are summarized here.

A useful frame of reference for discussing experimental methodology is to consider the design of an ideal experiment. Such an experiment would involve direct isotopic exchange between the two substances of interest. For example, the ideal experiment for determining the oxygen isotope fractionation factor between olivine and orthopyroxene would be one in which the two minerals are intimately mixed and allowed to equilibrate at the desired temperature until isotopic equilibrium is established. To confirm the attainment of equilibrium, a companion experiment would be carried out at the same temperature consisting of olivine and orthopyroxene with the same chemical composition and structural state but with an initial isotopic fractionation on the opposite side of the equilibrium value. Obtaining the same olivine-orthopyroxene fractionation factor in both experiments would constitute a successful experimental reversal. Additional criteria for an ideal experiment include no chemical and textural changes in the starting materials during the course of the experiment. That is, isotopic exchange is accomplished exclusively through a diffusional process, which in turn is driven solely by the free energy change for the exchange reaction.

For practical reasons, most, if not all, experimental studies depart to some extent from this ideal experiment. Firstly, a direct exchange between the phases of interest is

often not possible. For example, it would be impossible to obtain a clean physical separation between olivine and orthopyroxene (for isotopic analysis) after these minerals had been ground to a sufficiently fine grain size to yield reasonable amounts of isotopic exchange on laboratory time-scales. As a result, fractionation factors are often determined indirectly by exchanging phases with a common isotopic exchange medium in separate experiments, and combining the resulting data to obtain the fractionation factor of interest. The exchange media that have been used to date, H_2O, CO_2, H_2, $CaCO_3$, and $BaCO_3$ were chosen partly because they are easily separated from the phase of interest by physical or chemical techniques after the exchange experiment.

A second problem that plagues many exchange experiments is the sluggishness of exchange rates. In particular, the diffusion rates of oxygen and carbon in many minerals are slow enough to preclude a close approach to isotopic equilibrium in typical laboratory time scales through purely diffusional processes. As a consequence, many experiments in oxygen and carbon isotope systems induce exchange either by recrystallization of preexisting phases or crystallization of new phases (synthesis) during the experiment. Both procedures result in an experiment that is less than ideal. Synthesis experiments generally involve the inversion of a polymorph or crystallization of gels or oxide mixes. The free energy change associated with these processes is about 1000 times greater than those associated with isotope exchange reactions (Matthews et al. 1983b). These processes can also be very rapid and unidirectional, possibly resulting in kinetic rather than equilibrium isotopic fractionations. This was demonstrated elegantly by Matsuhisa et al. (1978) in hydrothermal experiments at 250°C, where quartz-water fractionations obtained by inverting cristobalite to quartz were about 3‰ different than those obtained by direct quartz-water exchange experiments. They interpreted these results to reflect a kinetic isotope effect associated with the crystallization of quartz from cristobalite. Similar non-equilibrium effects were noted by Matthews et al. (1983a) in crystallizing wollastonite and diopside from mixes of constituent oxides. In other cases, synthesis and direct exchange experiments appear to give comparable results (O'Neil and Taylor 1967; Matsuhisa et al. 1979; Lichtenstein and Hoernes 1992; Scheele and Hoefs 1992).

Despite the problems inherent to the mineral synthesis technique, this technique may be the only viable means of obtaining reasonable amounts of isotopic exchange in low temperature experiments ($T < 250°C$). With care, the technique may indeed provide reliable equilibrium fractionation factors. Criteria that have been used to suggest an approach to equilibrium fractionations in such experiments include controlled precipitation rates, an understanding of reaction pathways and the likelihood of kinetic fractionations associated with particular pathways, similar fractionations obtained in synthesis from different starting materials, and a concurrence of fractionation factors obtained with synthesis and direct exchange techniques (e.g. O'Neil and Taylor 1969; Scheele and Hoefs 1992; Bird et al. 1993; Kim and O'Neil 1997; Bao and Koch 1999). It should be emphasized, however, that even when these criteria are met, synthesis experiments cannot rigorously demonstrate the attainment of isotopic equilibrium.

Recrystallization of existing phases during the course of an experiment also involves driving forces other than solely those of the exchange reaction. However, the free energy change that drives recrystallization is approximately the same order of magnitude as that associated with isotopic exchange (Matthews et al. 1983b). As such, experiments involving recrystallization are less likely to incorporate kinetic effects than those requiring the growth of new phases. In contrast to this view, Sharp and Kirschner (1994) argued that recrystallization based experiments involving quartz do incorporate significant kinetic effects. In general, however, recrystallization experiments, although less than ideal, are clearly preferable to synthesis experiments, and often provide the best

available means of calibrating fractionation factors at moderate to high temperature.

Two additional features of isotope exchange experiments are useful in the acquisition of equilibrium fractionation data. Firstly, there is a substantial increase in oxygen isotope exchange rates with increasing pressure (Clayton et al. 1975; Matthews et al. 1983a,b; Goldsmith 1991). Thus, for a given experimental run time, experiments performed at higher pressure show a closer approach to equilibrium and thereby provide more tightly constrained data. Secondly, because isotope exchange reactions run in both forward and reverse directions involve exchange of the same element between phases, it is reasonable to assume that they have nearly identical reaction rates. On the basis of this assumption, Northrop and Clayton (1966) developed the following equation for extracting equilibrium oxygen and carbon isotope fractionation factors from partially exchanged experimental data:

$$\ln \alpha^{i} = \ln \alpha^{eq} - 1/F \, (\ln \alpha^{f} - \ln \alpha^{i})$$

where the superscripts *i, f* and *eq* refer to the initial, final and equilibrium fractionations, respectively, and F is the fractional approach to equilibrium during the experiment. This equation indicates that if forward and reverse directions of an isotope exchange reaction have the same exchange rates, then data from three or more companion experiments run at the same conditions, and for the same amount of time should be linear when plotted as $\ln \alpha^{i}$ versus $(\ln \alpha^{f} - \ln \alpha^{i})$. The slope of this line gives the fractionation approach to equilibrium and the y intercept gives the extrapolated equilibrium fractionation factor. This method becomes progressively more reliable as F approaches unity because the intercept between the plotted line and the y-axis occurs at higher angles. The slightly modified version of this equation developed for hydrogen isotope exchange experiments is (Suzuoki and Epstein 1976):

$$(\alpha^{i} - 1) = (\alpha^{eq} - 1) - 1/F \, (\alpha^{f} - \alpha^{i})$$

More recently, Criss (1999, p. 204) derived a different equation for extracting an equilibrium fractionation factor ($\alpha_{A\text{-}B}$) from a pair of exchange experiments (labeled 1 and 2) that has not proceeded completely to equilibrium:

$$(1-\mathrm{H})(\alpha^{eq})^2 + [\mathrm{H}\alpha_1^i + \mathrm{H}\alpha_2^f - \alpha_2^i - \alpha_1^f](\alpha^{eq}) + [\alpha_1^f \alpha_2^i - \mathrm{H}\alpha_2^f \alpha_1^i] = 0$$

where

$$\mathrm{H} = \left(\frac{\mathrm{R}_\mathrm{B}^i}{\mathrm{R}_\mathrm{B}^f}\right)_1 \left(\frac{\mathrm{R}_\mathrm{B}^f}{\mathrm{R}_\mathrm{B}^i}\right)_2$$

and R_B is the isotope ratio (e.g. $^{18}O/^{16}O$) of phase B. The quadratic formula is used to solve the equation for α^{eq}. Criss (1999) proposed that this equation yields more exact and more correct results than the commonly used equation of Northrop and Clayton (1966). In practice, the difference in equilibrium fractionation factors obtained with the two equations is small in most cases.

Hydrothermal- and carbonate-exchange techniques. The majority of available experimental fractionation data are for oxygen isotope fractionations involving minerals. Much of the data, particularly the early data, were obtained using water as the isotopic exchange medium. These experiments were either done at ambient pressure (typically synthesis experiments), or in cold-seal pressure vessels at pressures of 1 to 3 kbar (e.g. O'Neil and Taylor 1967; O'Neil et al. 1969; Clayton et al. 1972). Later experiments were done in a piston cylinder apparatus (at ~15 kbar) to exploit the pressure enhancement of exchange rates (Clayton et al. 1975; Matsuhisa et al. 1979; Matthews et al. 1983a,b).

Even though there were some differences in experimental methodologies, the agreement between the various studies was in general excellent for some of the major mineral-water systems (e.g. albite-water, quartz- and calcite-water systems). Matthews et al. (1983a) and Matthews (1994) provide compilations of mineral-pair fractionation factors derived from the high-temperature hydrothermal experiments.

Despite the apparent success of the hydrothermal technique, there are a number of theoretical and practical drawbacks to this method of experimentation. Under hydrothermal conditions, some minerals dissolve excessively, melt, or react to form hydrous phases, making them unsuited to this type of investigation. Furthermore, the high vibrational frequencies of the water molecule results in complex temperature-dependencies for mineral-H_2O fractionations (Fig. 3), thereby making it difficult to extrapolate fractionations outside the experimentally investigated temperature range. To overcome some of these difficulties, Clayton et al. (1989) developed a technique that uses $CaCO_3$ rather than water as the common isotope exchange medium. Rosenbaum et al. (1994) used a variation of this technique with $BaCO_3$ as the exchange medium. Advantages of the so-called carbonate-exchange technique include: (1) the ability to carry out experiments at high temperatures (up to 1400° C) because of the high thermal stability of many mineral-carbonate systems, (2) the avoidance of problems associated with mineral solubility and its potential effect on fractionation factors, (3) ease of mineral separation, and (4) the relative ease and high precision of carbonate isotopic analysis. Extrapolation of experimental data is also simplified in that anhydrous mineral-carbonate fractionations should be approximately linear through the origin on fractionation plots at temperatures above 600° C (Clayton et al.1989). There now exists a large body of oxygen isotope fractionation data for minerals acquired with the carbonate-exchange technique (summarized in Table 5).

Other experimental techniques. There have been several other recent advances in experimental techniques for determining fractionation factors for oxygen, carbon, and hydrogen isotope systems. CO_2 has successfully been used as an exchange medium for determining carbon or oxygen isotope fractionation factors for melts, glasses and carbonate, silicate and oxide minerals at both high and low pressure (Mattey et al. 1990; Chacko et al. 1991; Stolper and Epstein 1991; Scheele and Hoefs 1992; Matthews et al. 1994; Rosenbaum 1994; Palin et al. 1996; Fayek and Kyser 2000). Vennemann and O'Neil (1996) used H_2 gas as an exchange medium in low-pressure experiments to obtain hydrogen isotope fractionation factors for hydrous minerals. Horita (2001) was able to obtain tightly reversed carbon isotope fractionation data in the notoriously sluggish CO_2-CH_4 system by using transition-metal catalysts to accelerate exchange rates. Fortier et al. (1995) and Chacko et al. (1999) used the ion microprobe to obtain oxygen and hydrogen isotope analyses, respectively, of run products in magnetite-water and epidote-water exchange experiments. The latter study was novel in that it used millimeter-sized, single crystals of epidote instead finely ground epidote powder as starting material, and then analyzed the outer 0.5-2 μm of the isotopically exchanged crystals with an ion microprobe. The advantage of such an approach is that it allows D/H fractionation factors to be determined in experiments in which most or all of the isotopic exchange occurs by a diffusional process, rather than by a combination of diffusion and recrystallization (i.e. an ideal exchange experiment). The disadvantage of the approach is that the precision of hydrogen isotope analyses on the ion microprobe is currently a factor of 2 to 4 poorer than can obtained by conventional methods. That precision will no doubt improve with advances in instrumentation. Figure 15 shows Chacko et al.'s (1999) data for the epidote-H_2O system. Despite initial fractionations that were in most cases far from equilibrium, the companion experiments at each temperature were successful in bracketing the equilibrium fractionation factor within analytical error. This technique should be useful

Table 5. Coefficients for mineral-pair oxygen isotope fractionation factors.

	Cal	Ab	Mu	F-Phl	An	Phl	*Ap	Di	Gr	Gh	Fo	Ru	Mt	Prv
Qtz	0.38	0.94	1.37	1.64	1.99	2.16	2.51	2.75	3.15	3.50	3.67	4.69	6.29	6.80
Cal		0.56	0.99	1.26	1.61	1.78	2.13	2.37	2.77	3.12	3.29	4.31	5.91	6.42
Ab			0.43	0.70	1.05	1.22	1.57	1.81	2.21	2.56	2.73	3.75	5.35	5.86
Mu				0.27	0.62	0.79	1.14	1.38	1.78	2.13	2.30	3.32	4.92	5.43
F-Phl					0.35	0.52	0.87	1.11	1.51	1.86	2.03	3.05	4.65	5.16
An						0.17	0.52	0.76	1.72	1.51	1.68	2.70	4.30	4.81
Phl							0.35	0.59	0.99	1.34	1.51	2.53	4.13	4.64
Ap								0.24	0.64	0.99	1.16	2.18	3.78	4.29
Di									0.40	0.75	0.92	1.94	3.54	4.05
Gr										0.35	0.52	1.54	3.14	3.65
Gh											0.17	1.19	2.79	3.30
Fo												1.02	2.62	3.13
Ru													1.60	2.11
Mt														0.51

Coefficients for mineral-pair fractionation factors of the form $1000 \ln \alpha = A \times 10^6 / T^2(K)$, where the coefficient A is given in the table.

Equations should not be extrapolated below ~600°C. All data derived from experiments using the carbonate-exchange technique. Qtz = quartz; Cal = calcite; Ab = albite; Mu = muscovite; F-Phl = fluorophlogopite; An = anorthite; Phl = hydroxyphlogopite; Ap = apatite; Di = diopside; Gr = grossular; Gh = gehlenite; Fo = forsterite; Ru = rutile; Mt = magnetite; Prv = $CaTiO_3$ - perovskite. Data from Clayton et al. (1989), Chiba et al. (1989); Chacko et al. (1989, 1996), Gautason et al. (1993), Fortier and Lüttge (1995), and Rosenbaum and Mattey (1995).

*The equation for apatite is not the same as that given in Fortier and Lüttge (1995). Following Chacko et al.'s (1996) suggestion for hydrous minerals, Fortier and Lüttge's 500-800°C apatite-calcite fractionation data have been regressed by a straight line through the origin on a plot of $1000 \ln \alpha$ vs. $10^6/T^2$.

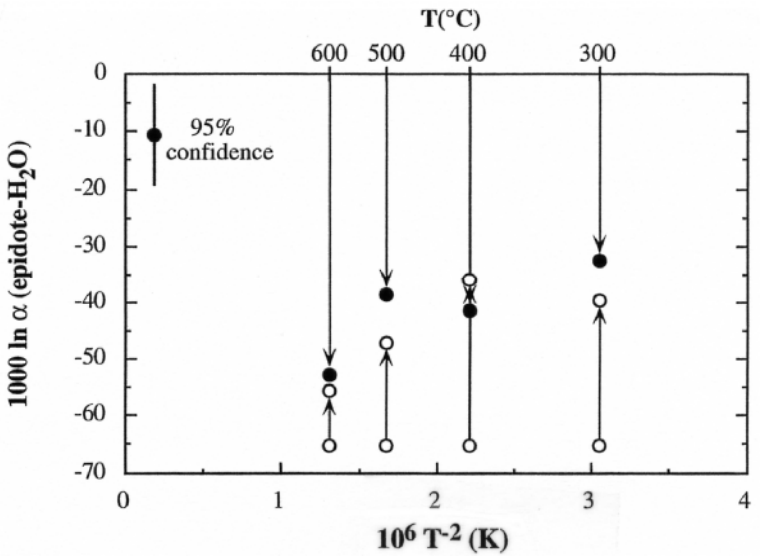

Figure 15. Experimental D/H fractionation data in the epidote-water system plotted as a function of 10^6 T^{-2} (modified after Chacko et al. 1999). The experiments involved exchange between water and large, single crystals of epidote. The isotopically exchanged crystals were analyzed by ion microprobe. Note that equilibrium fractionation factor was bracketed within analytical error (±6-10‰) to temperatures as low as 300°C.

for determining D/H fractionation factors in other mineral-water systems. On a more general level, micro-analytical techniques such as the ion microprobe hold great promise for isotope exchange experiments in that they open up the possibility of extending these experiments to significantly lower temperature.

SUMMARY OF FRACTIONATION FACTORS

Appendices 2-4 are an annotated list of published experimental and natural sample calibrations of oxygen, carbon and hydrogen isotope fractionation factors applicable to geological systems. The reader is referred to the Introduction section for sources of information on fractionation factors derived from theoretical and bond-strength methods. In this section, we extract from the larger tabulation some sets of fractionation data that have wide applicability. Our goal is to provide an overview of the current state of knowledge on these key fractionations, and to highlight areas where more work needs to be done. A summary of this type is necessarily subjective, and the reader is encouraged to consult the references given in this section and in the bibliography for alternative points of view.

Oxygen isotope fractionation factors

Mineral-pair fractionations. As detailed above, there currently exists two large sets of experimental data on oxygen isotope fractionation factors between minerals, one obtained using water, and the other using carbonate as the isotopic exchange medium. Mineral-pair fractionation factors derived from the two data sets are generally in good agreement except for fractionations involving quartz or calcite (Clayton et al. 1989; Chiba et al. 1989; Chacko 1993, Matthews 1994). The discrepancies are enigmatic because both hydrothermal and carbonate-exchange experiments meet many of the criteria listed above for an ideal exchange experiment. Moreover, the discrepancies cannot be attributed to inter-laboratory differences as most of both data sets were

acquired at the same laboratory. Hu and Clayton (in press) provided a resolution to this paradox with an experimental investigation of the oxygen isotope salt effect on quartz-H_2O and calcite-H_2O fractionations at high pressure and temperature. They found a significant salt effect in the quartz-H_2O system but no salt effect in otherwise comparable experiments in the calcite-H_2O system. The implications of these results are profound. If salt was the only dissolved constituent in the aqueous fluid, the magnitude of the salt effect (Γ) should be identical in both sets of experiments. The fact that $\Gamma_{qtz\text{-}fluid}$ is different than $\Gamma_{calcite\text{-}fluid}$ indicates that minerals also dissolve appreciably at experimental conditions, and importantly, that the nature of the dissolved mineral species significantly affects fractionations in mineral-H_2O systems. Thus, mineral-pair fractionation factors derived from different sets of mineral-H_2O experiments may not be internally consistent because the characteristics of the fluid phase may vary with the mineral under investigation. To ensure internal consistency, two minerals must be exchanged with the same fluid. Hu and Clayton (in press) tested this idea with three-phase experiments in the quartz-calcite-H_2O and phlogopite-calcite-H_2O systems. The mineral-fluid fractionation factors derived from these three-phase experiments are different than those obtained in two-phase mineral-fluid experiments. However, the quartz-calcite and phlogopite-calcite fractionation factors derived from the three-phase experiments are the same as those obtained in the two-phase mineral-calcite experiments of Clayton et al. (1989) and Chacko et al. (1996). These results indicate that, in a choice between the two data sets, the carbonate-exchange technique provides the better mineral-pair fractionation data.

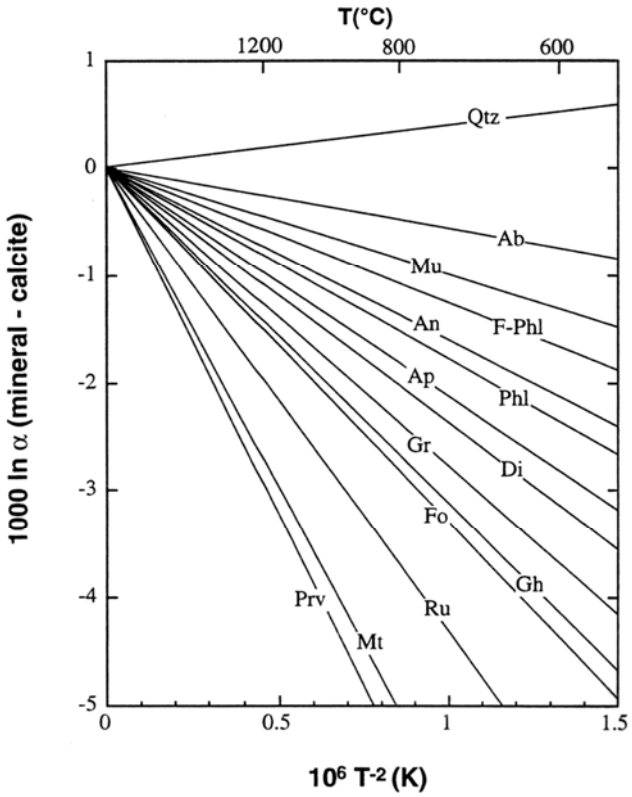

Figure 16. Summary of mineral-calcite fractionation factors given by the carbonate-exchange technique. All data have been fit by straight lines through the origin. Abbreviations and sources of data given in Table 5.

Mineral-calcite fractionation factors obtained with the carbonate-exchange technique are shown in graphical form in Figure 16. Each fractionation line shown on the plot is constrained by sets of experiments conducted at two to five different temperatures from 500 to 1300° C. These mineral-calcite fractionation data can be combined to obtain a large matrix of mineral-pair fractionation factors (Table 5). The straight-line equations given in Table 5 are adequate for calculating fractionation factors at high temperature but

should not be used at temperatures of below about 600° C.Clayton and Kieffer (1991) developed a methodology for extrapolating these fractionation data to lower temperatures. With the calculated partition function ratios for calcite serving as a baseline (Chacko et al. 1991), they used the theoretical calculations (Becker 1971; Kieffer 1982) to constrain the basic shape of each fractionation curve. They then applied a correction factor to the calculated partition function ratios of individual minerals to optimize agreement between theory and experiment. It should be noted that the magnitude of the correction factor required to bring the calculations into agreement with the experiments was small for all minerals except rutile (Clayton and Kieffer 1991; Chacko et al. 1996). The advantage of this fitting procedure is that it allows experimental data, which necessarily must be obtained over a limited temperature range, to be extrapolated to lower temperature in a manner that is theoretically justifiable**.** Table 6 gives polynomial expressions for calculating the reduced partition function ratios for minerals derived through this fitting procedure.

Table 6. Reduced partition function ratios for minerals.

Mineral	1000 ln β
Calcite	$11.781\,x - 0.420\,x^2 + 0.0158\,x^3$
Quartz	$12.116\,x - 0.370\,x^2 + 0.0123\,x^3$
Albite	$11.134\,x - 0.326\,x^2 + 0.0104\,x^3$
Muscovite	$10.766\,x - 0.412\,x^2 + 0.0209\,x^3$
Anorthite	$9.993\,x - 0.271\,x^2 + 0.0082\,x^3$
Phlogopite	$9.969\,x - 0.382\,x^2 + 0.0194\,x^3$
F-phlogopite	$10.475\,x - 0.401\,x^2 + 0.0203\,x^3$
Diopside	$9.237\,x - 0.199\,x^2 + 0.0053x^3$
Forsterite	$8.236\,x - 0.142\,x^2 + 0.0032\,x^3$
Rutile	$7.258\,x – 0.125\,x^2 + 0.0033\,x^3$
Magnetite	$5.674\,x - 0.038\,x^2 + 0.0003\,x^3$

Polynomial expressions describing oxygen reduced partition function ratios (1000 ln β) for minerals where $x= 10^6/T^2(K)$. The equations are only applicable at temperatures above 400K. The fractionation factor between any two phases at a particular temperature is given by the algebraic difference in their 1000 lnβ values (1000 ln β_A – 1000 ln β_B). Expressions are from Clayton and Kieffer (1991) and Chacko et al. (1996).

Mineral-pair fractionation factors obtained with the carbonate-exchange technique have gained wide, but not universal, acceptance. In particular, Sharp and Kirschner (1994) questioned the validity of quartz-calcite fractionations given by this technique. Their natural sample calibration of this important system gave systematically larger fractionations than indicated by the experiments of Clayton et al. (1989). They attributed the discrepancy to a kinetic isotope effect in the experiments engendered by the rapid rate of quartz recrystallization relative to the rate of oxygen diffusion in the calcite exchange medium. We note, however, that diffusion rates of oxygen in quartz and calcite at 1000° C (Giletti and Yund 1984; Farver 1994) are rapid enough to isotopically homogenize small grains (radii < 3 μm) of these minerals by volume diffusion in 24 hours. Thus, the 1000° C quartz-calcite experiments, which used fine grained starting materials (diameter

1 to 10 μm) and were held at temperature for 24 hours, were of sufficiently long duration to establish a true diffusional equilibrium between the two minerals. The fractionation factor obtained by Clayton et al. in these high-temperature experiments is entirely consistent with their results at lower temperature (600-800°C), and does not agree with that given by the natural sample calibration. This suggests that the difference between the two calibrations has some other fundamental cause than the one proposed by Sharp and Kirschner. We believe the bulk of the evidence favors the experimental calibration. Nevertheless, given its importance, it seems prudent to attempt to re-determine fractionation factors in the quartz-calcite system with an independent method. For example, it may be possible to indirectly determine quartz-calcite fractionations through a combination of data from CO_2-quartz and CO_2-calcite experiments at high pressure and temperature.

Another mineral that bears further investigation is kyanite. Existing experimental and natural sample calibrations of quartz-kyanite oxygen isotope fractionations are widely discrepant (Sharp 1995; Tennie et al. 1998), as are three bond-strength estimates of these fractionations (Smyth and Clayton 1988; Hoffbauer et al. 1994; Zheng 1999a). Although the experimental data for kyanite were obtained with the carbonate-exchange technique (Tennie et al. 1998), these data are not entirely compatible with the rest of the carbonate-exchange data set because the experiments involved polymorphic inversion of andalusite to kyanite, rather than direct kyanite-carbonate exchange. As such, it cannot unambiguously be shown that the fractionations measured in the experiments represent true equilibrium values. The highly refractory nature of kyanite in terms of oxygen isotope exchange makes it a difficult mineral to work with from both an experimental and natural sample perspective. However, that same characteristic potentially makes it a very useful mineral for elucidating the metamorphic history of rocks. Additional studies, although difficult, should be pursued.

Mineral-fluid oxygen isotope fractionations at low temperature. Unlike the case for high-temperature fractionations between minerals, the current status of our knowledge on oxygen isotope fractionation between minerals and fluids/gases at low-temperatures (<200°C) is far from satisfactory. Although isotopic fractionation factors of many rock-forming minerals have been calculated over a wide range of temperature by theoretical and bond-strength methods discussed in the previous sections, the accuracy of these results needs to be examined by independent experimental studies. Because of extremely sluggish isotopic exchange by direct reactions (dissolution-precipitation and diffusion) between most minerals and aqueous fluids at low temperatures, virtually all experimental studies conducted to date employed various methods of synthesis by means of homogeneous precipitation from solutions and replacement of reactant minerals followed by aging. As noted previously, the attainment of isotopic equilibrium in such studies can only be inferred. Furthermore, the number of minerals amenable to low temperature synthesis on laboratory time-scales is very limited because of high activation energies of nucleation and growth.

Probably the best constrained fractionation data at this temperature range is for carbonate minerals. Oxygen isotope fractionations have been determined for a number of metal carbonates through synthesis experiments involving either precipitation of a mineral from solution or replacement of a pre-existing carbonate mineral (Fig. 17). A striking feature of these results is that all the carbonate-water fractionation curves are positioned parallel to one another in a similar but not identical order of ^{18}O enrichment as observed at higher temperature in the experiments of O'Neil et al. (1969) (Fig. 8). Agreement between these experimental results, and theoretical and increment method calculations by Golyshev et al. (1981) and Zheng (1999b), respectively, is not entirely

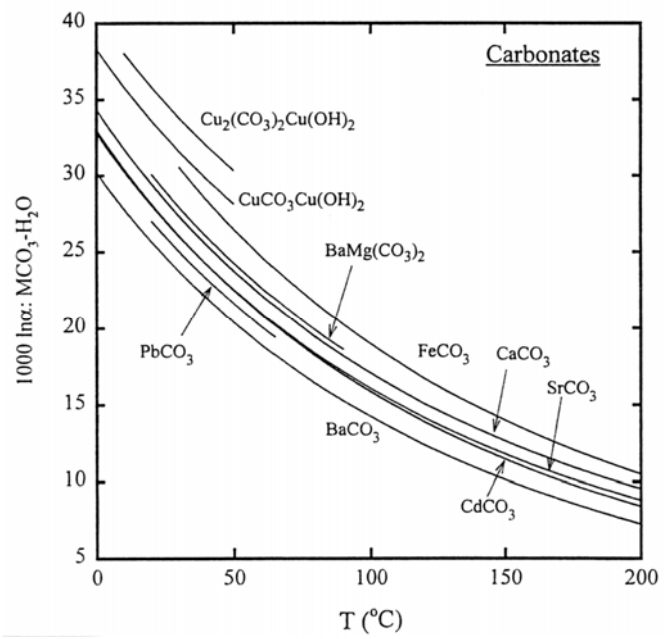

Figure 17. Plot of experimentally determined oxygen isotope fractionation factors between various metal carbonates and water at low temperatures. The carbonates were synthesized by precipitation from solution or replacement of calcite. Data sources: $CaCO_3$ (calcite), $SrCO_3$, and $BaCO_3$ – O'Neil et al. (1969), corrected in Friedman and O'Neil (1977); $CdCO_3$ – Kim and O'Neil (1997); $PbCO_3$ – Melchiorre et al. (2001); $CuCO_3Cu(OH)_2$ – Melchiorre et al. (1999); $(CuCO_3)_2Cu(OH)_2$ – Melchiorre et al. (2000); $BaMg(CO_3)_2$ – Bottcher (2000).

satisfactory. In particular, the order of ^{18}Oenrichment indicated by the numerical calibration methods is not the same, with the largest discrepancies for Pb (theoretical) and Cd (increment) carbonates. Furthermore, the experimental study of Tarutani et al. (1969) indicates that aragonite is slightly enriched in ^{18}O relative to calcite at 25° C, whereas the increment method predicts a large fractionation in the opposite direction. In terms of its applicability to natural samples, the most important of these carbonate-water systems is the calcite-water system. The detailed experimental study of Kim and O'Neil (1997) examined the effect of precipitation rate and solution ionic strength on calcite-water fractionations between 0 and 40° C. They found that precipitation rate had essentially no effect on the measured fractionations whereas solutions of high ionic strength resulted in systematically larger, disequilibrium fractionations. The equation reported by Kim and O'Neil (1997) for equilibrium calcite-water fractionations at low temperature is:

$$1000 \ln \alpha = 18.03 (10^3 T^{-1}) - 32.42$$

The situation for other minerals at low temperature is less satisfactory - as in the case of the iron oxides. Several fractionation factors proposed for magnetite-water exhibit an extremely wide range (Fig. 18). Empirical-theoretical calculations (Becker and Clayton 1976; Rowe et al. 1994) and empirical calculations by the increment method (Zheng 1995) predicted very negative values for this fractionation. The curve by O'Neil and Clayton (1964) is based on an extrapolation of results from high-temperature exchange experiments to one analysis of natural magnetite sample of teeth from marine chiton. Recent results of cultured biogenic magnetite samples at low temperatures (Zhang et al. 1997; Mandernack et al. 1999) together with those of magnetite obtained from modern geothermal system (Blattner et al. 1983) point to more positive values of magnetite-water fractionation (Fig. 18).

Oxygen isotopic fractionations between various Fe(III)-oxides and water are even more poorly constrained (Fig. 19). In addition to equations based on isotopic analysis of natural hematite in low-temperature environments (Clayton and Epstein 1961; Clayton 1963), several investigators recently reported fractionation factors for hematite and goethite obtained from laboratory synthesis experiments. They show a large (>10‰ variation especially at temperatures below 40° C, depending on reaction pathways and solution compositions (e.g. pH). Mineral precipitates at low temperatures tend to be

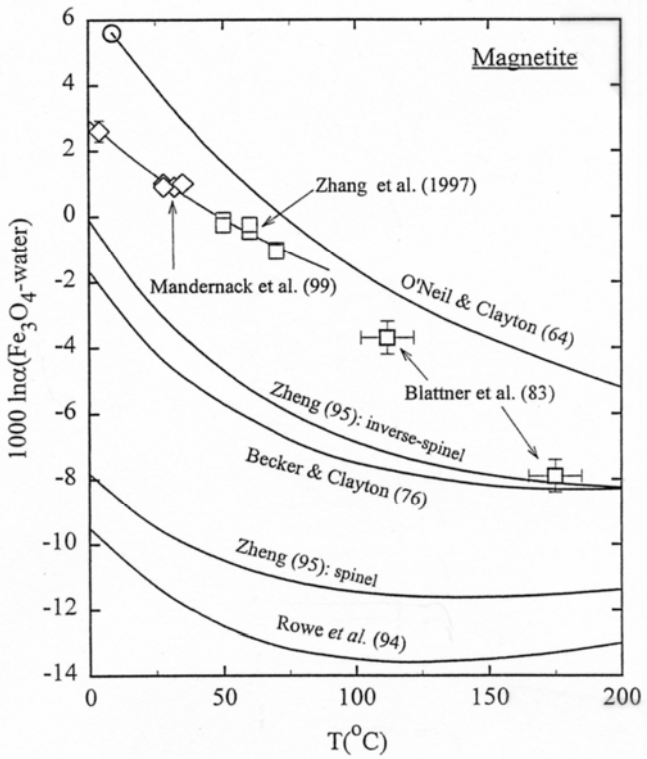

Figure 18. Plot of oxygen isotope fractionation factor between magnetite and water at low temperatures. Data sources: Becker and Clayton (1976) and Rowe et al. (1994) - empirical-theoretical calculations; Zheng (1995) - empirical increment method; O'Neil and Clayton (1964) - extrapolation of high-temperature experimental results to an analysis of magnetite teeth from marine chiton; Blattner et al. (1983) – natural samples from active geothermal system in New Zealand; Zhang et al. (1997) – extracellular magnetite produced by Fe(III)-reducing bacteria in culture; Mandernack et al. (1999) – magnetite produced intracellular by magnetotactic bacteria in culture.

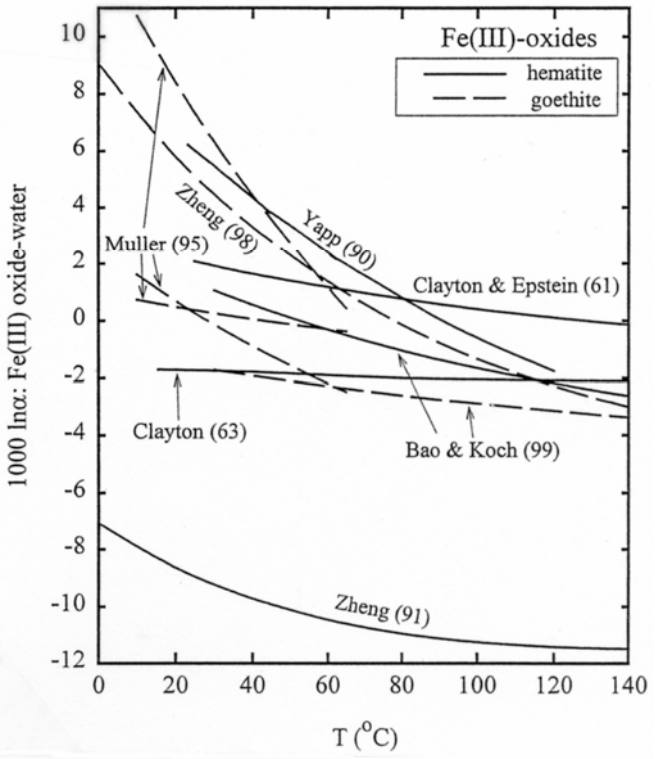

Figure 19. Plot of oxygen isotope fractionation factor between Fe(III) oxides (hematite and goethite) and water at low temperatures. Data sources: Zheng (1991, 1998) – increment method; Clayton and Epstein (1961), and Clayton (1963) – empirical calibration based on natural samples; Yapp (1990), Müller (1995), and Bao and Koch (1999) – laboratory synthesis experiments via different reaction pathways.

poorly crystalline and fine-grained (<100 nm) with large amounts of adsorbed water. These characteristics pose not only technical problems in handling and isotopic analysis (drying and rapid redox reactions), but also fundamental questions regarding equilibrium fractionation factors for nano-sized particles with large specific surface areas.

One way to facilitate isotopic exchange between minerals and water at low temperatures is by means of microbial and enzymatic activities. Examples are intra- and

extra-cellular biological precipitation of magnetite as mentioned above (Zhang et al. 1997; Mandernack et al. 1999), and enzymatic isotopic exchange between phosphate and water (Blake et al. 1998). It is likely that biological activities result in isotopic effects different from inorganic equilibrium fractionations. Such "isotopic biosignatures" may be recognizable in the rock record, and thus serve as a tool in the search for ancient life.

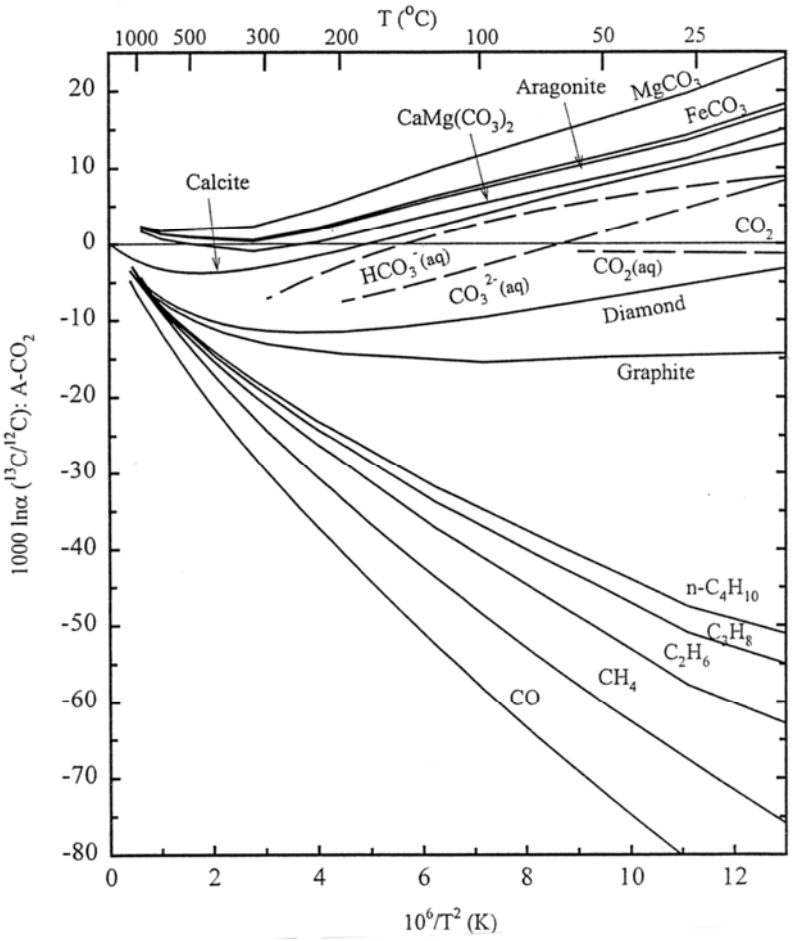

Figure 20. Plot of carbon isotope fractionation between various geologic materials and gaseous CO_2. Data sources: calcite – calculations by Chacko et al. (1991); aragonite, $CaMg(CO_3)_2$, $MgCO_3$ and $FeCO_3$, – calculations by Golyshev et al. (1981); HCO_3^-(aq) – experimental results by Malinin et al. (1967); CO_3^{2-}(aq) – calculations by Halas et al. (1997); CO_2(aq) – experimental results by Zhang et al. (1995); diamond and graphite – Bottinga (1969b); CO and CH_4 – Richet et al. (1977); hydrocarbons – Galimov (1985).

Carbon isotope fractionation factors

Figure 20 shows the general pattern of equilibrium ^{13}C enrichment among various geologic materials, exclusive of biological compounds, relative to gaseous CO_2. Because only a limited number of carbon-bearing systems have been investigated experimentally, this plot is constructed largely from theoretical calculations by Bottinga (1969b), Galimov (1985), Richet et al. (1977), Golyshev et al. (1981), Chacko et al. (1991), and Halas et al. (1997). There is a strong positive correlation between ^{13}C enrichment and the oxidation state or number of covalent bonds of carbon. Carbonate minerals, as a group, are the most enriched in ^{13}C, whereas CO and light hydrocarbons are the most depleted.

The magnitude of ^{13}C isotopic fractionations of various gaseous species (CO and hydrocarbon) relative to CO_2 decreases rapidly with increasing temperature, so that T^{-3} (K) (and even higher-order) terms are required to describe these curves numerically. There are minima in the fractionation curves of calcite, graphite and diamond, and fractionation crossovers are indicated for dissolved CO_2 species (HCO_3^- and CO_3^{2-}), calcite, and possibly other carbonate minerals.

Of the various fractionation curves shown on Figure 20, the best studied system involving a mineral is the system calcite-CO_2, which has been investigated theoretically and experimentally. Direct exchange experiments between calcite and CO_2 at high pressure (1-13 kbar) and temperature (400-1200°C) by Chacko et al. (1991), Scheele and Hoefs (1992), and Rosenbaum (1994) showed that CO_2 is enriched in ^{13}C by 2 to 3.5‰ relative to calcite over this temperature range. These experimental data are in marked disagreement with the calculations of Golyshev et al. (1981), which, over the same temperature range, indicate much smaller calcite-CO_2 fractionations, and even fractionations of the opposite sign. This casts serious doubt on the magnitude of carbonate-CO_2 fractionations given by Golyshev et al.'s calculations for other carbonate minerals (Fig. 20), although the order of ^{13}C enrichment amongst the carbonates indicated by those calculations may be correct. There is excellent agreement between the high-temperature experimental data and the theoretical calculations of Chacko et al. (1991). However, the same calculations gave fractionations that differed by 1.6-2.0‰ from those obtained in experiments involving slow, controlled precipitation of calcite from supersaturated solutions at 10-40°C (Romanek et al. 1992). In fact, the calculations for calcite are very similar to experimental aragonite-CO_2 fractionations obtained over the same temperature range (Romanek et al. 1992). Further investigations are needed to resolve this discrepancy at low temperatures in this very important system.

As originally suggested by Valley and O'Neil (1981), the calcite-graphite system is an important one, and can potentially serve as a very effective geothermometer in metamorphosed carbonate rocks. There are several theoretical and natural sample calibrations of fractionations in this system (Valley and O'Neil 1981; Wada and Suzuki 1983; Morikiyo 1984; Chacko et al. 1991; Kitchen and Valley 1995; Polyakov and Kharlashina 1995) (Fig. 14), and also an experimental calibration (Scheele and Hoefs 1992) derived from a combination of data from CO_2-graphite and CO_2-calcite experiments. In the temperature range 600-1200°C, the experimental calibration indicates markedly larger fractionations than given by the other calibrations. This discrepancy likely reflects a problem with the CO_2-graphite experiments, which, in order to overcome the problem of low exchange rates, used a very high graphite to CO_2 ratio. Although such a procedure greatly enhances exchange rates, the measured fractionations may represent those between CO_2 and graphite surface atoms rather than between CO_2 and bulk graphite (see Hamza and Broecker 1974 for a discussion of surface effects). There is good to excellent agreement between natural sample calibrations of Valley and O'Neil (1981) and Kitchen and Valley (1995), which are based on high-temperature natural sample data, and the theoretical calibration of Polyakov and Kharlashina (1995), which takes into account the significant pressure effect on fractionations in this system. Although the matter remains controversial, in our opinion, the current best estimate of equilibrium fractionations in the calcite-graphite system is given by the calibration of Polyakov and Kharlashina.

A recent experimental study on carbon isotope fractionation in the system CO_2-CH_4 (Horita 2001) showed that results of theoretical calculations by Richet et al. (1977) are accurate (to ±0.9‰) over the temperature range from 200 to 600°C. However, in the application of fractionation data for C-O-H gases, perhaps a more important question is

rates and mechanisms of isotopic exchange in natural environments. Many experimental studies indicate that isotopic exchange among gaseous species of the C-O-H system is driven by a series of elemental chemical reactions rather than by simple intermolecular collisions between the gaseous species of interest. It is also known that homogeneous gaseous reactions are very sluggish, and that these reactions can be enhanced tremendously by heterogeneous reactions on the surface of solids or minerals. Gaseous species of the C-O-H system (particularly CO_2-CH_4) from sedimentary and geothermal systems commonly appear to be out of isotopic equilibrium (Ohmoto 1986; Horita 2001). Many natural materials, however, can catalyze isotopic exchange among C-O-H gases. In this context, kinetic isotopic fractionation may be more important than equilibrium fractionation in the study of C-O-H gases at low to moderate (perhaps up to 500-600° C) temperatures.

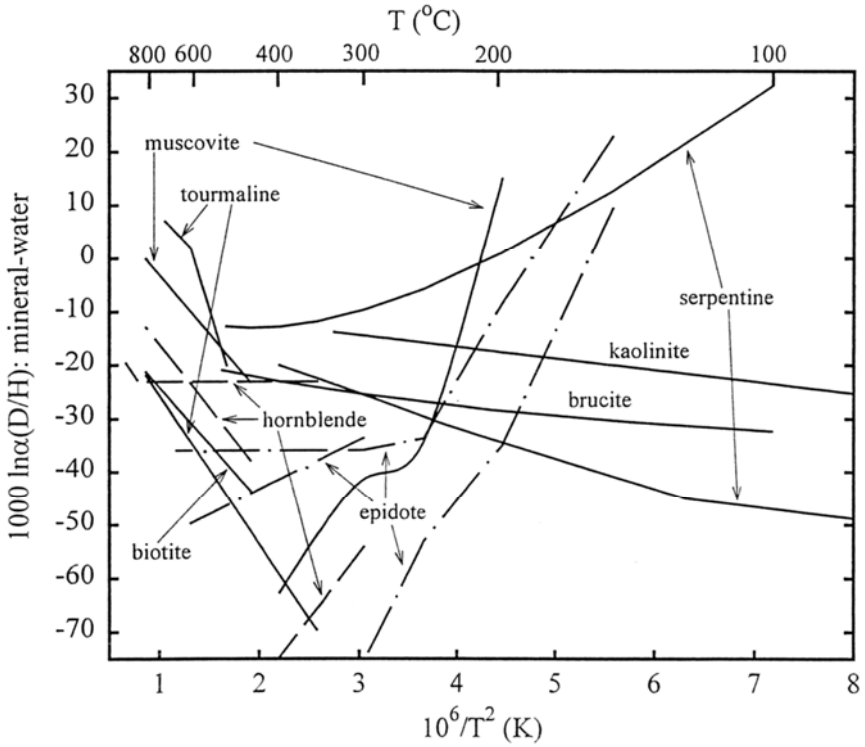

Figure 21. Plot of hydrogen isotope fractionation between various hydrous minerals and water. Note the large discrepancies of existing calibrations of epidote-water and hornblende-water fractionations. Data sources: serpentine – Wenner and Taylor (1973) and Sakai and Tsutsumi (1978); kaolinite – Gilg and Sheppard (1996); brucite – modified after Satake and Matsuo (1984); epidote – Graham et al. (1980), Vennemann and O'Neil (1996), and Chacko et al. (1999); hornblende – Suzuoki and Epstein (1976), Graham et al. (1984), and Vennemann and O'Neil (1996); muscovite – Suzuoki and Epstein (1976) and Vennemann and O'Neil (1996); biotite – Suzuoki and Epstein (1976); tourmaline – Blamart et al. (1989) and Jibao and Yaiqian (1997).

Hydrogen isotope fractionation factors

Figure 21 summarizes some of the available data on D/H fractionation factors in hydrous mineral-H_2O systems. These fractionations are mainly derived from experimental data, but also include calibrations based on natural samples. The plot shows a bewildering array of shapes for mineral-water fractionation curves. Moreover, as noted by Vennemann and O'Neil (1996), there are major, unresolved discrepancies between published experimental calibrations as regards the magnitude of fractionation factors in

individual mineral-water systems. This is well illustrated by the hornblende-water and epidote-water systems, where three independent experimental determinations in each system show marked differences in the magnitude of fractionation factors, and the shape of fractionation curves. As discussed earlier, differences in experimental pressures can account for some, but not all of the differences in the measured fractionation factors (Horita et al. 1999; Horita et al., in press). Differences in the experimental procedures of the various studies undoubtedly also contribute to the discrepancies. However, a review of these procedures does not reveal an obvious 'best' calibration. The difference in hornblende-H_2O (or actinolite-H_2O) fractionations given by the Suzuoki and Epstein (1976) and Graham et al. (1984) experiments is particularly unsettling because, except for the mineral to fluid ratio in the experimental charges, these studies used broadly similar procedures.

The lack of consensus on D/H fractionations in mineral-water systems limits the confidence with which these data can be used to estimate the hydrogen isotope compositions of fluids that have interacted with rocks. To resolve these issues, additional careful studies are required that systematically investigate the effect of mineral composition, fluid composition, confining pressure, and mineral to fluid ratio on D/H fractionation factors in these systems. A complementary avenue of research would be the development of theoretical methods for calculating D/H partition function ratios for hydrous minerals. Even if such calculations could not accurately predict the magnitude of fractionations, they would provide a useful framework for fitting and extrapolating experimental data.

CONCLUSIONS

In his concluding thoughts in the 1986 MSA review volume, O'Neil anticipated that experimental developments then underway would help to resolve major discrepancies in experimental, theoretical and natural sample estimates of equilibrium oxygen isotope fractionation factors between minerals. That expectation has to a large extent been realized. There is now considerably better agreement on high-temperature oxygen isotope fractionation factors for a significant number of common rock-forming minerals. However, as noted above, there still remains controversy, or lack of sufficient data on fractionations for some important minerals including quartz and kyanite. Additional experiments and carefully designed studies of natural samples should help to resolve some of these difficulties. Important insights can also be gained from further theoretical studies. In particular, the theoretical methodology developed by Kieffer (1982) has proven to be remarkably successful in predicting oxygen isotope fractionation factors for silicates. Her work should be expanded to include calculations for the aluminosilicate polymorphs, amphiboles, oxides, high-pressure mantle minerals, and other minerals that have not been, or may not be readily amenable to experimental investigation. The new methods of theoretical calculation developed over the past decade, such as the *ab initio* (Patel et al. 1991), and perturbation theory (Polyakov and Kharlashina 1995; Polyakov and Mineev 2000) methods, show great promise, and should also be refined and extended.

In contrast to the situation described above, there is a general lack of consensus on oxygen, carbon and hydrogen isotope fractionation factors for many important mineral-fluid systems, particularly at low temperature. It is clear that many different variables may affect the magnitude of fractionation factors measured in these systems including among others mineral composition, mineral zoning, solution composition, precipitation rate, and biological activity. Although the potential significance of these variables has long been appreciated, recent developments in experimental and analytical techniques,

including some of those described in this chapter, make it possible to investigate their effects on a more detailed and precise level.

ACKNOWLEDGMENTS

We respectfully dedicate this chapter to Professor Robert N. Clayton and the late Professor Julian R. Goldsmith in honor of their landmark contributions to our understanding of stable isotope fractionation in geological systems. TC thanks Neil Banerjee and Suman De for helpful comments on an earlier version of this manuscript, and Karlis Muehlenbachs for many discussions. We are very grateful to Bob Clayton, James Farquhar, Val Ferreira, Bob Luth and John Valley for timely reviews. Their comments materially improved the manuscript and caught some serious errors. Any remaining errors or omissions are entirely our responsibility. TC's research is supported by a Canadian NSERC research grant. The work of DRC and JH is sponsored by the Division of Chemical Sciences, Geosciences, and Biosciences, Office of Basic Energy Sciences, U.S. Department of Energy under contract DE-AC05-00OR22725, Oak Ridge National Laboratory, managed and operated by UT-Battelle, LLC.

REFERENCES

Addy SK, Garlick GD (1974) Oxygen isotope fractionation between rutile and water. Contrib Mineral Petrol 45:119-121

Agrinier P (1991) The natural calibration of $^{18}O/^{16}O$ geothermometers: Application to the quartz-rutile pair. Chem Geol 91:49-64

Anderson AT II, Clayton RN, Mayeda TK (1971) Oxygen isotope thermometry of mafic igneous rocks. J Geol 79:715-729

Arnason B. (1969) Equilibrium constant for the fractionation of deuterium between ice and water. J Phys Chem 73:3191-3194

Bao H, Koch PL (1999) Oxygen isotope fractionation in ferric oxide-water systems: low-temperature synthesis. Geochim Cosmochim Acta 63:599-613

Bechtel A, Hoernes S (1990) Oxygen isotope fractionation between oxygen of different sites in illite minerals: A potential single-mineral thermometer. Contrib Mineral Petrol 104:463-470

Becker RH (1971) Carbon and oxygen isotope ratios in iron-formation and associated rocks from the Hammersley Range of Western Australia and their implications. PhD Dissertation, University of Chicago

Becker RH, Clayton RN (1976) Oxygen isotope study of a Precambrian banded iron-formation. Hamersley Range, Western Australia. Geochim Cosmochim Acta 40:1153-1165

Berndt ME, Seal RR, II, Shanks WC, III, Seyfried WE Jr (1996) Hydrogen isotope systematics of phase separation in subseafloor hydrothermal systems: Experimental calibration and theoretical models. Geochim Cosmochim Acta 60:1595-1604

Bigeleisen J (1961) Statistical mechanics of isotope effects on the thermodynamic properties of condensed systems. J Chem Phys 34:1485-1493

Bigeleisen J (1965) Chemistry of isotopes. Science 147:463-471

Bigeleisen J, Mayer MG (1947) Calculation of equilibrium constants for isotopic exchange reactions. J Phys Chem 13:261-267

Bird MI, Longstaffe FJ, Fyfe WS, Bildgen P (1993) Oxygen-isotope fractionation in titanium-oxide minerals at low temperature. Geochim Cosmochim Acta 57:3083-3091

Bird MI, Longstaffe FJ, Fyfe WS, Takaki K, Chivas AR (1994) Oxygen-isotope fractionation in gibbsite: synthesis experiments versus natural samples. Geochim Cosmochim Acta 58:5267-5277

Blake RE, O'Neil JR, Garcia GA (1998) Effects of microbial activity on the $\delta^{18}O$ of dissolved inorganic phosphate and textual features of synthetic apatites. Am Mineral 83:1516-1531

Blamart D, Pichavant M, Sheppard SMF (1989) Experimental determination of the D/H isotopic fractionation between tourmaline and water at 600, 500 °C and 3 kbar. C R Acad Sci Paris 308:39-44

Blattner P (1973) Oxygen from liquids for isotopic analysis, and a new determination of αCO_2-H_2O at 25°C. Geochim Cosmochim Acta 37:2691-2693

Blattner P, Bird GW (1974) Oxygen isotope fractionation between quartz and K-feldspar at 600°C. Earth Planet Sci Lett 23:21-27

Blattner P, Braithwaite WR, Glover RB (1983) New evidence on magnetite oxygen isotope geothermometers at 175°C and 112°C in Wairakei steam pipelines (New Zealand). Isotope Geosci 1:195-204

Bopp P, Heinzinger K, Klemm A (1977) Oxygen isotope fractionation. Z Naturforschung 32a:1419-1425

Bottcher WE (1994) $^{13}C/^{12}C$ partitioning during synthesis of $Na_2Ca(CO_3)_2 2H_2O$. J Chem Soc Chem Commun, p 1485

Bottcher WE (2000) Stable isotope fractionation during experimental formation of norsethite ($BaMg[CO_3]_2$): A mineral analogue of dolomite. Aquatic Geochem 6:201-212

Bottinga Y (1968) Calculations of fractionation factors for carbon and oxygen isotopic exchange in the system calcite-carbon dioxide-water. J Phys Chem 72:800-808

Bottinga Y (1969a) Calculated fractionation factors for carbon and hydrogen isotope exchange in the system calcite-carbon dioxide-graphite-methane-hydrogen-water vapor. Geochim Cosmochim Acta 33:49-64

Bottinga Y (1969b) Carbon isotope fractionation between graphite, diamond and carbon dioxide. Earth Planet Sci Lett 5:301-307

Bottinga Y, Craig H (1969) Oxygen isotope fractionation between CO_2 and water, and the isotopic composition of marine atmospheric CO_2. Earth Planet Sci Lett 5:285-295

Bottinga Y, Javoy M (1973) Comments on oxygen isotope geothermometry. Earth Planet Sci Lett 20:250-265

Bottinga Y, Javoy M (1975) Oxygen isotope partitioning among the minerals and triplets in igneous and metamorphic rocks. Rev Geophys Space Phys 13:401-418

Brandriss ME, O'Neil JR, Edlund MB, Stoermer EF (1998) Oxygen isotope fractionation between diatomaceous silica and water. Geochim Cosmochim Acta 62:1119-1125

Brenninkmeijer CAM, Kraft P, Mook WG (1983) Oxygen isotope fractionation between CO_2 and H_2O. Isotope Geosci 1:181-190

Capuano RM (1992) The temperature-dependence of hydrogen isotope fractionation between clay minerals and water: Evidence from a geopressured system. Geochim Cosmochim Acta 56:2547-2554

Carothers WW, Adami LH, Rosenbauer RJ (1988) Experimental oxygen isotope fractionation between siderite-water and phosphoric acid liberated CO_2-siderite. Geochim Cosmochim Acta 52:2445-2450

Cerrai E, Marchetti C, Renzoni, R, Roseo L, Silvestri M, Villani S (1954) A thermal method for concentrating heavy water. Chem Engin Prog Symp Ser 50, No 11, Nuclear Engineering-Part I, p 271-280

Chacko T (1993) Experimental studies of equilibrium oxygen and carbon isotope fractionation between phases. *In* Luth RW (ed) Experiments at High Pressure and Application to the Earth's Mantle. Mineral Assoc Canada Short Course 21:357-384

Chacko T, Mayeda TK, Clayton RN (1989) Oxygen isotope fractionations in the system gehlenite-calcite. EOS Trans Am Geophys Union 70:489

Chacko T, Mayeda TK, Clayton RN, Goldsmith JR (1991) Oxygen and carbon isotope fractionations between CO_2 and calcite. Geochim Cosmochim Acta 55:2867-2882

Chacko T, Hu X, Mayeda TK, Clayton RN, Goldsmith JR (1996) Oxygen isotope fractionations in muscovite, phlogopite, and rutile. Geochim Cosmochim Acta 60:2595-2608

Chacko T, Riciputi LR, Cole DR, Horita J (1999) A new technique for determining equilibrium hydrogen isotope fractionation factors using the ion microprobe: Application to the epidote-water system. Geochim Cosmochim Acta 63:1-10

Chen C-H, Liu K-K, Shieh Y-N (1988) Geochemical and isotopic studies of bauxitization in the Tatun volcanic area, northern Taiwan. Chem Geol 68:41-56

Chiba H, Kusakabe M, Hirano S, Matsuo S, Somiya S (1981) Oxygen isotope fractionation factors between anhydrite and water from 100 to 550°C. Earth Planet Sci Lett 53:55-62

Chiba H, Chacko T, Clayton RN, Goldsmith JR (1989) Oxygen isotope fractionations involving diopside, forsterite, magnetite, and calcite: Application to geothermometry. Geochim Cosmochim Acta 53:2985-2995

Clayton RN (1963) High-temperature isotopic thermometry. *In* Nuclear Geology on Geothermal Areas. Cons Naz Ric Lab Geol Nucl, p 222-229

Clayton RN (1981) Isotopic thermometry. *In* Newton RC, Navrotsky A, Wood BJ (eds) The Thermodynamics of Minerals and Melts. Springer-Verlag, Berlin, p 85-109.

Clayton RN (1986) High temperature isotope effects in the early solar system. *In* Valley JW, Taylor HP Jr, O'Neil JR (eds) Stable Isotopes in High Temperature Geological Processes. Rev Mineral 16:129-140

Clayton RN, Epstein S (1961) The use of oxygen isotopes in high-temperature geological thermometery. J Geol 69:447-452

Clayton RN, Kieffer SW (1991) Oxygen isotope thermometer calibrations. *In* Taylor HP Jr, O'Neil JR, Kaplan IR (eds) Stable Isotope Geochemistry: A Tribute to Samuel Epstein. Geochem Soc Spec Pub 3:3-10.

Clayton RN, Jones BF, Berner RA (1968) Isotopic studies of dolomite formation under sedimentary conditions. Geochim Cosmochim Acta 32:415-432

Clayton RN, O'Neil JR, Mayeda TK (1972) Oxygen isotope exchange between quartz and water. J Geophys Res 77:3057-3067

Clayton RN, Goldsmith JR, Karel KJ, Mayeda TK, Newton RC (1975) Limits on the effect of pressure on isotopic fractionation. Geochim Cosmochim Acta 39:1197-1201

Clayton RN, Goldsmith JR, Mayeda TK (1989) Oxygen isotope fractionation in quartz, albite, anorthite, and calcite. Geochim Cosmochim Acta 53:725-733

Cole DR, Ripley EM (1999) Oxygen isotope fractionation between chlorite and water form 170 to 350°C: A preliminary assessment based on partial exchange and fluid/rock experiments. Geochim Cosmochim Acta 63:449-457

Compston W, Epstein S (1958) A method for the preparation of carbon dioxide from water vapor for oxygen isotopic analysis. EOS Trans Am Geophys Union 39:511

Craig H, Hom B (1968) Relationships of deuterium, oxygen-18, and chlorinity in the formation of sea ice. EOS Trans Am Geophys Union 216

Criss RE (1991) Temperature-dependence of isotopic fractionation factors. *In* Taylor HP Jr, O'Neil JR, Kaplan IR (eds) Stable Isotope Geochemistry: A Tribute to Samuel Epstein. Geochem Soc Spec Pub 3:11-16

Criss RE (1999) Principles of Stable Isotope Distribution. Oxford Univ Press, New York

Deines P (1977) On the oxygen isotope distribution among triplets in igneous and metamorphic rocks. Geochim Cosmochim Acta 41:1709-1730

Deuser WG, Degens ET (1967) Carbon isotope fractionation in the system CO_2(gas)- CO_2(aqueous)-HCO_3^- (aqueous). Nature 215:1033-1035

Dobson PF, Epstein S, Stolper EM (1989) Hydrogen isotope fractionation between coexisting vapor and silicate glasses and melts at low pressure. Geochim Cosmochim Acta 53:2723-2730

Dove MT, Winkler B, Leslie M, Harris MJ, Salje EKH (1992) A new interatomic model for calcite: applications to lattice dynamics studies, phase transition, and isotopic fractionation. Am Mineral 77:244-250

Downs WF, Touysinhthiphonexay Y, Deines P (1981) A direct determination of the oxygen isotope fractionation between quartz and magnetite at 600 and 800°C and 5 kbar. Geochim Cosmochim Acta 45:2065-2072

Driesner T (1996) Aspects of stable isotope fractionation in hydrothermal solutions. PhD dissertation, ETH-Zürich, 93 p

Driesner T (1997) The effect of pressure on deuterium-hydrogen fractionation in high-temperature water. Science 277:791-794

Driesner T, Seward TM (2000) Experimental and simulation study of salt effects and pressure/density effects on oxygen and hydrogen stable isotope liquid-vapor fractionation for 4 molal NaCl and KCl aqueous solutions to >400°C. Geochim Cosmochim Acta 64:1773-1784

Dugan JP, Borthwick J (1986) Carbon dioxide-water oxygen isotope fractionation factor using chlorine trifluoride and guanidine hydrochloride techniques. Analyt Chem 58:3052-3054

Dugan JP, Borthwick J, Harmon RS, Gagnier MA, Glahn JE, Kinsel EP, MacLeod S, Viglino JA (1985) Guanidine hydrochloride method for determination of water oxygen isotope ratios and the oxygen-18 fractionation between carbon dioxide and water at 25°C. Analyt Chem 57:1734-1736

Dunn SR, Valley JW (1992) Calcite-graphite isotope thermometry: a test for polymetamorphism in marble, Tudor gabbro aureole, Ontario, Canada. J Metam Geol 10:487-501

Eiler JM, Baumgartner LP, Valley JW (1992) Intercrystalline stable isotope diffusion: a fast grain boundary model. Contrib Mineral Petrol 112:543-557

Eiler JM, Kitchen N, Rahn TA (2000) Experimental constraints on the stable-isotope systematics of CO_2 ice/vapor systems and relevance to the study of Mars. Geochim Cosmochim Acta 64:733-746

Elcombe MM, Hulston JR (1975) Calculation of sulphur isotope fractionation between sphalerite and galena using lattice dynamics. Earth Planet Sci Lett 28:172-180

Emiliani C (1955) Pleistocene paleotemperatures. J Geol 63:538-578

Emrich K, Ehhalt DH, Vogel JC (1970) Carbon isotope fractionation during the precipitation of calcium carbonate. Earth Planet Sci Lett 8:363-371

Epstein S, Buchsbaum R, Lowenstam HA, Urey HC (1953) Revised carbonate-water isotopic temperature scale. Geol Soc Am Bull 64:1315-1326

Epstein S, Graf DL, Degens ET (1963) Oxygen isotope studies on the origin of dolomite. *In* Isotope and Cosmic Chemistry. H Craig et al. (eds) North-Holland, Amsterdam, p 169-180

Escande M, Decarreau A, Labeyrie L (1984) Etude experimentale de l'echangeabilite des isotopes de l'oxygene des smectites. C R Acad Sci Paris 299:707-710

Eslinger EV (1971) Mineralogy and oxygen isotope ratios of hydrothermal and low-grade metamorphic argillaceous rocks. PhD Dissertation, Case Western Reserve University, Cleveland, Ohio

Eslinger EV, Savin SM (1973) Mineralogy and oxygen isotope geochemistry of the hydrothermally altered rocks of the Ohaki-Broadlands, New Zealand geothermal area. Am J Sci 273:240-267

Eslinger EV, Savin SM, Yeh H (1979) Oxygen isotope geothermometry of diagenetically altered shales. SEPM Spec Publ 26:285-305

Farquhar J (1995) Strategies for high-temperature oxygen isotope thermometry. PhD Dissertation, University of Alberta

Farquhar J, Chacko T, Frost BR (1993) Strategies for high-temperature oxygen isotope thermometry: a worked example from the Laramie Anorthosite complex Wyoming USA. Earth Planet Sci Lett 117:407-422

Farver JR (1994) Oxygen self-diffusion in calcite: dependence on temperature and water fugacity. Earth Planet Sci Lett 121:575-587

Fayek M, Kyser TK (2000) Low temperature oxygen isotopic fractionation in the uraninite-UO_3-CO_2-H_2O system. Geochim Cosmochim Acta 64:2185-2197

Feng X, Savin SM (1993) Oxygen isotope studies of zeolites - stilbite, analcite, heulandite, and clinoptilolite; III. Oxygen isotope fractionation between stilbite and water or water vapor. Geochim Cosmochim Acta 57:4239-4247

Fontes JC, Gonfiantini R (1967) Fractionnement istopique de l'hydrogene dans l'eau de cristallisation du gypse. C R Acad Sc Paris 265:4-6

Fortier SM, Lüttge A (1995) An experimental calibration of the temperature-dependence of oxygen isotope fractionation between apatite and calcite at high temperature (350-800°C). Chem Geol 125:281-290

Fortier SM, Lüttge A, Satir M, Metz P (1994) Oxygen isotope fractionation between fluorphlogopite and calcite: An experimental investigation of temperature-dependence and F^-/OH^- effects. Eur J Mineral 6:53-65

Fortier SM, Cole DR, Wesolowski DJ, Riciputi LR, Paterson BA, Valley JW, Horita J (1995) Determination of equilibrium magnetite-water oxygen isotope fractionation factor at 350°C: a comparison of ion microprobe and laser fluorination techniques. Geochim Cosmochim Acta 59:3871-3875

Frantz JD, Dubessy J, Mysen B (1993) An optical cell for Raman spectroscopic studies of supercritical fluids and its application to the study of water to 500°C and 2000 bar. Chem Geol 106:9-26

Friedman I, O'Neil JR (1977) Compilation of Stable Isotope Fractionation Factors of Geochemical Interest. U SGeol Surv Prof Paper 440-KK

Friedman I, Gleason J, Sheppard RA, Gude AJ, III (1993) Deuterium fractionation as water diffuses into silicic volcanic ash. *In* Climate Change in Continental Isotopic Records. PK Swart et al. (eds) Am Geophys Union 321-323

Fritz P, Smith DGW (1970) The isotopic composition of secondary dolomites. Geochim Cosmochim Acta 34:1161-1173

Galimov EM (1985) The Biological Fractionation of Isotopes. Academic Press, Orlando, Florida

Garlick GD (1966) Oxygen isotope fractionation in igneous rocks. Earth Planet Sci Lett 1:361-368

Gautason B, Chacko T, Muehlenbachs K (1993) Oxygen isotope partitioning among perovskite ($CaTiO_3$), cassiterite (SnO_2) and calcite ($CaCO_3$). Geol Assoc Canada/ Mineral Assoc Canada Abstr Programs, Edmonton, Alberta, p A34

Gilg HA, Sheppard SMF (1996) Hydrogen isotope fractionation between kaolinite and water revisited. Geochim Cosmochim Acta 60:529-533

Gillet P, McMillan P, Schott J, Badro J, Grzechnik A (1996) Thermodynamic properties and isotopic fractionation of calcite from vibrational spectroscopy of ^{18}O-substituted calcite. Geochim Cosmochim Acta 60:3471-3485

Giletti BJ (1986) Diffusion effects on oxygen isotope temperatures of slowly cooled igneous and metamorphic rocks. Earth Planet Sci Lett 77:218-228

Giletti BJ, Yund RA (1984) Oxygen diffusion in quartz. J Geophys Res 89B:4039-4046

Girard J-P, Savin SM (1996) Intracrystalline fractionation of oxygen isotopes between hydroxyl and non-hydroxyl sites in kaolinite measured by thermal dehydroxylation and partial fluorination. Geochim Cosmochim Acta 60:469-487

Goldsmith JR (1991) Pressure-enhanced Al/Si diffusion and oxygen isotope exchange. *In* Ganguly J (ed) Diffusion, Atomic Ordering and Mass Transport. Springer-Verlag, Berlin, p 221-247

Golyshev SI, Padalko NL, Pechenkin, SA (1981) Fractionation of stable oxygen and carbon isotopes in carbonate systems. Geochem Int'l 18:85-99

Gonfiantini R, Fontes JC (1963) Oxygen isotopic fractionation in the water of crystallization of gypsum. Nature 200:644-646

Graham CM, Sheppard SMF, Heaton THE (1980) Experimental hydrogen isotope studies:hydrogen isotope fractionation in the systems epidote-H_2O, zoisite- H_2O and AlO(OH)-H_2O. Geochim Cosmochim Acta 44:353-364

Graham CM, Sheppard SMF (1980) Experimental hydrogen isotope studies, II. Fractionations in the systems epidote-NaCl-H_2O, epidote-$CaCl_2$-H_2O and epidote-seawater, and the hydrogen isotope composition of natural epidote. Earth Planet Sci Lett 48:237-251

Graham CM, Harmon RS, Sheppard SMF (1984) Experimental hydrogen isotope studies: Hydrogen isotope exchange between amphibole and water. Am Mineral 69:128-138

Graham CM, Viglino JA, Harmon RS (1987) Experimental study of hydrogen-isotope exchange between aluminous chlorite and water and of diffusion in chlorite. Am Mineral 72:566-579

Grinenko VA, Mineyev SD, Devirts AL, Lagutina Ye P (1987) Hydrogen isotope fractionation in the lizardite-water system at 100°C and 1 atm. Geochem Int'l 24:100-104.

Grootes PM, Mook WG, Vogel JC (1969) Isotopic fractionation between gaseous and condensed carbon dioxide. Z Physik 221:257-273

Grossman EL, Ku T-L (1986) Oxygen and carbon isotope fractionation in biogenic aragonite: temperature effects. Chem Geol 59:59-74

Gu Z (1980) Determination of the separation facto for isotopic exchange reaction between H_2O and CO_2 at 25°C. He Huaxue Yu Fangshe Huaxue 2:112-115 (in Chinese)

Halas S, Wolacewicz W (1982) The experimental study of oxygen isotope exchange reaction between dissolved bicarbonate and water. J Chem Phys 76:5470-5472

Halas S, Szaran J, Niezgoda H (1997) Experimental determination of carbon isotope equilibrium fractionation between dissolved carbonate and carbon dioxide. Geochim. Cosmochim. Acta 61:2691-2695

Hamza MS, Epstein S (1980) Oxygen isotopic fractionation between oxygen of different sites in hydroxyl-bearing silicate minerals. Geochim Cosmochim Acta 44:173-182

Hamza MS, Broecker WS (1974) Surface effect on the isotopic fractionation between CO_2 and some carbonate minerals. Geochim Cosmochim Acta 38:669-681

Hariya U, Tsutsumi M (1981) Hydrogen isotopic composition of MnO(OH) minerals from manganese oxide and massive sulfide (Kuroko) deposits in Japan. Contrib Mineral Petrol 77:256-261

Hoering TC (1961) The physical chemistry of isotopic substances: The effect of physical changes in isotope fractionation. Carnegie Inst Washington Yearbook 60:201-204

Hoffbauer R, Hoernes S, Fiorentini E (1994) Oxygen isotope thermometry based on a refined increment method and its application to granulite-grade rocks from Sri Lanka. Precambrian Res 66:199-220

Horibe Y, Craig H (1995) D/H fractionation in the system methane-hydrogen-water. Geochim Cosmochim Acta 59:5209-5217

Horibe Y, Shigehara K, Takakuwa Y (1973) Isotope separation factor of carbon dioxide-water system and isotopic composition of atmospheric oxygen. J Geophys Res 78:2625-2629

Horita J (1989) Stable isotope fractionation factors of water in hydrated saline minerals-brine systems. Earth Planet Sci Lett 95:173-179

Horita J (2001) Carbon isotope exchange in the system CO_2-CH_4 at elevated temperatures. Geochim Cosmochim Acta 65:1907-1919

Horita J, Wesolowski DJ (1994) Liquid-vapor fractionation of oxygen and hydrogen isotopes of water from the freezing to the critical temperature. Geochim Cosmochim Acta 58:3425-3437

Horita J, Wesolowski DJ, Cole DR (1993a) The activity-composition relationship of oxygen and hydrogen isotopes in aqueous salt solutions: I. Vapor-liquid water equilibration of single salt solutions from 50 to 100°C. Geochim Cosmochim Acta 57:2797-2817

Horita J, Cole DR, Wesolowski DJ (1993b) The activity-composition relationship of oxygen and hydrogen isotopes in aqueous salt solutions: II. Vapor-liquid water equilibration of mixed salt solutions from 50 to 100°C and geochemical implications. Geochim Cosmochim Acta 57:4703-4711

Horita J, Cole DR, Wesolowski DJ (1994) Salt effects on stable isotope partitioning and their geochemical implications for geothermal brines. *In* Proc 19th Workshop on Geothermal Reservoir Engineering, Stanford University, p 285-290

Horita J, Cole DR, Wesolowski DJ (1995a) The activity-composition relationship of oxygen and hydrogen isotopes in aqueous salt solutions: III. Vapor-liquid water equilibration of NaCl solutions from to 350°C. Geochim Cosmochim Acta 59:1139-1151

Horita J, Wesolowski DJ, Cole DR (1995b) D/H and $^{18}O/^{16}O$ partitioning between water liquid and vapor in the system H_2O-Na-K-Ca-Mg-Cl-SO_4 from 0 to 350^{o}C. *In* Physical Chemistry of Aqueous Systems: Meeting the Needs of Industry. Proc 12th Int'l Conf on the Properties of Water and Steam. HJ White Jr et al. (eds) Begell House, p 505-510

Horita J, Cole DR, Wesolowski DJ, Fortier SM (1996) Salt effects on isotope partitioning and their geochemical implications: An overview. *In* Proc Todai Int'l Symp on Cosmochronology and Isotope Geoscience, p 33-36

Horita J, Cole DR, Wesolowski DJ (1997) Salt effects on oxygen and hydrogen isotope partitioning between aqueous salt solutions and coexisting phases at elevated temperatures. *In* Proc 5th Int'l Symp on Hydrothermal Reaction*s*. Gatlinburg, Tennessee, p 194-197

Horita J, Driesner T, Cole DR (1999) Pressure effect on hydrogen isotope fractionation between brucite and water at elevated temperatures. Science 286:1545 -1547

Horita J, Cole DR, Polyakov VB, Driesner T (in press) Experimental and theoretical study of pressure effects on hydrogen isotope fractionation in the system brucite-water at elevated temperatures. Geochim Cosmochim Acta

Hu G, Clayton RN (in press) Oxygen isotope salt effects at high pressure and high temperature, and the calibration of oxygen isotope geothermometers. Geochim Cosmochim Acta

James AT, Baker DR (1976) Oxygen isotope exchange between illite and water at 22°C. Geochim. Cosmochim. Acta 40:235-239

Javoy M, Pineau F, Iiyama I (1978) Experimental determination of the isotopic fractionation between gaseous CO_2 and carbon dissolved in tholeiitic magma. Contrib Mineral Petrol 67:35-39

Jenkin GRT, Farrow CM, Fallick AE, Higgins D (1994) Oxygen isotope exchange and closure temperatures in cooling rocks. J Metam Geol 12:221-235

Jibao G, Yaqian Q (1997) Hydrogen isotope fractionation and hydrogen diffusion in the tourmaline-water system. Geochim Cosmochim Acta 61:4679-4688

Kakiuchi M (1994) Temperature-dependence of fractionation of hydrogen isotopes in aqueous sodium chloride solutions. J Sol Chem 23:1073-1087

Kakiuchi M (2000) Distribution of isotopic molecules, H_2O, HDO, and D_2O in vapor and liquid phases in pure water and aqueous solution systems. Geochim Cosmochim Acta 64:1485-1492

Karlsson HR, Clayton RN (1990) Oxygen isotope fractionation between analcime and water: An experimental study. Geochim Cosmochim Acta 54:1359-1368

Kazahaya K (1986) Chemical and isotopic studies on hydrothermal solutions. PhD dissertation, Tokyo Inst Technology

Kawabe I (1978) Calculation of oxygen isotope fractionation in quartz-water system with special reference to the low temperature fractionation. Geochim Cosmochim Acta 42:613-621

Kendall C, Chou. I-M, Coplen TB (1983) Salt effect on oxygen isotope equilibria. EOS Trans Am Geophys Union 64:334-335

Kieffer SW (1982) Thermodynamic and Lattice vibrations of Minerals: 4.Application to phase equilibria, isotope fractionation, and high pressure thermodynamics properties. Rev Geophys Space Phys 20:827-849

Kim S-T, O'Neil JR (1997) Equilibrium and nonequilibrium oxygen isotope effects in synthetic carbonates. Geochim Cosmochim Acta 61:3461-3475

Kitchen NE, Valley JW (1995) Carbon isotope thermometry in marbles of the Adirondack Mountains, New York. J Metam Geol 13:577-594

Kita I, Taguchi S, Matsubaya O (1985) Oxygen isotope fractionation between amorphous silica and water at 34-93°C. Nature 314:83-34

Koehler G, Kyser TK (1996) The significance of hydrogen and oxygen stable isotopic fractionations between carnallite and brine at low temperature: Experimental and empirical results. Geochim Cosmochim Acta 60:2721-2726

Kohn MJ, Valley JW (1998a) Oxygen isotope geochemistry of amphiboles: isotope effects of cation substitutions in minerals. Geochim Cosmochim Acta 62:1947-1958

Kohn MJ, Valley JW (1998b) Effects of cation substitution in garnet and pyroxene on equilibrium oxygen isotope fractionations. J Metam Geol 16:625-639

Kohn MJ, Valley JW (1998c) Obtaining equilibrium oxygen isotope fractionations from rocks: theory and example. Contrib Mineral Petrol 132:209-224

Kotzer TG, Kyser TK, King RW, Kerrich R (1993) An empirical oxygen- and hydrogen-isotope geothermometer for quartz-tourmaline and tourmaline-water. Geochim Cosmochim Acta 57:3421-3426

Kulla JB (1979) Oxygen and hydrogen isotope fractionation factors determined in clay-water systems. PhD Dissertation, University of Illinois at Urbana-Champaign

Kulla JB, Anderson TF (1978) Experimental oxygen isotope fractionation between kaolinite and water. *In* Short Papers of the 4th International Congress, Geochronology, Cosmochronology, Isotope Geology. RE Zartman (ed) U S Geol Surv Open file Report 78-70, p 234-235

Kuroda Y, Hariya Y, Suzuoki T, Matsuo S (1982) D/H fractionation between water and the melts of quartz, K-feldspar, albite and anorthite at high temperature and pressure. Geochem J 16:73-78

Kusakabe M, Robinson BW (1977) Oxygen and sulfur isotope equilibria in the $BaSO_4$-HSO_4^--H_2O system from 110 to 350°C and applications. Geochim Cosmochim Acta 41:1033-1040

Kyser TK (1987) Equilibrium fractionation factors for stable isotopes. *In* Kyser TK (ed) Stable Isotope Geochemistry of Low Temperature Fluids. Mineral Assoc Canada Short Course 13:1-84

Labeyrie L (1974) New approach to surface seawater paleotemperatures using $^{18}O/^{16}O$ ratios in silica of diatom frustules. Nature 248:40-41

Lambert SJ, Epstein S (1980) Stable isotope investigations of an active geothermal system in Valles Caldera, Jemez Mountains, New Mexico. J Volcan Geotherm Res 8:111-129.

Lawrence JR, Taylor HP Jr (1971) Deuterium and oxygen-18 correlation: Clay minerals and hydroxides in Quaternary soils compared to meteoric waters. Geochim Cosmochim Acta 35:993-1003

Lawrence JR, Taylor HP Jr (1972) Hydrogen and oxygen isotope systematics in weathering profiles. Geochim Cosmochim Acta 36:1377-1393

Lecuyer C, Grandjean P, Sheppard SMF (1999) Oxygen isotope exchange between dissolved phosphate and water at temperatures ≤135°C: Inorganic versus biological fractionations. Geochim Cosmochim Acta 63:855-862

Lehmann M, Siegenthaler U (1991) Equilibrium oxygen- and hydrogen-isotope fractionation between ice and water. J Glaciol 37:23-26

Lesniak PM, Sakai H (1989) Carbon isotope fractionation between dissolved carbonate (CO_3^{2-}) and CO_2(g) at 25° and 40°C. Earth Planet Sci Lett 95:297-301

Lichtenstein U, Hoernes S (1992) Oxygen isotope fractionation between grossular-spessartine garnet and water: an experimental investigation. Eur J Mineral 4:239-249

Liu K-K, Epstein S (1984) The hydrogen isotope fractionation between kaolinite and water. Isotope Geosci 2:335-350

Lloyd RM (1968) Oxygen isotope behavior in the sulfate-water system. J Geophys Res 73:6099-6110

Lowenstam HA (1962) Magnetite in denticle capping in recent chitons (polyplacophora). Geol Soc Am Bull 73:435

Majoube M (1971a) Fractionnement en ^{18}O entre la glace et la vapeur d'eau. J Chim Phys 68:625-636

Majoube M (1971b) Fractionnement en oxygene 18 et en deuterium entre l'eau et sa vapeur. J Chim Phys 68:1423-1436

Majzoub M (1966) Une methode d'analyse isotopique de l'oxygene sur des microquantites d'eau determination des coefficients de partage a l'equilibre de l'oxygene 18 entre H_2O et CO_2, D_2O et CO_2. J Chim Phys 63:563-568

Malinin SD, Kropotiva OI, Grinenko VA (1967) Experimental determination of equilibrium constants for carbon isotope exchange in the system CO_2(gas)-HCO_3^-(sol) under hydrothermal conditions. Geochem Int'l 4:764-771

Mandernack KW, Bazylinski DA, Shanks WC III, Bullen TD (1999) Oxygen and iron isotope studies of magnetite produced by magnetotactic bacteria. Science 285:1892-1896

Marumo K, Nagasawa K, Kuroda Y (1980) Mineralogy and hydrogen isotope composition of clay minerals in the Ohnuma geothermal area, northeastern Japan. Earth Planet Sci Lett 47:255-262

Matsubaya O, Sakai H (1973) Oxygen and hydrogen isotopic study on the water of crystallization of gypsum from the Kuroko type mineralization. Geochem J 7:153-165

Matsuhisa Y, Matsubaya O, Sakai H (1971) BrF_5 technique for the oxygen isotopic analysis of silicates and water. Mass Spectrometer 19:124-133

Matsuhisa Y, Goldsmith JR, Clayton RN (1979) Oxygen isotopic fractionation in the system quartz-albite-anorthite-water. Geochim Cosmochim Acta 43:1131-1140

Matsuo S, Friedman I, Smith GI (1972) Studies of Quaternary saline lakes. I. Hydrogen isotope fractionation in saline minerals. Geochim Cosmochim Acta 36:427-435

Mattey DP (1991) Carbon dioxide solubility and carbon isotope fractionation in basaltic melt. Geochim Cosmochim Acta 55:3467-3473

Mattey DP, Taylor WR, Green DH, Pillinger CT (1990) Carbon isotopic fractionation between CO_2 vapour, silicate and carbonate melts: An experimental study to 30 kbar. Contrib Mineral Petrol 104:492-505

Matthews A (1994) Oxygen isotope geothermometers for metamorphic rocks. J Metam Geol 12**:**211-219

Matthews A, Katz A (1977) Oxygen isotope fractionation during the dolomitization of calcium carbonate. Geochim Cosmochim Acta 41:1431-1438

Matthews A, Schliestedt M (1984) Evolution of blueschist and greenschist rocks of Sifnos, Cylades, Greece. Contrib Mineral Petrol 88:150-163

Matthews A, Beckinsale RD, Durham JJ (1979) Oxygen isotope fractionation between rutile and water and geothermometry of metamorphic eclogites. Mineral Mag 43:405-413

Matthews A, Goldsmith JR, Clayton RN (1983a) Oxygen isotope fractionations involving pyroxenes: The calibration of mineral-pair geothermometers. Geochim Cosmochim Acta 47:631-644

Matthews A, Goldsmith JR, Clayton RN (1983b) On the mechanisms and kinetics of oxygen isotope exchange in quartz and feldspars at elevated temperatures and pressures. Geol Soc Am Bull 94:396-412

Matthews A, Goldsmith JR, Clayton RN (1983c) Oxygen isotope fractionation between zoisite and water. Geochim Cosmochim Acta 47:645-654

Matthews A, Palin, JM, Epstein S, Stolper EM (1994) Experimental study of $^{18}O/^{16}O$ partitioning between crystalline albite, albitic glass, and CO_2 gas. Geochim Cosmochim Acta 58:5255-5266

McCrea JM (1950) On the isotopic chemistry of carbonates and a paleotemperature scale. J Chem Phys 18:849-857

McMillan P (1985) Vibrational spectroscopy in the mineral sciences. *In* Kieffer SW, Navrotsky A (eds) Microscopic to Macroscopic—Atomic Environments to Mineral Thermodynamics. Rev Mineral 14:9-63

Melchiorre EB, Criss RE, Rose TP (1999) Oxygen and carbon isotope study of natural and synthetic malachite. Econ Geol 94:245-259

Melchiorre EB, Criss RE, Rose TP (2000) Oxygen and carbon isotope study of natural and synthetic azurite. Econ Geol 95:621-628.

Melchiorre EB, Williams PA, Bevins RE (2001) A low temperature oxygen isotope thermometer for cerussite, with applications at Broken Hill, New South Wales, Australia. Geochim Cosmochim Acta 65:2527-2533

Merlivat L, Nief G (1967) Fractionnement isotopique lors de changements d'etat solide-vapeur et liquide-vapeur de l'eau a des temperatures inferieures a 0°C. Tellus 19:122-127

Mineev SD, Grinenko VA (1996) The pressure influence on hydrogen isotopes fractionation in the serpentine-water system. V M Goldschmidt Conf Abstr 1:404

Mizutani Y, Rafter TA (1969) Oxygen isotopic composition of sulfate-Part 3. Oxygen isotopic fractionation in the bisulfate ion-water system. New Zealand J Sci 12:54-59

Mook WG, Bommerson JC, Staverman WH (1974) Carbon isotope fractionation between dissolved bicarbonate and gaseous carbon dioxide. Earth Planet Sci Lett 22:169-176

Morikiyo T (1984) Carbon isotopic study on coexisting calcite and graphite in the Ryoke metamorphic rocks, northern Kiso district. Contrib Mineral Petrol 87:251-259

Morse PM (1929) Diatomic molecules according to the wave mechamics. II. Vibrational levels. Phys Rev 34:57-64

Müller J (1995) Oxygen isotopes in iron (III) oxides: A new preparation line; mineral-water fractionation factors and paleo-environmental considerations. Isotopes Environ Health Stud 31:301-302

Nahr T, Botz R, Bohrmann G, Schmidt M (1998) Oxygen isotopic composition of low-temperature authigenic clinoptilolite. Earth Planet Sci Lett 160:369-381

Northrop DA, Clayton RN (1966) Oxygen-isotope fractionations in systems containing dolomite. J Geol 74:174-196

Noto M, Kusakabe M (1997) An experimental study of oxygen isotope fractionation between wairakite and water. Geochim Cosmochim Acta 61:2083-2093

Ohmoto H (1986) Stable isotope geochemistry of ore deposits. *In* Valley JW, Taylor HP Jr, O'Neil JR (eds) Stable Isotopes in High Temperature Geological Processes. Rev Mineral 16:491-559

O'Neil, JR (1963) Oxygen isotope fractionation studies in mineral systems. PhD Dissertation, University of Chicago

O'Neil JR (1968) Hydrogen and oxygen isotope fractionation between ice and water. J Phys Chem 723:683-3684.

O'Neil JR (1986) Theoretical and experimental aspects of isotopic fractionation. *In* Valley JW, Taylor HP Jr, O'Neil JR (eds) Stable Isotopes in High Temperature Geological Processes. Rev Mineral 16:1-40

O'Neil JR, Clayton RN (1964) Oxygen isotope geothermometry. *In* Isotope and Cosmic Chemistry (eds., H. Craig et al.) North-Holland, Amsterdam, p157-168

O'Neil JR, Epstein S (1966) A method for oxygen isotope analysis of milligram quantities of water and some of its applications. J Geophys Res 71:4955-4961

O'Neil JR, Taylor HP Jr (1967) The oxygen isotope and cation exchange chemistry of feldspars. J Geophys Res 74:6012-6022

O'Neil JR, Taylor HP Jr (1969) Oxygen isotope equilibrium between muscovite and water. Am Mineral 52:1414-1437

O'Neil JR, Barnes I (1971) C^{13} and O^{18} compositions in some fresh-water carbonates associated with ultramafic rocks and serpentines: western United States. Geochim Cosmochim Acta 35:687-697

O'Neil JR, Truesdell AH (1991) Oxygen isotope fractionation studies of solute-water interactions. *In* Taylor HP Jr, O'Neil JR, Kaplan IR (eds) Stable Isotope Geochemistry: A Tribute to Samuel Epstein, Geochem Soc Spec Pub 3:17-25

O'Neil JR, Clayton RN, Mayeda TK (1969) Oxygen isotope fractionation in divalent metal carbonates. J Chem Phys 51:5547-5558

O'Neil JR, Adami LH, Epstein S (1975) Revised value for the ^{18}O fractionation between CO_2 and water at 25°C. U S Geol Surv J Res 3:623-624

Palin JM, Epstein S, Stolper EM (1996) Oxygen isotope partitioning between rhyolitic glass/melt and CO_2: An experimental study at 550-950°C and 1 bar. Geochim Cosmochim Acta 60:1963-1973

Patel A, Price GD, Mendelssohn MJ (1991) A computer simulation approach to modelling the structure, thermodynamics and oxygen isotope equilibria of silicates. Phys Chem Minerals 17:690-699

Pineau F, Shilobreeva, S, Kadik A, Javoy M (1998) Water solubility and D/H fractionation in the system basaltic andesite-H_2O at 1250°C and between 0.5 and 3 kbars. Chem Geol 147:173-184

Polyakov VB (1997) Equilibrium fractionation of iron isotopes: estimation from Mössbauer spectroscopy data. Geochim Cosmochim Acta 61:4213-4217

Polyakov VB (1998) On anharmonic and pressure corrections to the equilibrium isotopic constants for minerals, Geochim Cosmochim Acta 62:3077-3088

Polyakov VB, Kharlashina NN (1994) Effect of pressure on equilibrium isotopic fractionation. Geochim Cosmochim Acta 58:4739-4750

Polyakov VB, Kharlashina NN (1995) The use of heat capacity data to calculate carbon dioxide fractionation between graphite, diamond, and carbon dioxide: A new approach. Geochim Cosmochim Acta 59:2561-2572

Polyakov VB, Mineev SD (2000) The use of Mössbauer spectroscopy in stable isotope geochemistry. Geochim Cosmochim Acta 64:849-865

Poulson SR, Schoonen MAA (1994) Variations of the oxygen isotope fractionation between $NaCO_3^-$ and water due to the presence of NaCl at 100-300°C. Chem Geol (Isotope Geosci Sec) 116:305-315

Pradahananga TM, Matsuo S (1985a) Intracrystalline site preference of hydrogen isotopes in borax. J Phys Chem 89:72-76

Pradahananga TM, Matsuo S (1985b) D/H fractionation in sulfate hydrate-water systems. J Phys Chem 89:1869-1872

Richet P, Bottinga Y, Javoy M (1977) A review of hydrogen, carbon, nitrogen, oxygen, sulphur, and chlorine stable isotope fractionation among gaseous molecules. Ann Rev Earth Planet Sci 5:65-110

Richet P, Roux J, Pineau F (1986) Hydrogen isotope fractionation in the system H_2O-liquid $NaAlSi_3O_8$: new data and comments on D/H fractionation in hydrothermal experiments. Earth Planet Sci Lett 78:115-120

Richter R, Hoernes S (1988) The application of the increment method in comparison with experimentally derived and calculated O-isotope fractionations. Chem Erde 48:1-18

Rolston JH, Hartog J den, Butler JP (1976) The deuterium isotope separation factor between hydrogen and liquid water. J Phys Chem 80:1064-1067

Romanek CS, Grossman EL, Morse JW (1992) Carbon isotopic fractionation in synthetic aragonite and calcite: Effects of temperature and precipitation rate. Geochim Cosmochim Acta 56:419-430

Rosenbaum JM (1993) Room temperature oxygen isotope exchange between liquid CO_2 and H_2O. Geochim Cosmochim Acta 57:3195-3198

Rosenbaum JM (1994) Stable isotope exchange between carbon dioxide and calcite at 900°C. Geochim Cosmochim Acta 58:3747-3753

Rosenbaum JM (1997) Gaseous, liquid and supercritical H_2O and CO_2: oxygen isotope fractionation behavior. Geochim Cosmochim Acta 61:4993-5003

Rosenbaum JM, Mattey DP (1995) Equilibrium garnet-calcite oxygen isotope fractionation. Geochim Cosmochim Acta 59:2839-2842

Rosenbaum JM, Kyser TK, Walker D (1994) High temperature oxygen isotope fractionation in the enstatite-olivine-$BaCO_3$ system. Geochim Cosmochim Acta 58:2653-2660

Rowe MW, Clayton RN, Mayeda TK (1994) Oxygen isotopes in separated components of CI and CM meteorites. Geochim Cosmochim Acta 58:5341-5347

Rubinson M, Clayton RN (1969) Carbon-13 fractionation between aragonite and water. Geochim Cosmochim Acta 33:997-1002

Rye RO, Stoffregen RE (1995) Jarosite-water oxygen and hydrogen isotope fractionations: Preliminary experimental data. Econ Geol 90:2336-2342

Rye RO, Bethke PM, Wasserman MD (1992) The stable isotope geochemistry of acid-sulfate alteration. Econ Geol 87:240-262

Saccocia PJ, Seewald JS, Shank WC III (1998) Hydrogen and oxygen isotope fractionation between brucite and aqueous NaCl solutions from 250-450°C. Geochim Cosmochim Acta 62:485-492

Sakai H, Tsutsumi M (1978) D/H fractionation factors between serpentine and water at 10° to 500°C and 2000 bar water pressure, and the D/H ratios of natural serpentine. Earth Planet Sci Lett 40:231-242

Satake H, Matsuo S (1984) Hydrogen isotopic fractionation factor between brucite and water in the temperature range from 100 to 510°C. Contrib Mineral Petrol 86:19-24

Sato RK, McMillan PF (1987) Infrared spectra of the isotopic species of alpha quartz. J Phys Chem 91:3494-3498

Savin SM, Lee M (1988) Isotopic studies of phyllosilicates. *In* Bailey SW (ed) Hydrous Phyllosilicates (exclusive of micas). Rev Mineral 19:189-219

Scheele N, Hoefs J (1992) Carbon isotope fractionation between calcite, graphite and CO_2: An experimental study. Contrib Mineral Petrol 112:35-45

Schauble E, Rossman GR, Taylor, HP (2001) Theoretical estimates of equilibrium Fe-isotope fractionations from vibrational spectroscopy. Geochim Cosmochim Acta 65:2487-2497

Schütze H (1980) Der Isotopenindex—eine Inkrementenmethode zur näherungsweisen Berechnung von Isotopenaustauschgleichgewichten zwischen kristallinen Substanzen. Chem Erde 39:321-334

Schwarcz HP (1966) Oxygen isotope fractionation between host and exsolved phases in perthite. Geol Soc Am Bull 77:879-882

Sharp ZD (1995) Oxygen isotope geochemistry of the Al_2SiO_5 polymorphs. Am J Sci 295:1-19

Sharp ZD, Kirschner DL (1994) Quartz-calcite oxygen isotope thermometry: a calibration based on natural isotopic variations. Geochim Cosmochim Acta 58:4491-4501

Sheppard SMF, Schwarcz HP (1970) Fractionation of carbon and oxygen isotopes and magnesium between coexisting metamorphic calcite and dolomite. Contrib Mineral Petrol 26:161-198

Sheppard SMF, Gilg HA (1996) Stable isotope geochemistry of clay minerals. Clay Minerals 31:1-24

Sheppard SMF, Nielsen RL, Taylor HP Jr (1969) Oxygen and hydrogen isotope ratios of clay minerals from porphyry copper deposits. Econ Geol 64:755-777

Shilobreyeva SN, Devirts AL, Kadik AA, Lagutina YP (1992) Distribution of hydrogen isotopes in basalt liquid-water equilibrium at 3 kbar and 1250°C. Geochem Int'l 29:130-134

Shmulovich K, Landwehr D, Simon K, Heinrich W (1999) Stable isotope fractionation between liquid and vapor in water-salt systems up to 600°C. Chem Geol 157:343-354

Smyth JR (1989) Electrostatic characterization of oxygen sites in minerals. Geochim Cosmochim Acta 53:1101-1110

Smyth JR, Clayton RN (1988) Correlation of oxygen isotope fractionations and electrostatic site potentials in silicates. EOS Trans Am Geophys Union 69:1514

Sofer Z (1978) Isotopic composition hydration water in gypsum. Geochim Cosmochim Acta 42:1141-1149

Sofer Z, Gat JR (1972) Activities and concentrations of oxygen-18 in concentrated aqueous salt solutions: Analytical and geophysical implications. Earth Planet Sci Lett 15:232-238

Sofer Z, Gat JR (1975) The isotope composition of evaporating brines: Effects of the isotopic activity ratio in saline solutions. Earth Planet Sci Lett 26:179-186

Sommer MA, Rye D (1978) Oxygen and carbon isotope internal thermometry using benthic calcite and aragonite foraminifera pairs. Short Papers, 4th Int'l Conf. Geochron Cosmochron Isotope Geol, U S Geol Surv Open File Rep. 78-701, p 408-410

Spindel W, Stern MJ, Monse EU (1970) Further study on temperature-dependences of isotope effects. J Chem Phys 52:2022-2035

Staschewski D (1964) Experimentelle bestimmung der O^{18}/O^{16}-trennfaktoren in den systemen CO_2/H_2O und CO_2/D_2O. Berichte Bunsengesell 68:454-459

Stern MJ, Spindel W, Monse EU (1968) Temperature-dependences of isotope effects. J Chem Phys 48:2908-2919

Stewart MK (1974) Hydrogen and oxygen isotope fractionation during crystallization of mirabilite and ice. Geochim Cosmochim Acta 38:167-172

Stewart MK, Friedman I (1975) Deuterium fractionation between aqueous salt solutions and water vapor. J Geophys Res 80:3812-3818

Stoffregen RE, Rye RO, Wasserman MD (1994) Experimental studies of alunite: I. ^{18}O-^{16}O and D-H fractionation factors between alunite and water at 250-450°C. Geochim Cosmochim Acta 58:903-916

Stolper E, Epstein S (1991) An experimental study of oxygen isotope partitioning between silica glass and CO_2 vapor. *In* Taylor HP Jr, O'Neil JR, Kaplan IR (eds) Stable Isotope Geochemistry: A Tribute to Samuel Epstein. Geochem Soc Spec Pub 3:35-51

Suess, VH (1949) Das gleichgewicht $H_2 + HDO = HD + H_2O$ und die weiteren Austauschgleichgewichte im System H_2, D_2, und H_2O. Z Naturforschung 4a:328-332

Sushchevskaya TM, Ustinov VI, Nekrasov IY, Gavrilov YY, Grinenko VA (1985) The oxygen-isoope fractionation factor in cassiterite synthesis. Geochem Int'l 23:57-60

Suzuoki T, Kimura T (1973) D/H and $^{18}O/^{16}O$ fractionation in ice-water system. Mass Spectrom 21:229-233

Suzuoki T, Epstein S (1976) Hydrogen isotope fractionation between OH-bearing minerals and water. Geochim Cosmochim Acta 40:1229-1240

Szaran J (1997) Achievement of carbon isotope equilibrium in the system HCO_3^- (solution)-CO_2 (gas). Chem Geol 142:79-86

Tarutani T, Clayton RN, Mayeda TK (1969) The effect of polymorphism and magnesium substitution on oxygen isotope fractionation between calcium carbonate and water. Geochim Cosmochim Acta 33:987-996

Taube H (1954) Use of oxygen isotope effects in the study of hydration of ions. J Phys Chem 58:523-528
Taylor BE (1976) Origin and significance of C-O-H fluids in the formation of Ca-Fe-Si skarn, Osgood Mountains, Humboldt County, Nevada. PhD Dissertation, Stanford University
Taylor BE, Westrich HR (1985) Hydrogen isotope exchange and water solubility in experiments using natural rhyolite obsidian. EOS Trans Am Geophys Union 66:387.
Taylor HP Jr (1974) The application of oxygen and hydrogen isotope studies to problems of hydrothermal alteration and ore deposition. Econ Geol 69:843-883
Taylor HP Jr, Epstein S (1962) Relationship between O^{18}/O^{16} ratios in coexisting minerals of igneous and metamorphic rocks. Part I. Principles and experimental results. Geol. Soc Am Bull 73:461-480
Tennie A, Hoffbauer R, Hoernes S (1998) The oxygen isotope fractionation behaviour of kyanite in experiment and nature. Contrib Mineral Petrol 133:346-355
Truesdell AH (1974) Oxygen isotope activities and concentrations in aqueous salt solutions at elevated temperatures: Consequences for isotope geochemistry. Earth Planet Sci Lett 23:387-396
Turner JV (1982) Kinetic fractionation of carbon-13 during calcium carbonate precipitation. Geochim Cosmochim Acta 46:1183-1191
Urey HC (1947) The thermodynamic properties of isotopic substances. J Chem Soc (London), p 562-581
Usdowski E, Hoefs J (1993) Oxygen isotope exchange between carbonic acid, bicarbonate, carbonate, and water: A re-examination of the data of McCrea (1950) and an expression for the overall partitioning of oxygen isotopes between the carbonate species and water. Geochim Cosmochim Acta 57:3815-3818
Usdowski E, Michaelis J, Bottcher ME, Hoefs J (1991) Factors for the oxygen isotope equilibrium fractionation between aqueous and gaseous CO_2, carbonic acid, bicarbonate, carbonate, and water (19°C). Z Phys Chemie 170:237-249
Ustinov VI, Grinenko VA (1990) Determining isotope-equilibrium constants for mineral assemblages. Geochem Int'l 27 (10):1-9
Valley JW, O'Neil JR (1981) $^{13}C/^{12}C$ exchange between calcite and graphite: a possible thermometer in Grenville marbles. Geochim Cosmochim Acta 45:411-419
Valley JW, Taylor HP Jr, O'Neil JR (eds) (1986) Stable Isotopes in High Temperature Geological Processes. Rev Mineral, Vol 16
Valley JW, Chiarenzelli JR, McLelland JM (1994) Oxygen isotope geochemistry of zircon. Earth Planet Sci Lett 126:187-206
Van Hook WA (1975) Condensed phase isotope effects, especially vapor pressure isotope effects: aqueous solutions. *In* Rock PA (ed) Isotopes and Chemical Principles. Am Chem Soc Symp 11:101-130.
Vennemann TW, O'Neil JR (1996) Hydrogen isotope exchange between hydrous minerals and molecular hydrogen: I. A new approach for the determination of hydrogen isotope fractionation at moderate temperature. Geochim Cosmochim Acta 60:2437-2451
Vitali F, Longstaffe FJ, Bird MI, Caldwell WGE (2000) Oxygen-isotope fractionation between aluminum-hydroxide phases and water at <60°C: Results of decade-long synthesis experiments. Clays & Clay Minerals 48:230-237
Vitali F, Longstaffe FJ, Bird MI, Gage KL, Caldwell WGE (2001) Hydrogen-isotope fractionation in aluminum hydroxides: Synthesis products versus natural samples from bauxites. Geochim Cosmochim Acta 65:1391-1398
Vogel JC, Grootes PM, Mook WG (1970) Isotopic fractionation between gaseous and dissolved carbon dioxide. Z Phys 230:225-238
Wada H, Suzuki H (1983) Carbon isotopic thermometry calibrated by dolomite-calcite solvus temperatures. Geochim Cosmochim Acta 47:697-706.
Wendt I (1968) Fractionation of carbon isotopes and its temperature-dependence in the system CO_2-gas-CO_2 in solution and HCO_3-CO_2 in solution. Earth Planet Sci Lett 4:64-68
Wenner DB, Taylor HP Jr (1971) Temperatures of serpentinization of ultramafic rocks based on $^{18}O/^{16}O$ fractionations between coexisting minerals and magnetite. Contrib Mineral Petrol 32:165-185
Wenner DB, Taylor HP Jr (1973) Oxygen and hydrogen isotope studies of the serpentinization of ultramafic rocks in oceanic environments and continental ophiolite complexes. Am J Sci 273:207-239
Williams AE, McKibben MA (1989) A brine interface in the Salton Sea geothermal system, California: Fluid geochemical and isotopic characterization. Geochim Cosmochim Acta 53:1905-1920
Xu B-L, Zheng Y-F (1999) Experimental studies of oxygen and hydrogen isotope fractionations between precipitated brucite and water at low temperatures. Geochim Cosmochim Acta 63:2009-2018
Yapp CJ (1987) Oxygen and hydrogen isotope variations among goethites (FeOOH) and the determination of paleotemperatures. Geochim Cosmochim Acta 51:355-364.
Yapp CJ (1990) Oxygen isotopes in iron (III) oxides 1. Mineral-water fractionation factors. Chem Geol 85:329-335
Yapp CJ, Pedley MD (1985) Stable hydrogen isotopes in iron oxides. II. D/H variations among natural goethites. Geochim Cosmochim Acta 49:487-495

Yaqian Q, Jibao G (1993) Study of hydrogen isotope equilibrium and kinetic fractionation in the ilvaite-water system. Geochim Cosmochim Acta 57:3073-3082

Yeh H-W (1980) D/H ratios and late-stage dehydration of shales during burial. Geochim Cosmochim Acta 44:341-352

Yeh H-W, Savin SM (1977) The mechanism of burial metamorphism of argillaceous sediments: 3. Oxygen isotope evidence. Geol Soc Am Bull 88:1321-1330

Zhang C, Liu S, Phelps TJ, Cole DR, Horita J, Fortier SM, Elless M, Valley JW (1997) Physiochemical, mineralogical, and isotopic characterization of magnetite-rich iron oxides formed by thermophilic iron-reducing bacteria. Geochim Cosmochim Acta 61:4621-4632

Zhang CL, Horita J, Cole DR, Zhou J, Lovley DR, Phelps TJ (2001) Temperature-dependent oxygen and carbon isotope fractionations of biogenic siderite. Geochim Cosmochim Acta 65:2257-2271

Zhang L, Liu J, Zhou H, Chen Z (1989) Oxygen isotope fractionation in the quartz-water-salt system. Econ Geol 84:1643-1650

Zhang L, Liu J, Chen Z, Zhou H (1994) Experimental investigations of oxygen isotope fractionation in cassiterite and wolframite. Econ Geol 89:150-157

Zhang J, Quay PD, Wilbur DO (1995) Carbon isotope fractionation during gas-water exchange and dissolution of CO_2. Geochim Cosmochim Acta 59:107-114

Zheng Y-F (1991) Calculation of oxygen isotope fractionation in metal oxides. Geochim Cosmochim Acta 55:2299-2307

Zheng Y-F (1993) Calculation of oxygen isotope fractionation in hydroxyl-bearing silicates. Earth Planet Sci Lett 120:247-263

Zheng Y-F (1996) Oxygen isotope fractionations involving apatites: application to paleotemperature determination. Chem Geol 127:177-187

Zheng Y-F (1997) Prediction of high-temperature oxygen isotope fractionation factors between mantle minerals. Phys Chem Mineral 24:356-364

Zheng Y-F (1999a) Calculation of oxygen isotope fractionation in minerals. Episodes 22:99-106

Zheng Y-F (1999b) Oxygen isotope fractionation in carbonate and sulphate minerals. Geochem J 33:109-126

Zheng Y-F, Metz P, Satir M, Sharp ZD (1994a) An experimental calibration of oxygen isotope fractionation between calcite and forsterite in the presence of a CO_2-H_2O liquid. Chem Geol 116:17-27

Zheng Y-F, Metz P, Satir M (1994b) Oxygen isotope fractionation between calcite and tremolite: An experimental study. Contrib Mineral Petrol 118:249-255

APPENDICES

Appendix 1. Definition of commonly used terms and symbols.

Term	Symbol	Definition
Force (spring) constant	k	spring stiffness
Reduced mass	μ	$m_1m_2/(m_1+m_2)$ diatomic molecules where m is the mass
Planck's constant	h	$6.62608x10^{-34}$ J-sec
Boltzmann's constant	k_b	$1.380658x10^{-23}$J/K
Vibrational frequency	ν	$(1/2\pi)(k/\mu)^{0.5}(sec^{-1})$
Wave number	ω	$\omega = \nu/c$ (cm^{-1})
Velocity of light (vacuum)	c	$2.99792x10^{10}$cm/sec
Frequency shift	$\Delta\nu$	$\nu - \nu^*$
Frequency shift factor	----	$\nu^*/\nu = \omega^*/\omega$
Zero Point Energy	ZPE	$h\nu/2$
Change in ZPE	ΔZPE	ZPE - ZPE* = $h\Delta\nu/2$
Symmetry number	σ	Number of equivalent ways to orient a molecule in space
U	U	$h\nu/k_bT$
Number of atoms in a compound	s	s = number of atoms in a gaseous compound (e.g., s=3 for CO_2), or in the unit cell of crystalline solids (e.g., s = 9 in quartz - Si_3O_6)
r	r	Number of atoms of the element being exchanged in the substance of interest (e.g., r = 2 for oxygen isotope exchange in CO_2; r = 6 in Si_3O_6)
Mass of element	m, m*	Atomic mass of element being exchanged
Partition Function Ratio	Q*/Q	Equation (9) – gases Equation (11) – solids
Reduced Partition Function Ratio	f	$(Q^*/Q)(m/m^*)^{3r/2}$
β value (factor)	β	$f^{1/r}$
Fractionation Factor	α or $10^3 \ln\alpha$	$\alpha_{A-B} = \frac{R_A}{R_B} = \frac{\beta_A}{\beta_B}$ where R is an isotope ratio
Isotope salt effect	Γ	$\Gamma = \frac{\alpha_{\text{A-aqueous soln}}}{\alpha_{\text{A-pure water}}}$ where A is a reference phase

The asterisk in all cases denotes a substance made with the heavy isotope

Appendix 2. Oxygen isotope fractionation factors: calibrations based on experiments or natural samples.

#	Phases	Reference	[1]Method	[2]1000 ln α	T(°C)	Comments
	Gases, Liquid, Ice:					
1	H_2O: ice-vapor	Majoube (1971a)	Ex	11839/T-28.224	-33.4 - 0	
2	H_2O: ice-liquid	O'Neil (1968)	Ex	+3.0	0?	Slow growth of ice in a stirred water.
3	H_2O: ice-liquid	Craig and Hom (1968)	Ex	+2.65,+2.70	0?	Freezing from 4‰ chlorinity and seawater.
4	H_2O: ice-liquid	Suzuki and Kimura (1973)	Ex	+2.8±0.1	0?	
5	H_2O: ice-liquid	Stewart (1974)	Ex	+2.2	-10	Freezing from 2.5m NaCl soln.
6	H_2O: ice-liquid	Lehmann and Siegenthaler (1991)	Ex	+2.91±0.03	0	Slow growth of ice in a stirred water.
7	H_2O: liquid-vapor	Majoube (1971b)	Ex	$1.137\ (10^6/T^2) - 0.4156\ (10^3/T) - 2.0667$	0-100	Slow distillation of liquid water.
8	H_2O: liquid-vapor	Horita and Wesolowski (1994), and all references therein	Ex	$-7.685 + 6.7123\ (10^3/T) - 1.6664\ (10^6/T^2) + 0.35041\ (10^9/T^3)$	0-374	High precision experimental calibration using three different apparatus to cover the full temperature range. This large dataset was combined with selected earlier experimental studies to generate the calibration curve.
9	CO_2:solid-vapor	Eiler et al. (2000)	Ex	2868/T–14.5	130-150(K)	By sublimation-condensation and isotopic exchange.
10	CO_2:liquid-vapor	Grootes et al. (1969)	Ex	+0.06 to +1.03	220-303(K)	Liquid-vapor equilibration for >4 hr.
11	CO_2(liq)- H_2O(l)	Rosenbaum (1993)	Ex	+41.94±0.27	25.3	Direct exchange at P=100-200 bar.
12	CO_2-H_2O(l)	Compton and Epstein (1958), Staschewski (1964), Mazjoub (1966), O'Neil and Epstein (1966), Bottinga and Craig (1969), Matsuhisa et al. (1971), Blattner (1973), Horibe et al. (1973), O'Neil et al. (1975), Gu (1980), Brenninkmeijer et al. (1983), Dugan et al. (1985), and Dugan and Borthwick (1986)	Ex	+39.89 to +41.53 $10^3(\alpha-1) = 17604/T - 17.93$ (Brenninkmeijer et al., 1983)	25 5-100	Large number of measurements at room temperature. Brenninkmeijer et al. combined their own and earlier experimental results. Fractionations adjusted such that $\alpha(CO_2\text{-}H_2O)$ at 25°C = 1.0412.
13	CO_2-H_2O(l)	Truesdell (1974)	Ex	$3.97\ (10^6/T^2) + 0.31$	130-350	Experiments at P=28 bars. Fractionations adjusted to $\alpha(CO_2\text{-}H_2O)$ at 25°C = 1.0412.
	Dissolved Species:					
14	CO_2 (aq)- H_2O	Usdowski and Hoefs (1993)	Ex	+56.3	19	Based on data by McCrea (1950) and Usdowski et al. (1991).
15	H_2CO_3 (aq)- H_2O	Usdowski and Hoefs (1993)	Ex	+38.7, +38.8	19, 25	Based on data by McCrea (1950) and Usdowski et al. (1991).
16	HCO_3^- (aq)- H_2O	Usdowski and Hoefs (1993)	Ex	+34.0, +34.5	19, 25	Based on data by McCrea (1950) and Usdowski et al. (1991).
17	CO_3^{2-} (aq)- H_2O	Usdowski and Hoefs (1993)	Ex	+18.1, +18.2	19, 25	Based on data by McCrea (1950) and Usdowski et al. (1991).
18	HCO_3^- (aq)- H_2O	Halas and Wolacewicz (1982)	Ex	$2.92\ (10^6/T^2) - 2.66$	25-45	0.03m $NaHCO_3$ soln.
19	$NaCO_3^-$ (aq)- H_2O	Poulson and Schoonen (1994)	Ex	$2.7\ (10^6/T^2) - 5.7$	100-300	0.1M Na_2CO_3+0.1M NaOH+0-4M NaCl soln.
20	HSO_4^-(aq)- H_2O	Lloyd (1968)	Ex	$3.251\ (10^6/T^2) - 5.6$	72.5-348	Direct exchange between dissolved Na_2SO_4 and water at pH=4-9.
21	HSO_4^-(aq)- H_2O	Mizutani and Rafter (1969)	Ex	$2.88\ (10^6/T^2) - 4.1$	110-200	Direct exchange between dissolved H_2SO_4 and water.
22	$H_2PO_4^-$(aq)- H_2O	Lecuyer et al. (1999)	Ex	$18.35\ (10^3/T) - 32.29$	75-135	Direct exchange between dissolved KH_2PO_4 and water at pH=5. 28-100% exchange. Extrapolated values more than 10‰ greater than results of biogenic phosphates.

	Hydrated Salts:					
23	carnallite($KMgCl_3 \cdot 6H_2O$) – H_2O	Horita (1989)	Ex	+7.5 to +8.8	10-40	By precipitation and aging 30-67 days. Determined on the activity scale of brines.
24	carnallite($KMgCl_3 \cdot 6H_2O$) – H_2O	Koehler and Kyser (1996)	Ex	-0.1 to +1.3	22-45	By synthesis and exchange.
25	bischofite($MgCl_2 \cdot 6H_2O$) – H_2O	Horita (1989)	Ex	+7.6 to +8.2	10-40	By precipitation and aging 30-67 days. Determined on the activity scale of brines.
26	tachyhydrite($CaMg_2Cl_6 \cdot 12H_2O$) – H_2O	Horita (1989)	Ex	+9.5	25	By precipitation and aging 30-67 days. Determined on the activity scale of brines.
27	gypsum ($CaSO_4 \cdot 2H_2O$)- H_2O	Gonfiantini and Fontes (1963), and Matsubaya and Sakai (1973), and Sofer (1978)	Ex	+2.9 to +4.1	17-57	Slow precipitation.
28	mirabilite ($Na_2SO_4 \cdot 10H_2O$)- H_2O	Stewart (1974)	Ex	+1.4 to +2.0	0-25	Synthesis from aqueous solutions. Determined on the composition scale of brine.
	Carbonates:					
29	aragonite/calcite-H_2O	McCrea (1950)	Ex	$\delta^{18}O=15.7\ (10^3/T) - 54.2$ (Florida seawater) $\delta^{18}O=16.4\ (10^3/T) - 57.6$ (Cape Cod seawater)	-1.2 to 79.8	Slow precipitation by CO_2 degassing.
30	calcite-H_2O	Epstein et al. (1953)	Mx	$2.73\ (10^6/T^2) - 2.71$	7-30	Combination of data obtained from biogenic precipitation of calcite in tank experiments and analysis of natural samples. Regression line fit through data given in Epstein et al. (1953) after recalculation following the method outlined in Tarutani et al. (1969).
31	calcite-H_2O	O'Neil et al. (1969)	Ex	$2.78\ (10^6/T^2) – 2.89$ corrected in Friedman and O'Neil (1977)	0-500	200-500°C experiments involved exchange between carbonate minerals and ammonium chloride solutions. P=1 kbar. Experiments at 0 and 25 involved controlled precipitation of carbonate minerals from bicarbonate solutions. P= 1 atm. 100% exchange in all experiments.
	calcite-H_2O	Clayton et al. (1975)	Ex	1.22 - 1.33 (500°) 0.01 - 0.10 (700°C)	500, 700	Pressure effects investigated to 20 kbars in pure water.
32	strontianite ($SrCO_3$)-H_2O	O'Neil et al. (1969)	Ex	$2.69\ (10^6/T^2) - 3.24$ corrected in Friedman and O'Neil (1977)	0-500	As above.
33	witherite ($BaCO_3$) - H_2O	O'Neil et al. (1969)	Ex	$2.57\ (10^6/T^2) - 4.23$ corrected in Friedman and O'Neil (1977)	0-500	As above.
34	cerrusite ($PbCO_3$) - H_2O	O'Neil et al. (1969)	Ex	4.51, 6.92	240, 201	No equation given.
35	rhodochrosite ($MnCO_3$) - H_2O	O'Neil et al. (1969)	Ex	6.76	240	As above.
36	otavite ($CdCO_3$) - H_2O	O'Neil et al. (1969)	Ex	2.95, 5.97	320, 250	As above.

37	calcite-H_2O	Kim and O'Neil (1997)	Ex	18.03 (10^3/T) - 32.42	10-40	Low-T controlled precipitation experiments.
38	witherite ($BaCO_3$) - H_2O	Kim and O'Neil (1997)	Ex	2.63 ($10^6/T^2$) - 4.04	0-500	Low-T controlled precipitation experiments combined with the high-T experiments of O'Neil et al. (1969). Revised acid fractionation factors used in recalculating the isotopic compositions of $BaCO_3$ determined in O'Neil et al. (1969).
39	otavite ($CdCO_3$) - H_2O	Kim and O'Neil (1997)	Ex	2.76 ($10^6/T^2$) - 3.96	0-500	As above.
40	siderite ($FeCO_3$)- H_2O	Carothers et al. (1988)	Ex	3.13($10^6/T^2$) - 3.50	33-197	Slow addition of $FeCl_2$ soln to $NaHCO_3$ soln.
41	siderite ($FeCO_3$)- H_2O	Zhang et al. (2001)	Ex	2.56 ($10^6/T^2$) + 1.69	45-75	Based on microbial siderite precipitated by thermophilic Fe(III)-reducing bacteria in culture.
42	malachite ($CuCO_3Cu(OH)_2$)- H_2O	Melchiorre et al. (1999)	Ex	2.66 ($10^6/T^2$) + 2.66	0-50	Replacement of calcite with Cu^{2+}-bearing soln.
43	azurite ($(CuCO_3)_2Cu(OH)_2$)- H_2O	Melchiorre et al. (2000)	Ex	2.67 ($10^6/T^2$) + 4.75	10-45	Replacement of calcite with Cu^{2+}-bearing soln.
44	cerussite($PbCO_3$)- H_2O	Melchiorre et al. (2001)	Ex	2.63 ($10^6/T^2$) - 3.58	20-65	Replacement of calcite with Pb^{2+}-bearing soln.
45	norsethite ($BaMg(CO_3)_2$) - H_2O	Bottcher (2000)	Ex	2.83 ($10^6/T^2$) - 2.85	20-90	Formed from $BaCO_3$ and $MgCO_3 3H_2O$ in $NaHCO_3$ soln.
46	hydromagnesite($Mg_4(OH)_4(CO_3)_3$)- H_2O	O'Neil et al. (1971)	Ex	+31.19, +37.08	0, 25	Slow precipitation from $Mg(HCO_3)_2$ soln.
47	dolomite-H_2O	Clayton et al. (1968)	N	+34.5	20±5	Based on sedimentary dolomite from Deep Springs Lake, California.
48	dolomite-H_2O	Northrop and Clayton (1966)	Ex	3.20 ($10^6/T^2$) - 2.00	300-510	Direct exchange. 3-50% exchange. P= 1 kbar.
49	dolomite-H_2O	Matthews and Katz (1977)	Ex	3.06 ($10^6/T^2$) - 3.24	252-295	Hydrothermal dolomitization of calcite or aragonite in the presence of Ca-Mg-Sr chloride solutions. P= 1 atm.
50	protodolomite-H_2O	Fritz and Smith (1970)	Ex	+23.4 to +31.6 3.2 ($10^6/T^2$) – 2.0	25-78.6	Precipitated from a Ca-Mg-CO_3 soln. The equation is based on extrapolation to the 25°C datum of Clayton et al. (1968).
51	CO_2-calcite	O'Neil and Epstein (1966)	Ex	1.93 ($10^6/T^2$) + 3.92	350-610	Direct exchange experiments using very large calcite to CO_2 ratio. Measured values may represent surface fractionations rather than true equilibrium fractionations. P=0.3 bars.
52	CO_2-dolomite	O'Neil and Epstein (1966)	Ex	1.31 ($10^6/T^2$) + 3.62	350-610	As above.
53	CO_2-calcite	Chacko et al. (1991)	Ex	$-0.038435 + 5.0077x - 1.0703x^2 + 0.15452x^3 - 0.014366x^4 + 0.00073624x^5 - 0.000015567x^6$, where $x=10^6/T^2$	400-800	Direct exchange. 39-94% exchange. P=10 kbar. Equation represents theoretical calculations that closely fit the experimental data. The equation reproduces the calculated fractionations from 273-4000K.
54	CO_2-calcite	Scheele and Hoefs (1992)	Ex	5.92-2.31	500-1200	Aragonite starting material inverted to calcite during the experiment. No equation given but fractionations generally larger than those given by Chacko et al. (1991) by ~0.5‰.

55	CO_2-calcite	Rosenbaum (1994)	Ex	3.30	900	Direct exchange. 97% exchange. P=12.5 kbar
56	aragonite-calcite	Tarutani et al. (1969)	Ex	0.6	25	Combination of data from experiments in which calcite or aragonite were slowly precipitated from aqueous bicarbonate solutions.
57	aragonite-calcite	Grossman and Ku (1986)	N	0.76 - 0.017T(°C)	0-25	Based on the analysis of aragonitic foraminifer *Hogelundia* and coexisting calcitic foraminifer *Uvigerina*. Large scatter about the regression line indicates that the apparent temperature dependence is not statistically significant.
58	dolomite-calcite	Epstein et al. (1963)	Ex	+0.9	550	Dolomitization of natural calcite with $CaCl_2$ soln
59	dolomite-calcite	Northrop and Clayton (1966)	Ex	0. 50 ($10^6/T^2$)	300-510	Combination of dolomite-H_2O experiments of Northrop and Clayton (1966) and calcite-H_2O experiment of O'Neil (1963).
60	dolomite-calcite	O'Neil and Epstein (1966)	Ex	0.56 ($10^6/T^2$) + 0.45	350-610	Combination of CO_2-calcite and CO_2-dolomite experiments.
61	dolomite-calcite	Sheppard and Schwarz (1970)	N	0.45 ($10^6/T^2$) - 0.40	100-650	Based on analysis of co-existing calcite-dolomite pairs in regionally metamorphosed marbles and calcareous schists. Temperatures derived from calcite-dolomite solvus thermometry.
	Silica Group:					
62	quartz-calcite	Clayton et al. (1989)	Ex	0.38 ($10^6/T^2$)	600-1000	Direct exchange. 72-99% exchange. P=15 kbar.
63	quartz-calcite	Sharp and Kirschner (1994)	N	0.87 ($10^6/T^2$)	100-700	Primarily based on analyses of low-grade marbles and veins.
64	quartz-H_2O	Clayton et al. (1972)	Ex	2.51 ($10^6/T^2$) - 1.96	500-750	Direct exchange. 100% exchange. P=1 kbar.
65	quartz- H_2O	Bottinga and Javoy (1973)	Mx	4.10 ($10^6/T^2$) - 3.7	500-800	Based on selected experimental data from Clayton et al. (1972), theoretical considerations and data from natural samples.
66	quartz-H_2O	Matsuhisa et al. (1979)	Ex	2.05 ($10^6/T^2$) - 1.14	500-800	Direct exchange. 87-100% exchange. P=15 kbar.
67	quartz-H_2O	Matsuhisa et al. (1979)	Ex	3.34 ($10^6/T^2$) - 3.31	250-500	Direct exchange. 36-87% exchange. P=15 kbar.
68	quartz-H_2O	Matthews et al. (1983b)	Ex	1.44, 3.99, 9.12	600, 400, 250	Three isotope technique. No equation given but data fits equation of Matsuhisa et al (1979).
69	quartz-H_2O	Zhang et al. (1989)	Ex	3.306 ($10^6/T^2$) – 2.71	180-550	Conversion of silica gel to quartz in up to 40wt-% NaCl, NaF, and KCl. Little salt effect observed.
70	amorphous silica-H_2O	Kita et al. (1985)	Ex	3.52 ($10^6/T^2$) - 4.35	34-93	Based on the analysis of amorphous silica precipitating in geothermal power plant waters.
71	biogenic silica-H_2O	Labeyrie (1974)	N	41.2 - 0.25T(°C)	4-27	Based on the analysis of sponge spicules and diatoms formed under known conditions.
72	biogenic silica-water	Brandriss et al. (1998)	Ex	15.56 (10^3/T)-20.92	3.6-20.0	Based on cultured fresh water diatoms. 3-4‰ smaller than Labeyrie (1974).
73	quartz-microcline	Blattner and Bird (1974)	Ex	1.8	600	Quartz and alkali feldspar directly exchanged in the presence of a common water or KCl solution.
74	quartz-cassiterite(SnO_2)	Zhang et al. (1994)	Ex	+8.5, +6.9	400, 500	Reaction between silica gel and amorphous SnO_2 in the presence of water.
	Feldspars:					
75	albite-calcite	Clayton et al. (1989)	Ex	-0.56 ($10^6/T^2$)	600-800	Direct exchange. 88-100% exchange. P=11-16 kbar.
76	albite-H_2O	O'Neil and Taylor (1967)	Ex	2.91 ($10^6/T^2$) - 3.41	350-800	Alkali exchange with aqueous chloride solutions. Found no difference in the fractionation behavior of Na- and K-feldspar. 100% exchange. P=1 kbar.

77	albite-H_2O	Bottinga and Javoy (1973)	Mx	3.13 ($10^6/T^2$) - 3.7	500-800	Based on experimental data from O'Neil and Taylor (1967), theoretical considerations and data from natural samples.
78	albite-H_2O	Matsuhisa et al. (1979)	Ex	1.59 ($10^6/T^2$) - 1.16	500-700	Direct exchange. 79-100% exchange. P=7-15 kbar. P=7-12 kbar.
79	albite-H_2O	Matsuhisa et al. (1979)	Ex	2.39 x$10^6/T^2$-2.51	400-500	Direct exchange. 50-79% exchange. P=12 kbar.
80	albite-H_2O	Matthews et al. (1983b)	Ex	0.95, 1.38	600, 500	Three isotope technique. No equation given but data fits equation of Matsuhisa et al (1979). P=15 kbar.
81	anorthite-calcite	Clayton et al. (1989)	Ex	-1.59 ($10^6/T^2$)	600-800	Direct exchange. 95-100% exchange. P=9-12 kbar.
82	anorthite-H_2O	O'Neil and Taylor (1967)	Ex	2.15 ($10^6/T^2$) - 3.82	500-800	Exchange of Ba feldspar or anorthite with $CaCl_2$ solutions. 96-100% exchange. P=1 kbar.
83	anorthite-H_2O	Bottinga and Javoy (1973)	Mx	2.09 ($10^6/T^2$) ^{2}- 3.70	500-800	Based on experimental data from O'Neil and Taylor (1967), theoretical considerations and data from natural samples.
84	anorthite-H_2O	Matsuhisa et al. (1979)	Ex	1.04 ($10^6/T^2$) - 2.01	500-750	Direct exchange. 100% exchange. P=4-10 kbar.
85	anorthite-H_2O	Matsuhisa et al. (1979)	Ex	1.49 ($10^6/T^2$) - 2.81	400-500	Direct exchange. 95-100% exchange. P=2-4 kbar.
86	anorthite-H_2O	Matthews et al. (1983b)	Ex	-1.31	600	Three isotope technique. Less than 50% exchange. P=7 kbar.
	Olivine:					
87	forsterite-calcite	Chiba et al. (1989)	Ex	-3.29 ($10^6/T^2$)	700-1300	Direct exchange. 61-100% exchange. P= 15-16 kbar.
88	forsterite-calcite	Zheng et al. (1994a)	Ex	-3.17 ($10^6/T^2$) - 0.44	600-900	Exchange of forsterite and calcite in the presence of a CO_2-H_2O fluid. 60-90% exchange. P=3-12 kbar.
89	forsterite-$BaCO_3$	Rosenbaum et al. (1994)	Ex	-1.95, -1.7, -2.12, -1.32, -1.16	1009-1409 in 100°C increments	No equation given but all points are similar to forsterite-calcite fractionations of Chiba et al. (1989) except the 1209°C datum.
	Garnet:					
90	grossular/andradite-calcite	Rosenbaum and Mattey (1995)	Ex	-2.77 ($10^6/T^2$)	800-1200	Direct exchange between $grossular_{0.7}$ $andradite_{0.19}$ $pyrope_{0.03}$ garnet and calcite. 60-97% exchange. P=23 kbar.
91	grossular-H_2O	Taylor (1976)	Ex	-1.6	600	Hydrothermal synthesis of grossular from gel. P= 2 kbar.
92	andradite-H_2O	Taylor (1976)	Ex	-3.28	600	Hydrothermal synthesis of andradite from gel. P= 2 kbar.
93	grossular/spessartine-H_2O	Lichtenstein and Hoernes (1992)	Ex	-2.1	750	Direct exchange between grossular and spessartine rich garnet and water. Both sets of experiments yielded nearly identical fractionation factors. 56-59% exchange. P=16 kbar. Synthesis experiments at 750°C yield a spessartine-H_2O fractionation of –2.5.
94	grossular- H_2O	Matthews (1994)	Ex	-1.77, -1.51	700, 800	Direct exchange of grossular with 0.86M NaF solution. 90-92% exchange. P=1.6-2.0 kbar. No equation given.
95	grossular-andradite	Kohn and Valley (1998b)	N	0.6 to 0.8	727	Based on analysis of coexisting garnet-wollastonite pairs in granulite-facies calc-silicates.
96	garnet-quartz	Bottinga and Javoy (1975)	N	-2.88 ($10^6/T^2$)	>500	Based on quartz-garnet data on natural samples where temperatures for those samples were determined by the Bottinga and Javoy (1973) calibrations of the feldspar-quartz, feldspar-muscovite or feldspar-magnetite isotope thermometers.

97	garnet-zircon	Valley et al. (1994)	N	0	800-1000	Based on analysis of garnet-zircon pairs from the Adirondack mountains.
	Aluminosilicate					
98	kyanite-calcite	Tennie et al. (1998)	Ex	-2.62 ($10^6/T^2$)	625-725	Isotopic exchange induced by polymorphic inversion of andalusite to kyanite in the presence of calcite. P=13 kbar.
99	kyanite-quartz	Sharp (1995)	N	-2.17 ($10^6/T^2$)	535-1300	Based on the analysis of coexisting quartz, kyanite and garnet and an assumed Δ(qtz-grt) = $3.1x10^6/T^2$.
100	sillimanite-quartz	Sharp (1995)	N	-2.36 ($10^6/T^2$)	535-1300	Based on the analysis of coexisting quartz, sillimanite and garnet and an assumed Δ(qtz-grt) = $3.1x10^6/T^2$.
	Sorosilicates					
101	zoisite-H_2O	Matthews et al. (1983c)	Ex	0.49, 0.20, -0.33, -0.5, -0.62	400, 450, 500, 600, 700	Direct exchange at 600 and 700°C using the three isotope method. 54-65% exchange. Synthesis from glass in 400-600°C experiments. Results from direct exchange and synthesis experiments agree at 600. No equation given.
102	epidote-quartz	Matthews and Schliestedt (1984)	Ex	- (1.56 + 1.92β_{Ps})($10^6/T^2$)		Based on the experimental zosite-water and quartz-water calibrations of Matthews et al. (1983b) and Matsuhisa et al. (1979). Effect of Fe^{3+} substitution is estimated using the grossular/andradite data of Taylor (1976). β_{Ps} is the mole fractionation of pistacite ($Ca_2Fe_3Si_3O_{12}OH$) component in the epidote.
103	gehlenite-calcite	Chacko et al. (1989)	Ex	-3.12 ($10^6/T^2$)	700-1000	Direct exchange. 90-100% exchange. P=15 kbar.
	Cyclosilicates:					
104	tourmaline-quartz	Kotzer et al. (1993)	N	-1.0 ($10^6/T^2$) – 0.39	200-600	Based on the analysis of co-existing quartz, muscovite and tourmaline from several ore deposits. Temperatures based on quartz-muscovite fractionations compiled by Eslinger et al. (1979).
	Pyroxenes:					
105	diopside-calcite	Chiba et al. (1989)	Ex	-2.37 ($10^6/T^2$)	600-1200	Direct exchange. 61-100% exchange. P=15-16 kbar.
106	enstatite- $BaCO_3$	Rosenbaum et al. (1994)	Ex	-0.97, -1.20, -1.5, -1.2, -1.11	1009-1409 in 100°C increments	Direct exchange. 91-100% exchange. P= 30 kbar. No equation given. Experimental data are non-linear with respect to $1/T^2$ even at these high temperatures.
107	diopside-H_2O	Matthews et al (1983a)	Ex	-1.27, -1.08, -0.98	600, 700, 800	Direct exchange using three-isotope method. 55- 79% exchange. P=13-18 kbar. No equation given.
108	wollastonite- H_2O	Matthews et al (1983a)	Ex	-1.41, -1.37, -1.19, -1.03	500, 600, 700, 800	Direct exchange using three-isotope method. 46-100% exchange. P=9-20 kbar. No equation given.
109	hedenbergite- H_2O	Matthews et al (1983a)	Ex	-1.00	700	Direct exchange using three-isotope method. 52-73% exchange. P=13 kbar. No equation given.
110	jadeite- H_2O	Matthews et al (1983a)	Ex	0.37, 0.21	500, 600	Direct exchange using three-isotope method. 20-39% exchange. P=16-18 kbar. No equation given.
	Amphiboles:					
111	tremolite-calcite	Zheng et al. (1994b)	Ex	-3.80 ($10^6/T^2$) + 1.67	520-680	Exchange of tremolite and calcite in the presence of a CO_2-H_2O fluid. 48-81% exchange. P=3-10 kbar. Extrapolation to equilibrium fractionations at 520, 560, 580°C are suspect because of unequal exchange rates in companion experiments at each of those temperatures.

112	amphibole-quartz	Bottinga and Javoy (1975)	N	$-3.15\ (10^6/T^2) + 0.30$	>500	Based on natural quartz-amphibole data where temperatures were determined by the Bottinga and Javoy (1973) calibrations of the feldspar-quartz, feldspar-muscovite or feldspar-magnetite isotope thermometers.
	Micas:					
113	muscovite-calcite	Chacko et al. (1996)	Ex	$-0.99\ (10^6/T^2)$	550-650	Direct exchange. 80-100% exchange. P=15 kbar. Linear equation fit through the origin. Equation should not be extrapolated below 500°C.
114	phlogopite-calcite	Chacko et al. (1996)	Ex	$-1.78\ (10^6/T^2)$	650-800	Direct exchange. 98-100% exchange. P=15 kbar. Equation as in muscovite-calcite.
115	fluorophlogopite-calcite	Chacko et al. (1996)	Ex	$-1.26\ (10^6/T^2)$	500-800	Direct exchange. 44-90% exchange. P=15 kbar. Equation as in muscovite-calcite. Fluorophlogopite has F/(F+OH)=1
116	fluorophlogopite-calcite	Fortier et al. (1994)	Ex	$-1.84\ (10^6/T^2) + 0.43$	400-800	Direct exchange. 31-91% exchange. P=11 kbar. Equation as in muscovite-calcite. Fluorophlogopite has F/(F+OH)=0.75. Experimental data for this mixed fluoro-hydroxy phlogopite fall in between the equations for end-member hydroxy- and flurophlogopite-calcite fractionations given by Chacko et al. (1996).
117	muscovite-H_2O	O'Neil and Taylor (1969)	Ex	$2.38\ (10^6/T^2) - 3.89$	400-650	Experiments involved synthesis of muscovite from gels or reaction of paragonite or kaolinite with KCl solutions.
118	muscovite-H_2O	Bottinga and Javoy (1973)	Mx	$1.90\ (10^6/T^2) - 3.10$	500-800	Based on the experimental data of O'Neil and Taylor (1969), natural samples, and theoretical estimate of the effect of OH groups on fractionation behavior.
119	muscovite-quartz	Matthews and Schliestedt (1984)	Ex	$-1.55\ (10^6/T^2)$	500-650	Based on the experimental muscovite-water and quartz-water calibrations of O'Neil and Taylor (1969) and Matsuhisa et al. (1979) with a straight line constrained to go through the origin.
120	biotite-quartz	Bottinga and Javoy (1975)	N	$-3.69\ (10^6/T^2) + 0.60$		Based on natural quartz-biotite data where temperatures were determined by the Bottinga and Javoy (1973) calibrations of the feldspar-quartz, feldspar-muscovite or feldspar-magnetite isotope thermometers.
	Other Hydrous Phyllosilicates:					
121	chlorite- H_2O	Wenner and Taylor (1971)	N	$1.56\ (10^6/T^2) - 4.70$	150-400	Based on the analysis of natural chlorites and coexisting minerals in metasediments.
122	chlorite- H_2O	Cole and Ripley (1999)	Ex	$2.693\ (10^9/T^3)$ $- 6.342\ (10^6/T^2)$ $+ 2.969\ (10^3/T)$	150-400	Direct exchange at 350°C. 12% exchange. P=0.25 kbar. This high temperature datum is combined with results from granite-fluid experiments at 170-300°C in which chlorite is formed by alteration of biotite.
123	kaolinite- H_2O	Eslinger (1971)	Mx	$2.50\ (10^6/T^2) - 2.87$	0-350	Combination of single sample of hydrothermal kaolinite from Broadlands, New Zealand and model calculations.
124	kaolinite- H_2O	Kulla and Anderson (1978)	Ex	$2.42\ (10^6/T^2) - 4.45$	170-320	Hydrothermal synthesis of kaolinite from gels.

125	kaolinite- H_2O	Sheppard and Gilg (1996)	Mx	2.76 ($10^6/T^2$) - 6.75	0-350	Regression line fit through a combination of experimental data (Kulla and Anderson, 1978) and various natural occurrences.
126	smectite- H_2O	Escande et al (1984)	Ex	3.31 ($10^6/T^2$) - 4.82	25-95	Synthesis of Mg-rich smectite (stevensonite and saponite) under hydrothermal conditions. Savin and Lee (1988) point out that Escande et al.'s (1984) technique of analyzing smectites may have resulted in an overestimation of the smectite- H_2O fractionation factor.
127	smectite- H_2O	Savin and Lee (1988)	Mx	2.58 ($10^6/T^2$) - 4.19	0-350	Modification of the equation of Yeh and Savin (1977). Based on analysis of authigenic smecite formed at 1°C (Δ(sm-H_2O)=30.3 ‰), natural smectite-illite pairs, the quartz-illite curve of Eslinger and Savin (1973), and the quartz-H_2O curve of Matsuhisa et al. (1979).
128	smectite- H_2O	Sheppard and Gilg (1996)	Mx	2.55 ($10^6/T^2$) - 4.05	0-350	Regression line fit through a combination of experimental data (Kulla 1979) and various natural occurrences.
129	illite- H_2O	Savin and Lee (1988)	Mx	2.39 ($10^6/T^2$) - 4.19		Based on the natural sample quartz-illite curve of Eslinger and Savin (1973), and the quartz-H_2O curve of Matsuhisa et al. (1979).
130	illite- H_2O	James and Baker (1976)	Ex	23.4	22	Fractionation determined in experiments in which illite was suspended in 2N NaCl and 0.2N NaTPB-EDTA solution. The Northrop-Clayton extrapolation procedure indicates 140% exchange – a significant overshoot of the equilibrium fractionation. Thus, the derived fractionation factor may not be reliable.
131	illite- H_2O	Sheppard and Gilg (1996)	Mx	2.39 ($10^6/T^2$) - 3.76	0-350	Regression line fit through a combination of experimental data (O'Neil and Taylor, 1969) and various natural occurrences.
132	illite:framework-OH	Bechtel and Hoernes (1990)	N	-0.076 T(°C) + 30.42	200-300	Determined intra-mineral fractionation by thermal dehydration and partial fluorination methods. Hamza and Epstein (1980) and Girard and Savin (1996) also attempted on many hydrous minerals, but the techniques are incomplete and the results are umbigouous.
133	serpentine- H_2O	Wenner and Taylor (1971)	N	1.56 ($10^6/T^2$) - 4.70	150-400	Same equation as that for chlorite- H_2O.
	Oxides and Hydroxides:					
134	magnetite-calcite	Chiba et al. (1989)	Ex	-5.91 ($10^6/T^2$)	800-1200	Direct exchange. 82-100% exchange. P=15 kbar.
135	magnetite- siderite	Zhang et al. (2001)	Ex	-1.76 ($10^6/T^2$) - 9.43	45-75	Based on microbial siderite-water and magnetite-water fractionations established by thermophilic Fe(III)-reducing bacteria.
136	magnetite-H_2O	Lowenstam(1962)	N	5.6	9	Measurement of magnetite teeth from the species *Cryptochiton stelleri*, which grew in water at 9°C.
137	magnetite-H_2O	O'Neil (1963)	Ex	-5.5, -4.4	700, 800	Direct exchange. 84-94% exchange. Fractionations calculated by Matthews et al. (1983b) based on the experimental data of O'Neil (1963).

138	magnetite-H_2O	Bottinga and Javoy (1973)	N	-1.47 ($10^6/T^2$) - 3.70		Based on the analysis of feldspar-magnetite pairs from mafic lavas (Anderson et al.,1971), where solidification temperatures are relatively well known.
139	magnetite-H_2O	Blattner et al. (1983)	Ex	-3.7, -7.9	112, 175	Based on analysis of magnetite precipitated in steam pipelines of the Wairakei geothermal power station.
140	magnetite-H_2O	Fortier et al. (1995)	Ex	-8.60	350	Magnetite grown from fine-grained hematite. P = 1 kbar. Isotopic analysis by ion microprobe.
141	magnetite-rich FeO-H_2O	Zhang et al. (1997)	Ex	0.80 ($10^6/T^2$) – 7.74	45-75	Based on Fe_3O_4-rich iron oxides precipitated by Fe(III)-reduction by thermophilic bacteria in culture.
142	magnetite-H_2O	Mandernack et al . (1999)	Ex	0.79 ($10^6/T^2$) – 7.64	4-75	Based on microbial Fe_3O_4 grown within mangetotactic bacteria in culture and those of Zhang et al. (1997).
143	magnetite-quartz	Downs et al. (1981)	Ex	-7.8, -6.1	600, 800	Fayalite is oxidized to quartz and magnetite under hydrothermal conditions. P = 5 kbar. No equation given but regression line through the origin fitted to these two data points is in agreement with the results of Chiba et al. (1989).
144	hematite - H_2O	Clayton and Epstein (1961)	Mx	0.413 ($10^6/T^2$) - 2.56	25-120	Based on the analysis of co-existing quartz, calcite and hematite and experimental calcite-water fractionation factor of Clayton (1961).
145	hematite (geothite)-H_2O	Yapp (1990)	Ex	1.63 ($10^6/T^2$) - 12.3	25-120	Based on the synthesis of hematite ($T \geq 62°C$) or geothite ($T<62°C$) from $Fe(NO_3)_3$ solutions. Fractionation behavior of the two minerals was isotopically indistinguishable.
146	hematite - H_2O	Bao and Koch (1999)	Ex	0.733 ($10^6/T^2$) - 6.914	30-140	Synthesis of hematite from $FeCl_3$ solutions by the addition of $NaHCO_3$ solution. Fractionations are similar to Yapp (1990) at T>95°C but differ significantly at lower temperatures. The authors attribute the discrepancy to differences in the washing and drying protocols applied to the hematite precipitates.
147	goethite - H_2O	Müller (1995)	Ex	1.10 ($10^6/T^2$) - 12.1 (KOH) 0.3 ($10^6/T^2$) - 3.0 (NaOH) 2.76 ($10^6/T^2$) - 23.7 (hydrolysis)	10-65	Precipitation from $Fe(NO_3)_2$ soln by titrating KOH and NaOH solution, and by hydrolysis. The hydrolysis results differ significantly from the KOH and NaOH results.
148	goethite - H_2O	Bao and Koch (1999)	Ex	1.907 ($10^6/T^2$) - 8.004	35-140	Synthesis of geothite from $FeCl_3$ solutions by the addition of NaOH solution. See above for details.
149	akaganeite (β-FeOOH) - H_2O	Bao and Koch (1999)	Ex	3.927 ($10^6/T^2$) - 12.157	35-95	Synthesis of akaganeite by hydrolysis of $FeCl_3$ solutions.
150	rutile-calcite	Chacko et al. (1996)	Ex	-4.31 ($10^6/T^2$)	800-1000	Direct exchange. 53-90% exchange. P=15 kbar.
151	rutile-H_2O	Addy and Garlick (1974)	Ex	-4.1 ($10^6/T^2$) + 0.96	575-775	Exchange by crystallization of amorphous TiO_2 powder.
152	rutile-H_2O	Matthews et al. (1979)	Ex	-4.72 ($10^6/T^2$) +1.62	300-700	Exchange by controlled oxidation of Ti metal powder under hydrothermal conditions.
153	rutile-H_2O	Bird et al. (1993)	Ex	6.1, 3.0	22, 50	Synthesis of rutile from $TiCl_4$ solutions.
154	anatase-H_2O	Bird et al. (1993)	Ex	8.7, 4.9	22, 50	Synthesis of anatase from $TiCl_4$ solutions.
155	rutile-quartz	Matthews and Schliestedt (1984)	Ex	-4.54 ($10^6/T^2$)	500-700	Based on the experimental rutile-water and quartz-water calibrations of Matthews et al. (1979) and Matsuhisa et al. (1979).

156	rutile-quartz	Agrinier (1991)	N	-4.78 ($10^6/T^2$)	450-800	Based on the analysis of quartz, rutile pairs in metamorphic rocks, primarily eclogites. Temperatures based on the Bottinga and Javoy (1975) calibrations of the quartz-muscovite and quartz-garnet thermometers.
157	gibbsite – H_2O	Lawrence and Taylor (1971)	N	~+18	0-30	From analysis of samples from a large number of natural weathering profiles.
158	gibbsite – H_2O	Chen et al. (1988)	N	~+16	0-30	Based on the analysis of gibbsite from bauxite deposits in Taiwan.
159	gibbsite- H_2O	Bird et al. (1994)	Ex	1.31 ($10^6/T^2$) – 1.78	8-51	By synthesis and aging for 3-56 months.
160	gibbsite- H_2O	Vitali et al. (2000)	Ex	2.04 ($10^6/T^2$) – 3.61 ($10^3/T$) + 3.65	0-60	By synthesis and aging for 3-56 months.
161	brucite-H_2O	Saccocia et al. (1998)	Ex	9.54 ($10^6/T^2$) – 35.3 ($10^3/T$) + 26.58	250-450	Direct exchange with 3.2 and 10wt% NaCl soln. P=500 bar.
162	brucite-H_2O	Xu and Zheng (1999)	Ex	1.56 ($10^6/T^2$) – 14.1	15-120	Synthesis by hydrolysis of Mg_3N_2 and $MgCl_2$, and MgO.
163	uraninite(UO_2)-H_2O	Fayek and Kyser (2000)	Ex	16.58 ($10^6/T^2$) – 77.52($10^3/T$) + 77.48	100-300	Combined experimental results of UO_2-CO_2 exchange with CO_2 –H_2O of Truesdell (1974).
164	UO_3-H_2O	Fayek and Kyser (2000)	Ex	-2.21 ($10^6/T^2$) + 25.06($10^3/T$) – 49.50	100-300	Combined experimental results of UO_3-CO_2 exchange with CO_2 –H_2O of Truesdell (1974).
165	cassiterite(SnO_2)-H_2O	Zhang et al. (1994)	Ex	10.13 ($10^6/T^2$) – 26.09($10^3/T$) + 12.58	250-370	Synthesis from amorphous SnO_2 or $SnCl_2$ soln.
166	cassiterite(SnO_2)-H_2O	Sushchevskaya et al. (1985)	Ex	+14.5 (25°C) -1.1 to 0 (300-450°C)	25-450	Precipitation from $SnCl_2$ soln (25°C) and oxidation of Sn (300-450°C).
167	scheelite($CaWO_4$)-H_2O	Ustinov and Grinenko (1990)	Ex	+10.8, +1.8	25, 100	Precipitation.
168	wolframite[(Fe,Mn)WO_4]- H_2O	Zhang et al. (1994)	Ex	3.13 ($10^6/T^2$) – 6.42($10^3/T$) – 0.12	200-420	Synthesis from Na_2WO_4, $FeCl_2$, and $MnCl_2$ in the presence of up to 30wt% NaCl or NaF.
169	perovskite($CaTiO_3$)-calcite	Gautason et al. (1993)	Ex	-6.42 ($10^6/T^2$)	800-1000	Direct exchange. 67-99% exchange. P= 15 kbar.
	Sulfates:					
170	anhydrite- H_2O	Lloyd (1968)	Ex	3.878 ($10^6/T^2$) – 3.4	100-500	Direct exchange between anhydrite and water in 1N H_2SO_4 solution. P=690 bars.
171	anhydrite- H_2O	Chiba et al. (1981)	Ex	3.21 ($10^6/T^2$) – 4.72	100-550	Direct exchange between anhydrite and water in 1m NaCl, HCl or H_2SO_4 solutions. 28-98% exchange. P=1-1000 bars.
172	barite- H_2O	Kusakabe and Robinson (1977)	Ex	2.64 ($10^6/T^2$) – 5.3 (salt-effect not corrected)	110-350	Direct exchange between barite and water in 1m NaCl or 1mNaCl-1m H_2SO_4 solution. 26-98% exchange.
173	alunite(SO_4)- H_2O	Stoffregen et al. (1994)	Ex	3.09 ($10^6/T^2$) – 2.94	250-450	Cation exchange of natroanunite with 0.7m K_2SO_4. 8-95% exchange.
174	alunite(OH)- H_2O	Stoffregen et al. (1994)	Ex	2.28 ($10^6/T^2$) – 3.90	250-450	Cation exchange of natroanunite with 0.7m K_2SO_4. 8-95% exchange.
175	jarosite (SO_4)- H_2O	Rye and Stoffregen (1995)	Ex	1.43 ($10^6/T^2$) + 1.86	150-250	Cation exchange of natroanunite with H_2SO_4-K_2SO_4. 40-100% exchange.
176	jarosite(OH)- H_2O	Rye and Stoffregen (1995)	Ex	2.1 ($10^6/T^2$) – 8.77	150-250	Cation exchange of natroanunite with H_2SO_4-K_2SO_4. 40-100% exchange.

	Zeolites:					
177	analcime- H_2O	Karlsson and Clayton (1990)	Mx	2.78 ($10^6/T^2$) - 2.89	25-400	Combined results of direct exchange at 300-400°C and two natural samples.
178	analcime(channel-water)- H_2O	Karlsson and Clayton (1990)	Ex	1.01 ($10^6/T^2$) - 8.87	300-400	Direct exchange at 1.5-5.0 kbar.
179	stilbite- $H_2O_{(v)}$	Feng and Savin (1993)	Ex	-2.4 + 2.7 ($10^6/T^2$)	220-300	Direct exchange at low pressures (21 Torr).
180	wairakite- H_2O	Noto and Kusakabe (1997)	Ex	2.46 ($10^6/T^2$) - 1.76	250-400	Direct exchange at 0.5-1.5 kbar. 63-98% exchange.
181	wairakite (channel-water)- H_2O	Noto and Kusakabe (1997)	Ex	0.79 ($10^6/T^2$) - 3.07	250-400	Direct exchange at 0.5-1.5 kbar. 94-99% exchange.
182	clinoptilolite-water	Nahr et al. (1998)	N	+31.6±0.2, +26.6	25, 40	Based on analysis of authigenic clinoptilolite samples in oceanic sediments from three ODP sites.
	CO_2-Silicate/Melt/Glass:					
183	CO_2-silica glass	Stolper and Epstein (1991)	Ex	+2.14 to +4.30	550-950	Direct exchange between silica wool or power and CO_2 at 0.5 bar.
184	CO_2-silica glass	Matthews et al. (1994)	Ex	+2.10 to +3.11	750-950	Direct exchange between silica wool or power and CO_2 at 1 bar.
185	CO_2-albite glass	Matthews et al. (1994)	Ex	+3.58 to +4.75	750-950	Direct exchange between albite glass and CO_2 at 1 bar.
186	CO_2-albite	Matthews et al. (1994)	Ex	+3.36 to +4.74	750-950	Direct exchange between crystalline albite and CO_2 at 1 bar.
187	CO_2-rhyolitic glass/melt	Palin et al. (1996)	Ex	+2.95 to +5.08	550-950	Direct exchange between rhyolitic glass and CO_2 at 0.8-1.5 bar.

Notes: 1. Ex = experimental; N = natural sample; M = mixed experimental/natural sample calibration. 2. Equations given with temperature in Kelvin unless otherwise indicated.

Appendix 3. Carbon isotope fractionation factors: calibrations based on experiments or natural samples.

#	Phases	Reference	[1]Method	[2]1000 ln α	T(°C)	Comments
	$CO_2$and Aqueous Species:					
1	CO_2:solid-vapor	Eiler et al. (2000)	Ex	-0.2 to +0.4	130-150(K)	By sublimation-condensation and isotopic exchange.
2	CO_2:liquid-vapor	Grootes et al. (1969)	Ex	-0.57 to –0.14	220-303(K)	Liquid-vapor equilibration for >4 hr.
3	CO_2(aq)-CO_2(g)	Wendt (1968), Vogel et al. (1970), and Zhang et al. (1995)	Ex	0.0041 T(°C)-1.18 (Vogel) 0.0049 T(°C)-1.31 (Zhang)	0-60	^{13}C is depleted and ^{18}O is enriched in the aqueous phase.
4	HCO_3^-(aq)-CO_2(g)	Deuser and Degens (1967), Wendt (1968), Emrich et al. (1970), Mook et al. (1974), Turner (1982), Lesniak and Sakai (1989), and Zhang et al. (1995)	Ex	7.92 to 8.27 at 25°C with –0.064 to –0.141‰/°C gradient	5-60	Consistent results by many investigators.
5	HCO_3^-(aq)-CO_2(g)	Szaran (1997)	Ex	-0.0954 T(°C) + 10.41	7-70	Also investigated the relaxation time.
6	HCO_3^-(aq)-CO_2(g)	Malinin et al. (1967)	Ex	-7.3 to +7.5	23-286	Cross-over at about 150°C.
7	CO_3^{2-}(aq)-CO_2(g)	Turner (1982), Lesniak and Sakai (1989), Zhang et al. (1995) and Halas et al. (1997)	Ex	-1.5 to +8.5	4-80	Cross-over at about 67°C (Halas et al., 1997).
	Carbonates-Aqueous Solution:					
8	calcite-HCO_3^-(aq)	Rubinson and Clayton (1969)	Ex	0.9±0.2	25	Slow precipitation by CO_2 degassing.
9	calcite-CO_2(g)	Emrich et al. (1970)	Ex	9.61±0.28 at 25°C	20-60	Slow precipitation by CO_2 degassing.
10	calcite-HCO_3^-(aq)	Turner (1982)	Ex	1.83 to 2.26	25	Slow precipitation by adding NaOH to Ca-HCO_3 soln.
11	calcite-CO_2(g)	Romanek et al. (1992)	Ex	11.98 - 0.12 T(°C)	10-40	Controlled seeded precipitation at constant composition.
12	aragonite-HCO_3^-(aq)	Rubinson and Clayton (1969)	Ex	2.7±0.2	25	Slow precipitation by CO_2 degassing.
13	aragonite-CO_2(g)	Romanek et al. (1992)	Ex	13.88 - 0.13 T(°C)	10-40	Controlled seeded precipitation at constant composition.
14	siderite ($FeCO_3$) - HCO_3^-(aq)	Carothers et al. (1988)	Ex	-4.20 to +2.86	33-197	Slow injection of $FeCl_2$ soln to $NaHCO_3$ soln.
15	gaylussite ($Na_2CO_3 \cdot CaCO_3 \cdot 5H_2O$)- CO_3^{2-}(aq)	Matsuo et al. (1972)	Ex	1.9 to 3.1	8-35	Formed by mixing Na_2CO_3 and $CaCl_2$ solns.
16	trona ($Na_2CO_3 \cdot NaHCO_3 \cdot 2H_2O$)- CO_3^{2-}(aq)	Matsuo et al. (1972)	Ex	0.7 to 1.8	18-35	Formed from Na_2CO_3 and $NaHCO_3$ solns onto seed crystal.
17	pirssonite ($Na_2 \cdot Ca(CO_3)_2 \cdot 2H_2O$)- CO_3^{2-}(aq)	Bottcher (1994)	Ex	2.3 and 3.3	60-90	Reaction of $CaCO_3$ with Na_2CO_3 soln.
18	CO_2-malachite ($CuCO_3 \cdot Cu(OH)_2$)	Melchiorre et al. (1999)	Ex	-1.85 ($10^6/T^2$)+ 10.51	0-50	Replacement of calcite with Cu^{2+}-bearing soln.
19	norsethite ($BaMg(CO_3)_2$) - CO_2	Bottcher (2000)	Ex	1.78 ($10^6/T^2$) - 10.16	20-90	Formed from $BaCO_3$ and $MgCO_3 \cdot 3H_2O$ in $NaHCO_3$ soln.

	CO_2-Calcite/Graphite:					
20	CO_2-calcite	Chacko et al. (1991)	Ex	2.91 to 5.08 $-0.10028 + 5.4173x - 2.5076x^2 + 0.47193x^3 - 0.049501x^4 + 0.0027046x^5 - 0.000059409x^6$ where $x=10^6/T^2$	400-950	Direct exchange. 19-98% exchange. P=10 kbar. Large errors due to small degrees of exchange. Equation represents theoretical calculations that fit the experimental data of Chacko et al. (1991) and Rosenbaum (1994) within error. The data of Scheele and Hoefs (1992) are displaced to slightly larger fractionations. The equation reproduces the calculated fractionations from 273-4000K.
21	CO_2-calcite	Rosenbaum (1994)	Ex	2.70	900	Direct exchange. P=12.5 kbar.
22	CO_2-calcite	Scheele and Hoefs (1992)	Ex	$-3.46 (10^6/T^2) + 9.58 (10^3/T) - 2.72$	500-1200	Most experiments involved inversion of aragonite to calcite. P=1-5 kbar.
23	CO_2-graphite	Scheele and Hoefs (1992)	Ex	$4.53 (10^6/T^2) + 3.04$	600-1200	Direct exchange. 33-79% exchange. P=5-15 kbar. Small CO_2/C ratio (1/32) used in the experiments may have resulted in the incorporation of surface effects in the measured fractionations.
	Carbonates-Graphite/Diamond					
24	aragonite-calcite	Sommer and Rye (1978)	N	2.56 - 0.065T(°C)	0-25	Based on analysis of coexisting calcite and aragonite tests and shells.
25	dolomite-calcite	Sheppard and Schwarcz (1970)	N	$0.18 (10^6/T^2) + 0.17$	100-650	Based on analyses of coexisting pairs of metamorphic origin. Preliminary experimental results show much larger fractionations.
26	calcite-graphite	Valley and O'Neil (1981)	N	-0.00748 T(°C) + 8.68	610-760	Based on analyses of metamorphic samples from the Adirondack Mountains.
27	calcite-graphite	Wada and Suzuki (1983)	N	$5.6 (10^6/T^2) - 2.4$	400-680	Based on analyses of metamorphic aureole samples from central Japan.
28	calcite-graphite	Morikiyo (1984)	N	$8.9 (10^6/T^2) - 7.1$	270-650	Based on analyses of metamorphic aureole samples from central Japan.
29	calcite-graphite	Dunn and Valley (1992)	N	$5.81 (10^6/T^2) - 2.61$	400-800	Based on analyses of metamorphic samples from Tudor aureole, Canada.
30	calcite-graphite	Kitchen and Valley (1995)	N	$3.56 (10^6/T^2)$	700-800	Based on analyses of metamorphic samples from the Adirondack Mountains.
31	dolomite-graphite	Wada and Suzuki (1983)	N	$5.9 (10^6/T^2) - 1.9$	400-680	Based on analyses of metamorphic aureole samples from central Japan.
32	diamond-graphite	Hoering (1961)	Ex	0.3	>1700	Conversion of graphite to diamond at P=70 kbar.
	CO_2 in Melts:					
33	CO_2-CO_3^{2-} in melt	Javoy et al. (1978)	Ex	4.0 to 4.6	1120-1280	Solution of CO_2 into tholeiitic silicate melt at 7.0-8.4 kbar.
34	CO_2-CO_3^{2-} in melt	Mattey et al. (1990) and Mattey (1991)	Ex	1.8 to 2.7	1200-1400	Solution of CO_2 into silicate (sodamelilite and basalt) and carbonate melts at P=5-39 kbar.
	Gases:					
35	CO_2-CH_4	Horita (2001)	Ex	$26.70 - 49.137 (10^3/T) + 40.828 (10^6/T^2) - 7.512(10^9/T^3)$	200-600	Complete exchange catalyzed by Ni catalyst.

Notes: 1. Ex = experimental; N = natural sample; M = mixed experimental/natural sample calibration. 2. Equations given with temperature in Kelvin unless otherwise indicated.

Appendix 4. Hydrogen isotope fractionation factors: calibrations based on experiments or natural samples.

#	Phases	Reference	[1]Method	[2]1000 ln α	T(°C)	Comments
	Gases, Liquid, Ice					
1	H_2O: ice-vapor	Merlivat and Nief (1967)	Ex	$\log\alpha = -0.041 + 7.074/T^2$	-40 – 0	
2	H_2O: ice-liquid	O'Neil (1968)	Ex	+18.7±0.9	0?	Slow growth of ice in stirred water.
3	H_2O: ice-liquid	Craig and Hom (1968)	Ex	+19.5, +20.3	0?	Freezing from 4‰ chlorinity water and seawater.
4	H_2O: ice-liquid	Arnason (1969)	Ex	+20.6±0.7	0	Seeded-growth.
5	H_2O: ice-liquid	Suzuki and Kimura (1973)	Ex	+20.4±0.5	0?	
6	H_2O: ice-liquid	Stewart (1974)	Ex	+24	-10	Freezing from 2.5m NaCl soln.
7	H_2O: ice-liquid	Lehmann and Siegenthaler (1991)	Ex	+21.2±0.4	0	Slow growth of ice in stirred water.
8	H_2O: liquid-vapor	Majoube (1971b)	Ex	$24.844\ (10^6/T^2) - 76.248(10^3/T) + 52.612$	0-100	Slow distillation of liquid water.
9	H_2O: liquid-vapor	Horita and Wesolowski (1994), and all references therein	Ex	$1158.8\ (T^3/10^9) - 1620.1\ (T^2/10^6) + 794.84\ (T/10^3) + 2.9992\ (10^9/T^3) - 161.04$	0-374	High precision experimental calibration using three different apparatus to cover the full temperature range. This large dataset was combined with selected earlier experimental studies to generate the calibration curve.
10	CH_4-H_2	Horibe and Craig (1995)	Ex	$\alpha = 0.8994 + 183540/T^2$	200-500	Complete exchange with Ni-thoria catalyst.
11	$H_2O_{(v)}$-H_2	Suess (1949)	Ex	$\log\alpha = 203/T - 0.132$	80-200	
12	$H_2O_{(v)}$-H_2	Cerrai et al. (1954)	Ex	3.04 to 1.18 (α)	51-742	Dynamic exchange in a reactor with Pt catalyst.
13	$H_2O_{(liq)}$-H_2	Rolston et al. (1976)	Ex	$\ln\alpha = -0.2143 + 368.9/T + 27870/T^2$	7-97	Exchange catalyzed by Pt catalyst.
	Hydrated Salts:					
14	trona ($Na_2CO_3 \cdot NaHCO_3 \cdot 2H_2O$) – H_2O	Matsuo et al. (1972)	Ex	$1.420\ (10^7/T^2) + 2.356\ (10^4/T)$	8-35	Synthesis from aqueous solutions. Determined on the composition scale of brine.
15	gaylussite ($Na_2CO_3 \cdot CaCO_3 \cdot 5H_2O$) – H_2O	Matsuo et al. (1972)	Ex	-15 to -13	8-35	Synthesis from aqueous solutions. Determined on the composition scale of brine.
16	natron ($Na_2CO_3 \cdot 10H_2O$) – H_2O	Pradhananga and Matsuo (1985b)	Ex	+15 to +17	5-10	Synthesis from aqueous solutions. Determined on the composition scale of brine.
17	borax ($Na_2B_4O_7 \cdot 10H_2O$) – H_2O	Matsuo et al. (1972) Pradhananga and Matsuo (1985a)	Ex	0 to +2 +2 to +5	8-35 5-25	Synthesis from aqueous solutions. Determined on the composition scale of brine.
18	carnallite($KMgCl_3 \cdot 6H_2O$) – H_2O	Horita (1989)	Ex	-44 to -40	10-40	By precipitation and aging 30-67 days. Determined on the activity scale of brines.
19	carnallite($KMgCl_3 \cdot 6H_2O$) – H_2O	Koehler and Kyser (1996)	Ex	$-18.4\ (10^6/T^2) + 162$	22-45	By synthesis and exchange.
20	bischofite($MgCl_2 \cdot 6H_2O$) – H_2O	Horita (1989)	Ex	-47 to -37	10-40	By precipitation and aging 30-67 days. Determined on the activity scale of brines.
21	tachyhydrite($CaMg_2Cl_6 \cdot 12H_2O$) – H_2O	Horita (1989)	Ex	-46 to -36	25-40	By precipitation and aging 30-67 days. Determined on the activity scale of brines.
22	gypsum ($CaSO_4 \cdot 2H_2O$)- H_2O	Fontes and Gonfiantini (1967), Sofer (1978), and Matsubaya and Sakai (1973)	Ex	-15 to -20	17-57	Slow precipitation.
23	mirabilite ($Na_2SO_4 \cdot 10H_2O$)- H_2O	Stewart (1974) Pradhananga and Matsuo (1985b)	Ex	+13 to +19	0-25	Synthesis from aqueous solutions. Determined on the composition scale of brine.

24	episomite ($MgSO_4 \cdot 7H_2O$)- H_2O	Pradhananga and Matsuo (1985b)	Ex	-1	25	Synthesis from aqueous solutions. Determined on the composition scale of brine.
	Hydroxides:					
25	boehmite- H_2O	Suzuoki and Epstein (1976)	Ex	-66.2	400	Direct exchange. 93% exchange. P=1 kbar (Suzuoki, pers. commun.).
26	boehmite- H_2O	Graham et al. (1980)	Ex	-37.4, -36.2, -53.5, -49.9	150, 200, 280, 380	Direct exchange. 77-100% exchange. P = 2 kbar.
27	diaspore- H_2O	Graham et al. (1980)	Ex	-78.7	380	Direct exchange. 25% exchange. P = 4 kbar.
28	gibbsite- H_2O	Lawrence and Taylor (1971)	N	-15	0-30	From analysis of samples from a large number of natural weathering profiles.
29	gibbsite- H_2O	Chen et al. (1988)	N	-8	0-30	From analysis of samples from a large number of natural weathering profiles in Taiwan.
30	gibbsite- H_2O	Vitali et al. (2001)	Ex	-2±6	9-60	Synthesis over 10 years.
31	gibbsite- H_2O	Vitali et al. (2001)	N	-8±10	Ambient	Based on analysis of 12 samples from various localities in the tropics.
32	goethite- $H_2O_{(v)}$	Yapp and Pedley (1985)	Ex	-75.8, -89.9	100, 145	Direct exchange between natural goethite and water vapor. 52-75% exchange. P=1 bar. Corresponding oethite-H_2O(l) fractionations are –103.6 at both 100 and 145°C using the liquid-vapor fractionation curve of Horita et al. (1994).
33	goethite- $H_2O_{(l)}$	Yapp and Pedley (1985)	N	-105	~25	Based on the analysis of natural goethite and associated modern waters.
34	goethite- $H_2O_{(l)}$	Yapp (1987)	Ex	~-95	25, 62	Synthesis of goethite from $Fe(NO_3)_3$ solutions.
35	manganite- $H_2O_{(l)}$	Hariya and Tsutsumi (1981)	Ex	-211 to -192	150-250	Direct exchange at 500 bar. 46-90% exchange.
36	brucite-H_2O	Satake and Matsuo (1984)	Ex	$8.72\ (10^6/T^2) - 3.86\ (10^4/T) + 14.5$	144-510	Direct exchange. 58-100% exchange. P=1-1060 bars.
37	brucite-H_2O	Saccocia et al. (1998)	Ex	-32 to -22	250-450	Direct exchange with 3.2 and 10wt% NaCl soln. P=500 bar.
38	brucite-H_2O	Xu and Zheng (1999)	Ex	$4.88\ (10^6/T^2) - 22.54$	25-90	Synthesis by hydrolysis of Mg_3N_2 and $MgCl_2$. Large discrepancy with the data of Satake and Matsuo (1984).
39	brucite-H_2O	Horita et al. (1999)	Ex	-31.9 to –19.5	380	Increase with pressure from 150 to 8000 bar.
	Sorosilicates:					
40	epidote- H_2O	Graham et al. (1980)	Ex	$29.2\ (10^6/T^2) - 138.8$ -35.9	200-300 300-650	Direct exchange. 30-100% exchange. P=2-4 kbar. Epidote composition is pistacite (Fe/Fe+Al) = 0.29. Experiments indicate fractionation factor is independent of temperature in the 300-650°C temperature range.
41	epidote- H_2O	Chacko et al. (1999)	Ex	$9.3\ (10^6/T^2) - 61.9$	300-600	Direct exchange. Experiments done on large single crystals and analyzed with the ion microprobe. P = 1.2 – 2.2 kbar. Epidote composition is pistacite (Fe/Fe+Al) = 0.33.
42	epidote- H_2	Vennemann and O'Neil (1996)	Ex	$110.756\ (10^6/T^2) + 149.98\ (10^3/T) - 158.685$	150-400	Direct exchange of epidote with H_2 gas. 71-91% exchange. P = 0.3-2 bars. At 300°C, epidote-H_2O fractionations derived from these results are approximately 35‰ more negative than those reported in the direct epidote-H_2O exchange experiments of Graham et al. (1980) and Chacko et al. (1980). Epidote composition is pistacite (Fe/Fe+Al) = 0.30.
43	zoisite- H_2O	Graham et al. (1980)	Ex	$-15.07\ (10^6/T^2) - 27.73$	280-650	Direct exchange. 35-100% exchange. P= 4 kbar. Zoisite composition is pistacite (Fe/Fe+Al) = 0.03.
44	clinozoisite- H_2O	Graham et al. (1980)	Ex	-37.8, -37.2	300, 450	Direct exchange. 60-100% exchange. P= 2 kbar. Zoisite composition is pistacite (Fe/Fe+Al) = 0.09.

45	ilvaite – H_2O	Yaqian and Jibao (1993)	Ex	-105 (350-550°C) -29.95 ($10^6/T^2$) – 60.62 (550-750°C)	350-750	Direct exchange at P=50-203 bar. 50-100% exchange.
	Cyclosilicates:					
46	tourmaline- H_2O	Blamart et al. (1989)	Ex	-39.3 ($10^6/T^2$) + 63.4	500-600	Direct exchange at P=3 kbar. 72-92% exchange.
47	tourmaline- H_2O	Jibao and Yaqian (1997)	Ex	-27.9 ($10^6/T^2$) + 2.3	450-800	Direct exchange at P=150-250 bar. 11-81% exchange.
48	tourmaline- H_2O	Kotzer et al. (1993)	N	-27.2 ($10^6/T^2$) + 28.1	350-600	Based on the analysis of co-existing quartz, muscovite and tourmaline from several ore deposits. Temperatures based on quartz-muscovite oxygen isotope fractionations compiled by Eslinger et al. (1979).
	Amphiboles:					
49	hornblende- H_2O	Suzuoki and Epstein (1976)	Ex	-23.9 ($10^6/T^2$) + 7.9	400-700	Direct exchange. 19-100% exchange. Pressure unspecified. Composition of the hornblende not clearly specified but appears to actinolite or actinolitic hornblende.
50	pargasite- H_2O	Graham et al. (1984)	Ex	-21.86, -18.12	700, 850	Direct exchange. 83-90% exchange. P = 4-6 kbar.
51	ferroan pargasitic hornblende – H_2O	Graham et al. (1984)	Ex	-31.0 ($10^6/T^2$) + 1.1 -23.1	850-950 350-700	Direct exchange. 46-100% exchange. P = 2-8 kbar. Experiments indicate fractionation factor is independent of temperature in the 350-700°C temperature range.
52	hornblende- H_2	Vennemann and O'Neil (1996)	Ex	452, 326	300, 400	Direct exchange of hornblende with H_2 gas. 71-91% exchange. P = 2 bars. Fe^{3+} content of the hornblende decreased and water content increased during the experiment indicating that isotopic exchange was accompanied by partial reduction of Fe.
53	tremolite- H_2O	Graham et al. (1984)	Ex	-31.0 ($10^6/T^2$) +14.9 -21.7	650-850 350-650	Direct exchange. 75-99% exchange. P = 2-4 kbar. Experiments indicate fractionation factor is independent of temperature in the 350-650°C temperature range.
54	actinolite- H_2O	Graham et al. (1984)	Ex	-29	400	Direct exchange. 59% exchange. P = 2 kbar.
	Micas:					
55	muscovite- H_2O	Suzuoki and Epstein (1976)	Ex	-22.1 ($10^6/T^2$) + 19.1	450-750	Direct exchange. 39-100% exchange. P=1 kbar (Suzuoki, pers. commun.).
56	muscovite- H_2	Vennemann and O'Neil (1996)	Ex	316.851 ($10^6/T^2$) – 584.796 ($10^3/T$) + 515.684	200-400	Direct exchange of muscovite with H_2 gas. 13-80% exchange. P =0.4-2 bars.
57	lepidolite- H_2O	Suzuoki and Epstein (1976)	Ex	+15.4	650	Direct exchange. 45% exchange. P=1 kbar (Suzuoki, pers. commun.).
58	phlogopite – H_2O	Suzuoki and Epstein (1976)	Ex	-14.9, -9.9	575, 650	Direct exchange. 36-81% exchange. P=1 kbar (Suzuoki, pers. commun.). Biotite composition is Mg/(Fe+Mg) = 0.89.
59	biotite (Mg-rich) – H_2O	Suzuoki and Epstein (1976)	Ex	-21.3 ($10^6/T^2$) – 2.8	400-850	Direct exchange. 31-100% exchange. P=1 kbar (Suzuoki, pers. commun.). Biotite composition is Mg/(Fe+Mg) = 0.61.
60	biotite (Fe-rich) – H_2O	Suzuoki and Epstein (1976)	Ex	-38.0	650	Direct exchange. 100% exchange. P=1 kbar (Suzuoki, pers. commun.). Biotite composition is Mg/(Fe+Mg) = 0.33.
61	biotite- H_2	Vennemann and O'Neil (1996)	Ex	417.3, 293.0	300, 400	Direct exchange of biotite with H_2 gas. 31-64% exchange. P =2 bars. Extensive reduction of Fe^{3+} and increase in water accompanied isotopic exchange.

	Other Hydrous Phyllosilicates:					
62	chlorite- H_2O	Marumo et al. (1980)	N	-47 to -13	100-250	Based on the analysis of chlorites in drill core samples from the Ohnuma geothermal area, Japan. The authors propose that fractionations are independent of temperature over this temperature range but become systematically more negative with increasing Fe/(Fe+Mg) of chlorite. Graham et al. (1987) question the validity of these conclusions.
63	chlorite- H_2O	Taylor (1974)	N	-45 to -35	300-500	Based on natural samples.
64	chlorite- H_2O	Graham et al. (1987)	Ex	-28	500-700	Direct exchange. 47-100% exchange. P = 2 kbar. Experiments indicate fractionation factor is independent of temperature over this temperature range.
65	serpentine- H_2O	Wenner and Taylor (1973)	Mx	$1.56\ (10^6/T^2) - 4.70$	25-400	Based on analysis of natural deweylite, lizardite, antigorite and one preliminary experimental data of Suzuoki and Epstein .
66	serpentine- H_2O	Suzuoki and Epstein (1976)	Ex	-19.8	400	Direct exchange. 98% exchange. P=1 kbar (Suzuoki, pers. commun.).
67	serpentine- H_2O	Sakai and Tsutsumi (1978)	Ex	$2.75\ (10^7/T^2) - 7.69\ (10^4/T) + 40.8$	100-500	Direct exchange. 18-93% exchangeP = 2 kbar. Starting material is a commercial chrysotile asbestos fiber.
68	serpentine- H_2O	Grinenko et al (1987) Mineev and Grinenko (1996)	Ex	-40 to +35 (100°C) -23 to +6 (200°C)	100, 200	Direct exchange of natural lizardite and water. 11-20% exchange. P = 1-2500 bar. Similar to the semi-empirical calibration of Wenner and Taylor (1973). Attribute the large discrepancy with the results of Sakai and Tsutsumi (1978) to differences in experimental pressures.
69	kaolinite-H_2O	Suzuoki and Epstein (1976)	Ex	-23.7	400	Direct exchange. 90% exchange. P=1 kbar (Suzuoki, pers. commun.). Temperature is beyond the thermal stability limit of kaolinite.
70	kaolinite-H_2O	Lambert and Epstein (1980)	N	$-4.53\ (10^6/T^2) + 19.36$	<230	Based on analysis of samples from Valles Caldera, New Mexico, geothermal system.
71	kaolinite-$H_2O_{(v)}$	Liu and Epstein (1984)	Ex	-21.20to –9.6	250-352	Direct exchange with high kaolinite-water H ratio (80). 36-100% exchange. Combined with $H_2O_{(l)}$-$H_2O_{(v)}$ to obtain kaolinite-$H_2O_{(liq)}$ fractionation.
72	kaolinite-H_2O	Gilg and Sheppard (1996)	Mx	$-2.2\ (10^6/T^2) - 7.7$	0-330	Based on the experimental data of Sheppard et al. (1969) and Liu and Epstein (1984) at 300°C and various natural sample data from geothermal systems and weathering profiles (Marumo et al. 1980; Rye et al. 1992; Lawrence and Taylor 1972).
73	kaolinite- H_2	Vennemann and O'Neil (1996)	Ex	$-162.495\ (10^6/T^2) + 1241.164\ (10^3/T) - 1219.110$	150-275	Direct exchange of kaolinite with H_2 gas. 32-94% exchange. P =0.3-2 bars.
74	smectite-H_2O	Yeh (1980)	N	$-19.6\ (10^3/T) + 25$	25-120	Based on the analysis of smectites in deep Gulf Coast wells and assuming Δ=-41 at 25°C. See also Savin and Lee (1988) and Sheppard and Gilg (1996) for critique of these and other smectite-H_2O data.
75	illite/smectite-H_2O	Capuano (1992)	N	$-45.3\ (10^3/T) + 94.7$	0-150	Based on analysis of coexisting clay and water from Gulf Coast geopressured fields.

	Sulfates:					
76	alunite- H_2O	Stoffregen et al. (1994)	Ex	-6 to -19	250-450	Cation exchange of natroanunite with 0.7m K_2SO_4. 8-95% exchange.
77	jarosite- H_2O	Rye and Stoffregen (1995)	Ex	-50±12	150-250	Cation exchange of natroanunite with H_2SO_4-K_2SO_4. 40-100% exchange.
	Melts-Glass:					
78	$H_2O_{(v)}$-silicate glass	Dobson et al. (1989)	Ex	+35 to +51	530-850	Natural rhyolitic obsidian and synthetic albite-orthoclase glasses. P=1.4-2.8 bar.
79	$H_2O_{(liq)}$-rhyolite glass	Friedman et al. (1993)	N	+33	Ambient	Based on analysis of hydrated rhyolitic lava from Idaho and Katmai.
80	$H_2O_{(v)}$-silicate melt	Kuroda et al. (1982)	Ex	-54 to +33	800-1300	All at 20 kbar. D enriched in K-feldspar and albite melts and depleted in quartz and anorthite melts.
81	$H_2O_{(v)}$-rhyolite melt	Taylor and Westrich (1985)	Ex	+23.6	950	Synthesis and reversed isotope exchange experiments. D depleted in the melt.
82	$H_2O_{(v)}$-albite melt	Richet et al. (1986)	Ex	+8 to +25	870-1250	Used natural albite at 2 kbar. Contradict Kuroda et al. (1982).
83	$H_2O_{(v)}$-basalt melt	Shilobreyeva et al. (1992)	Ex	+18 to +25	1250	P=3 kbar. Deuterium depleted in the melt.
84	$H_2O_{(v)}$-basaltic andesite melt	Pineau et al. (1998)	Ex	+20 to +32	1250	Fractionation decreased with pressure from 0.5 to 3 kbar, due to increasing solubility of H_2O.

Notes: 1. Ex = experimental; N = natural sample; M = mixed experimental/natural sample calibration. 2. Equations given with temperature in Kelvin unless otherwise indicated.